PB-228 282

WASTE WATER RECHARGE AND DISPERSION IN POROUS MEDIA

John Austin Hoopes, et al

Massachusetts Institute of Technology

Prepared for:

Public Health Service

June 1965

DISTRIBUTED BY:

NTIS
National Technical Information Service
U. S. DEPARTMENT OF COMMERCE
5285 Port Royal Road, Springfield Va. 22151

PB 228 282

R65-55

HYDRODYNAMICS LABORATORY

Department of Civil Engineering
Massachusetts Institute of Technology

WASTE WATER RECHARGE AND DISPERSION IN POROUS MEDIA

by

John Austin Hoopes
and
Donald R.F. Harleman

June, 1965

Report No. 75

Prepared Under

Division of Water Supply and Pollution Control,
Public Health Service, National Institutes of Health,
U.S. Department of Health, Education,
and Welfare under Research Grant No. WP-347

Reproduced by
NATIONAL TECHNICAL
INFORMATION SERVICE
U S Department of Commerce
Springfield VA 22151

ABSTRACT

The recharge and disposal of treated and untreated waste waters in aquifers results in a mixing of these waters with the natural groundwater. The distribution and boundaries of the ensuing mixture are determined by dispersion and diffusion. This study incorporates the effects of these mixing processes in a mass conservation equation and derives solutions to this equation which predict the tracer distributions resulting from certain well recharging and disposal operations.

For uniform flow, the longitudinal and lateral dispersion coefficients (i.e. in the flow direction and transverse to it) are related to the seepage velocity, particle size, and media structure. These coefficients are determined from experimental measurements of the distribution of a dilute salt tracer in flow through a sand column.

The results are used in the prediction of the tracer distributions in confined aquifers during recharge or disposal operations by wells. A solution for the tracer distribution is obtained in the study of recharge by a single well. It is shown that convection and dispersion determine the tracer distribution near the well; whereas, at larger distances from the well, molecular diffusion and convection alone are important.

With a pair of wells, one recharging tracer fluid and the other pumping the mixture of tracer and native ground water, the solution for the tracer distribution indicates that lateral dispersion has a negligible influence on the tracer distribution, except very near the line joining the two wells. Molecular diffusion is also shown to be insignificant, except for small flow rates and large well spacings. Longitudinal dispersion determines the shape of the tracer distribution within the media; whereas, convection dominates the tracer distribution at the pumping well, except for short times.

ACKNOWLEDGEMENTS

This study was sponsored by the Division of Water Supply and Pollution Control, Public Health Service, National Institutes of Health, U.S. Department of Health, Education, and Welfare under Research Grant No. WP-347. Part of this study was made possible by the American Society of Civil Engineers who awarded the J. Waldo Smith Hydraulic Fellowship to Mr. John A. Hoopes for the academic year 1961-1962. In addition, support was obtained through a Ford Foundation loan from 1962-1964.

The authors are indebted to Professor Norman H. Brooks of the California Institute of Technology, who supervised the study during the first year of this investigation when Professors Harleman and Brooks were exchange Visiting Professors.

In addition, the interest and assistance of the faculty and research staff of the Hydrodynamics Laboratory in this study are deeply appreciated. The assistance of Khalid Mohtadullah in the experimental work, and of Edward Holley in the many discussions on questions both theoretical and experimental are appreciated. The help of Frank Perkins and Gerald Tlapa on some of the computer work is also gratefully acknowledged.

The IBM 7094 computer in the Computation Center at the Massachusetts Institute of Technology was used to conduct the numerical solutions of this investigation.

TABLE OF CONTENTS

ABSTRACT ii

ACKNOWLEDGEMENTS iii

LIST OF FIGURES AND TABLES vii

I. INTRODUCTION 1

II. LITERATURE REVIEW AND OBJECTIVES 4

2.1 Review of Previous Work 4

2.2 Objectives of this Investigation 10

III. LONGITUDINAL AND LATERAL DISPERSION 11

3.1 Theoretical Analysis 11

3.1.1 Convective-Dispersion Equation 11

3.1.2 Longitudinal Dispersion 13

3.1.3 Lateral Dispersion 14

3.2 Experimental Equipment and Procedure 24

3.2.1 Experimental Equipment 24

3.2.2 Longitudinal Dispersion Testing Procedure 29

3.2.3 Lateral Dispersion Testing Procedure 31

3.3 Analysis of Data 31

3.3.1 Longitudinal Dispersion 31

3.3.2 Lateral Dispersion 40

3.4 Presentation and Discussion of Results 45

3.4.1 Longitudinal Dispersion 45

3.4.2 Lateral Dispersion 55

IV. DISPERSION IN RADIAL FLOW AND FLOW BETWEEN TWO WELLS 61

4.1 Theoretical Developments 61
    4.1.1 General Convective-Dispersion Equation for Two-Dimensional Flows 61
    4.1.2 Dispersion in Steady Radial Flow from a Well in a Confined Aquifer 65
        4.1.2.1 Description of the Flow Field 65
        4.1.2.2 Convective-Dispersion Equation 67
    4.1.3 Dispersion in Steady Flow between a Recharging and a Pumping Well in a Confined Aquifer 79
        4.1.3.1 Description of the Flow Field 79
        4.1.3.2 Convective-Dispersion Equation 82
            a) Tracer Distribution with no Dispersion 84
            b) Tracer Distribution with Longitudinal Dispersion along the Streamlines 89
            c) Tracer Distribution with Lateral Dispersion across the Streamlines 100

4.2 Experimental Equipment and Procedure 105
    4.2.1 Radial and Two Well Flow Equipment 105
    4.2.2 Radial Flow Testing Procedure 112
    4.2.3 Two Well Flow Testing Procedure 114

4.3 Method of Analysis 115
    4.3.1 Radial Flow Dispersion 115
    4.3.2 Dispersion in Flow between Two Wells 118

4.4 Presentation and Discussion of Results 121

4.4.1 Radial Flow Dispersion 121

4.4.2 Dispersion in Flow between Two Wells 127

V. SUMMARY AND CONCLUSIONS 146

VI. REFERENCES 150

DEFINITION OF SYMBOLS 162

LIST OF FIGURES AND TABLES

Figure No. Page

3-1 Mass Flux Components in a Small Volume of a Packed Sand Column 12
3-2 Schematic Longitudinal Dispersion Column Setup and Typical Measurement 13
3-3 Schematic Column Setup and Typical Measurement for an Instantaneous Point Source Injection 15
3-4 Schematic Column Setup and Typical Measurement for a Continuous Point Source Injection 15
3-5 Longitudinal and Lateral Concentration Gradients for a Continuous Point Source Injection 21
3-6 Schematic Layout for Longitudinal and Lateral Dispersion Column Tests 25
3-7 Conductivity Probe 28
3-8 Wheatstone Bridge Circuit for Conductivity Probe 28
3-9 Plot of Exact and Approximate Concentration Distributions for Longitudinal Dispersion 33
3-10 Buildup to Steady Flow through a Packed Sand Column 36
3-11 Time Variation of Tracer Concentration at a Point During Longitudinal Dispersion Test 9, No. 2 Sand 38
3-12 c/c_0 versus $1-\xi'/2\sqrt{\xi'}$ for Longitudinal Dispersion Test 9, No. 2 Sand 39
3-13 c/c_{max} versus r for Lateral Dispersion Run 3 43
3-14 $\sqrt{\ln c/c_{max}}$ versus r for Lateral Dispersion Run 3 44
3-15 Correlation of D_1/ν and D_2/ν with $\mathbb{R} = wd_{50}/\nu$ 46
3-16 Correlation of D_1/ν and D_2/ν with $\mathbb{R}_k = w\sqrt{k}/\nu$ 47
3-17 Comparison of the Characteristics of the Ringed Electrode and Parallel Plate Probes 54

Figure No. Page

3-18 Measurement of Radial Tracer Variation with the Conductivity Probe 58

4-1 Streamline and Equipotential Line Pattern for a Steady, Two-Dimensional Flow 61

4-2 Flow Field and Co-ordinate System for Dispersion in Radial Flow from a Line Source 66

4-3 Comparisons of Numerical and Approximate Solutions for the Concentration Distribution in Radial Flow 73

4-4 Comparison of Numerical and Approximate Solutions for the Concentration Distribution in Radial Flow 74

4-5 Streamline and Equipotential Line Pattern for Flow between a Line Source and a Line Sink 80

4-6 Concentration Distribution at Pumping Well With and Without Dispersion Along Streamlines 88

4-7 Comparison of Numerical and Approximate Solutions for the Concentration Distribution along $\psi = 0$ at $\phi = 0$ and $\phi = \infty$ 99

4-8 General Layout of Well Recharge Apparatus 107

4-9 Schematic Section of Well Recharging Model 108

4-10 Conctruction and Operation Details of the Wells and Conductivity Probes 109

4-11 Plot of Relative Concentration, c/c_0, versus Time, t_*, for Three Radii in Radial Dispersion Test 3 119

4-12 Plot of c/c_0 versus $1-\xi$ for Radial Dispersion Test 3 120

4-13 Concentration Distribution on Line of Symmetry between the Wells for Run I 129

4-14 Concentration Distribution at the Pumping Well for Run I 130

4-15 Differential Piezometric Head Distribution for Run I 131

Figure No. Page

4-16 Concentration Distributions on Line of Symmetry between the Wells for Run II 132

4-17 Concentration Distribution at the Pumping Well for Run II 133

4-18 Differential Piezometric Head Distribution for Run II 134

4-19 Concentration Distributions on Line of Symmetry between the Wells for Run III 135

4-20 Concentration Distribution at the Pumping Well for Run III 136

4-21 Differential Piezometric Head Distribution for Run III 137

4-22 Distortion of Flow Pattern due to Probe Misalignment with Flow 142

Table No.

3-1 Summary of Longitudinal Dispersion Tests 48

3-2 Summary of Lateral Dispersion Tests 56

4-1 Summary of Radial Dispersion Tests 121

I. INTRODUCTION

The rapid growth of population, the expansion of industrial uses, and the increasing agricultural production will continue to make demands for quality and quantity of water exceeding the naturally available surface water and groundwater supplies. Coupled with the need for additional water is the requirement for disposal of used waters and waste materials. In the past, the solution to these problems often was to take and use as much water as one needed so long as the supply lasted and to dispose of the wastes in any manner possible. For groundwater supplies, the fruits of such practices have resulted in drastic declines of natural ground water levels, increased water costs due to increased pumping lifts, contamination of coastal groundwater basins with intruding salt water, and the contamination of aquifers by improper waste disposal. These conditions have led to the development of techniques for the replenishment of groundwater basins by artificial recharge and the development and implementation of management policies for the use and disposal of water based both upon an understanding of hydrologic phenomena and upon equitable legal doctrines.

Records of artificial recharging activities indicate that spreading basins were used in Europe in the early 1800's and in the western United States in the late 1800's. In more recent years, recharge of water by wells has also been used both to halt salt water intrusion and to replenish overdrawn basins. In addition, as natural fresh water supplies are being exhausted, artificial recharge is currently being accomplished by the reuse after treatment of sewage and industrial waste waters. The method of waste disposal by cesspools and septic tanks, which has been used for several centuries, discharges waste products directly into the ground, generally in the region above the groundwater table. On the other hand, chemical wastes, oil-field brines, and more recently radioactive wastes are being stored and disposed of by well injection into regions far below the groundwater table. The methods used for recharge and disposal in groundwater basins depend upon the local hydrology and geology of the area, the physical, chemical, and biological characteristics of the water and the cost of the project; however, this study will be confined to certain aspects of the method of well recharge and disposal.

The successful operation of a recharge or disposal well requires a knowledge of how the recharged water or wastes will be distributed throughout a groundwater basin and what effects there will be on the quality of the natural groundwater. The resulting water quality is a complex problem requiring an understanding of the effects of adsorption, decay, aeration, and dilution on the chemical, biological, and radiological constituents in the water as it moves through the soil. The movements and distribution of waters within a groundwater basin are studied using tracers and observation wells. The interpretation of such studies, however, requires a knowledge of the mechanics of miscible fluid displacement since tracers, recharged waters, and wastes are miscible with the natural groundwater.

In the last ten to fifteen years, a great deal of work has been directed toward an understanding of miscible displacement in porous media. Studies have shown that the mixing of fluids during displacement is dependent upon the magnitude and distribution of flow velocities within the media and upon the geometry of the porous structure. This mixing, which is greater than can be accounted for by molecular diffusion, is called dispersion, since it is caused by the flow through the porous medium. In well recharging or disposal operations, dispersion (or mixing) between the recharged (or disposed) water and the natural groundwater causes the boundary between the two fluids to be a gradual transition from the native to the recharged (or disposed) water. The extent of this dispersed region, which depends upon the local velocity and soil characteristics, can be predicted from the mass conservation requirement of the recharged water; however, before introducing the theoretical and experimental results of this study, a general review of earlier investigations, related to the study of well recharge and dispersion in porous media, will be made.

II. LITERATURE REVIEW AND OBJECTIVES

2.1 Review of Previous Work

Todd [114] has summarized in an anotated bibliography all of the artificial recharge activities in this country and abroad through 1954. This summary deals primarily with the various techniques of recharging which have been used and the problems encountered in their use. The chief problem in well recharging was the reduction in the rate of recharge due to clogging of the well screen and surrounding media by biological growths, chemical deposits, air binding, and the collection of fine materials. Various solutions to the problem of well clogging, which are based upon chemical additives, deaeration, and well redevelopment, were proposed.

In 1955, the Sanitary Engineering Research Laboratory [111] reported some experimental results on well recharge of a confined aquifer using both fresh and treated waste water. Similar recharging rates of the fresh water and the sewage plant effluent were maintained for a period of about 7 days. Then the well required redevelopment to remove the organic solids which had partially clogged the well. Bacteria in the waste water were adsorbed by the media within 100 feet of the well, independent of recharge rate or period of recharging. Chemical constituents in the water were not attenuated but were transported with the recharged water.

In 1957, Lau, Kaufman, and Todd [63] presented the results of the first investigation of dispersion in radial flow. They developed the conservation of mass equation; however, an error was introduced in the derivation, for the dispersion coefficient was assumed to be constant. Field tests, carried out in a thin, confined aquifer using three different tracers, indicated that chloride ion was the best tracer. However, the differences in shape and arrival time of the tracer distributions, recorded at several observation wells around the recharge well, indicated that the flow from the recharge well was not radial.

Ogata [77] in 1958 obtained an analytical solution for the radial flow-dispersion equation in integral form. As the integral could not be evaluated analytically, a numerical solution to the radial flow-dispersion equation was carried out; however, an error was made in the formulation of the finite difference scheme. Further discussion of this work will be given in section 4.1.2. In a second report in 1959, Lau, Kaufman, and Todd [65] presented the correct conservation of mass equation for radial flow through a confined sand bed. No solution of the radial dispersion equation was obtained; however, an approximate expression for the standard deviation of the tracer distribution was developed. Using this result, dispersion coefficients were evaluated from the model tests.

In the 1959 and 1961 biennial conferences on ground water recharge, Schiff [104] and [105], the results of field tests and experiences for a number of well recharge projects were discussed. Laboratory studies on well filter material, well flow in nonhomogeneous media, and longitudinal and radial flow dispersion were also discussed. In 1959, Richter and Chun [87] and Todd [115] summarized the methods and practices of various recharging and disposal activities in California and throughout the world. Extensive bibliographies on these subjects are included. In the 1959 conference on "Ground Disposal of Radioactive Wastes" [56], the influences of dispersion and adsorption on radioactive waste disposal were discussed as well as some field experiences with radioactive waste disposal at Hanford and other nuclear reactor sites. Incidents of contamination by sewage and chemical wastes and laboratory studies of the adsorption and travel of these pollutants through various types of soil are given in the "Symposium on Ground Water Contamination" [41].

Raimondi, Gardner, and Petrick [85] in 1959 gave a solution to the radial flow-dispersion equation with a modified dispersion term. This approach is based upon the assumption that dispersion in comparison with convection has a negligible influence on the concentration distribution away from the recharge well; a more detailed discussion is given in section 4.1.2. Cole, Cowan, and Jackson [26] present the results of some radial displacement tests in consolidated cores of porous media to determine optimum oil recovery for various amounts of a pentane slug injection.

In 1962, Banks, Jersate, and Owston [4] conducted experimental studies of dispersion in a diverging flow through a trapezoidal section; however, no analysis of the results was made due to errors in the measurement of the tracer distribution. Harpaz and Bear [49], 1963, present some of the results of laboratory and field tests on underground storage operations with a single recharging well and with two wells, one recharging and one pumping. An analytical solution, assuming immiscible displacement, is given for the two well flow case; however, no solution is given for either case including dispersion. Estimates of the longitudinal dispersion coefficient were made using the results of Lau's work [65].

A review of the literature on the head, velocity, streamline and potential line patterns produced by single and multiple well systems has not been made; however, this work is available in many standard books on ground water flows [34], [44], [50], [54], [73], [83], [115].

Studies on longitudinal and lateral dispersion in flow through porous media date from Kitagawa's work [58] in 1934; however, in the last ten to fifteen years, numerous investigators have presented theoretical models and experimental measurements of this phenomenon. The theoretical descriptions of dispersion have employed either a statistical analysis of the fluid particle motion through a porous media or a mass conservation requirement on a tracer travelling with the fluid.

Danckwerts [30], in 1953, used a statistical model which replaced the porous medium by a series of mixing cells. By specifying both the distribution of residence times of the fluid particles within the cells and the type of input to the cells, he predicted the shape and characteristics of the curve representing the effluent from the cells or idealized media. Beran [12] in 1955 studied longitudinal dispersion with a statistical model in which the distribution of probable positions of a fluid particle introduced at one point was assumed to be Gaussian. From this model, he obtained an expression for the tracer distribution in which the influence of molecular diffusion is shown to be additive to the spreading caused by longitudinal dispersion.

Rifai *et al* [89], in 1956, considered two models of longitudinal dispersion in uniform flow. The first assumed the porous medium to be comprised of a series of parallel capillary tubes of different diameters in which the distribution of a tracer was the same as derived by Taylor [112] for a single capillary tube but weighted by the distribution of diameters. In the second approach, a completely disordered medium, in which the future time and position of a fluid particle was described by a Galton probability distribution, was assumed. The distribution of a tracer introduced at one point was obtained, and for large distances and times, this distribution reduced to the normal or Gaussian form. Experimental measurements of tracer dispersion for two sands confirmed the theoretical predictions and indicated that the dispersion coefficient in laminar flow varied linearly with the velocity.

DeJong [32] in 1958 developed a statistical model for one dimensional flow which included the influence of both longitudinal and lateral dispersion in the distribution of a tracer, introduced at a point in the flow. The dispersion coefficients were shown to vary linearly with the velocity, pore size, and the distance from the point of tracer introduction. Scheidegger [102] in 1960 has summarized the results of his earlier work in 1954 [94], 1958, [96], and 1959 [99]. In these works, he obtains tracer distributions using a random walk analysis with and without autocorrelation. From two other models, he shows that the dispersion coefficient may vary either with the velocity or the velocity squared, if molecular diffusion is important.

Saffman [92] in 1959 and [93] in 1960 employed a random residence time model and obtained dispersion coefficients which varied linearly with the velocity. Simpson [108] in 1962 developed a statistical model for lateral dispersion in which the probability for lateral movement from one streamline to another was related to molecular diffusion. Experimental measurements of the lateral spread of a line source in a consolidated sandstone are reported.

Klinkenberg *et al* [59] in 1953 stated that longitudinal dispersion was the combined result of variations in pore size and structure, velocity variations within a pore, and turbulence (at high Reynolds numbers); whereas, lateral dispersion was primarily the result of intertwining of streamlines and molecular diffusion. They also presented solutions to the steady-state, convective-dispersion equation for a point source tracer introduction in one-dimensional flow. Kramers and Alberda [61] solved the convective-dispersion equation, including only longitudinal dispersion, for a sinusoidally varying input tracer concentration superimposed on a steady flow of fresh water. The damping and phase shift of the concentration wave were related to the longitudinal dispersion coefficient.

Ebach and White [37] in 1958 used both the sinusoidally varying and the pulse input concentration to measure longitudinal dispersion coefficients for a wide range of particle sizes, shapes, and Reynolds numbers. Blackwell [20] in 1959 reported on measurements of longitudinal and lateral dispersion for several sands over the Reynolds number range 0.002-4. At the smallest Reynolds numbers, the dispersion coefficients were approximately equal to the molecular diffusion coefficient, and near a Reynolds number of 1, the lateral dispersion coefficient was about 1/24 the longitudinal dispersion coefficient.

Bear [10] in 1960 solved the one-dimensional, convective-dispersion equation for steady and unsteady flow. In addition, the variance of the concentration distribution, resulting from a point source, is shown to be a second order tensor and equal to the product of twice the coefficient of dispersivity, a fourth rank tensor, and the displacement of the point source, a second rank tensor. Scheidegger [103], in 1961, assumed that the dispersion coefficient in any direction was equal to the product of the coefficient of dispersivity (a constant dependent upon the media structure) and the velocity components, parallel and perpendicular to that direction. Using this assumption, he found that the coefficient of dispersivity was a fourth rank tensor with 81 components which reduced to 21 for an isotropic media.

Ogata and Banks [78] in 1961, give the solution to the one-dimensional, convective dispersion equation for a step function imput of tracer. Ogata [79] in 1961, and [80] in 1964, presents the general integral solution, including longitudinal and lateral dispersion, for the concentration distribution resulting from a step function tracer introduction over a finite area. Bischoff and Levenspiel [18] and [19] in 1962 , obtained general solutions to the convective dispersion equation in one-dimensional flow through a column which account for the influences of a finite length of media, measurement of the tracer distribution below the media,and the introduction of the tracer above the media and over a finite area. In addition, the effect of radial variations in velocity and dispersion coefficients on the tracer measurements are predicted.

Harleman and Rumer [45] 1962, and [46] 1962, and [48] 1963 derived the convective-dispersion equation and showed that the dispersion coefficients at a point are related to the spatial variations of velocity and tracer concentration in a small volume about that point. The general dispersion tensor is obtained in a form similar to Scheidegger [103]; however, the dispersion coefficient in any direction may vary with the velocity to a power different from one. An experimental study of longitudinal dispersion in steady and unsteady flow and of lateral dispersion in steady flow was carried out for uniform and non-uniform media.

Bachmat and Bear [3], 1964, presented the convective-dispersion equation, assuming a linear relationship between the velocity and dispersion coefficient, in a general tensorial form which is applicable to uniform and non-uniform flows in any co-ordinate system.

2.2 Objectives of this Investigation

This study will attempt to define a method for the prediction of tracer distributions which result from the recharge of confined aquifers by wells. To develop these predictions, the basic features of miscible fluid displacement in homogeneous, isotropic media will be used.

In the first part of this investigation, longitudinal and lateral dispersion in uniform, laminar flow will be studied, and, since the flow within a few feet of a well may not be laminar, the existing knowledge of longitudinal and lateral dispersion in laminar flow will be extended into the laminar non-linear flow range [106] (i.e. to $\mathbb{R} = 100$). These results will be used in the prediction of tracer distributions resulting from the recharge of a single well and from the recharge and pumping of a pair of wells. Finally, a comparison of the analytical and measured tracer distributions will be made in order to show the relative importance of convection, dispersion, and diffusion on the displacement process in the laboratory model and field situation.

III. LONGITUDINAL AND LATERAL DISPERSION

3.1 Theoretical Analysis

3.1.1 Convective Dispersion Equation

In a homogeneous, isotropic sand column with uniform flow parallel to its axis, the distribution of a tracer introduced at a point or over an area can be obtained by considering the conservation of this substance in a small volume (including both sand particles and fluid). Using the notation as set forth in Figure 3-1, the conservation of tracer equation becomes

$$\frac{\partial c}{\partial t} + w\frac{\partial c}{\partial z} = \left(D_1+\mathcal{D}_m\right)\frac{\partial^2 c}{\partial z^2} + \left(D_2+\mathcal{D}_m\right)\frac{1}{r}\frac{\partial}{\partial r}\left(r\frac{\partial c}{\partial r}\right) + S \qquad (1)$$

where w, D_1, and D_2 are constants throughout the column and equal to the average seepage velocity, longitudinal dispersion coefficient and lateral dispersion coefficient respectively. c is the average concentration of tracer (mass of substance/mass of solution), and ρ is the average solution density (mass of solution/volume of solution) in the small volume. D_m is the molecular diffusion coefficient, θ is the porosity, and S is the rate of gain of tracer within the volume. It has been assumed that the tracer has the same density and viscosity as the bulk fluid. Rumer [45] in deriving equation (1) has shown that the dispersion coefficients D_1 and D_2 are related to the spatial variations of velocity and tracer within the small volume.

In this study of longitudinal and lateral dispersion, the tracer substance is conservative (i.e., no gains or losses within the sand bed); hence, S is equal to 0. In addition, for the range of flows to be studied, the mass transfer due to molecular diffusion is negligible compared to that due to dispersion, and thus, molecular diffusion in equation (1) will be neglected. With these conditions, equation (1) reduces to

$$\frac{\partial c}{\partial t} + w\frac{\partial c}{\partial z} = D_1\frac{\partial^2 c}{\partial z^2} + D_2 \frac{1}{r}\frac{\partial}{\partial r}\left(r\frac{\partial c}{\partial r}\right) \qquad (2)$$

Equation (2) is called the convective-dispersion equation, for it expresses the mass transfer due to convection, w, and dispersion, D_1 and D_2. It should be noted that equation (2) also holds for unsteady, uniform flows; however, in that case, w, D_1 and D_2 would become functions of time. For a further treatment of this problem, see Bear [10] and Rumer [91]. For the study presented herein, the flow will be assumed steady.

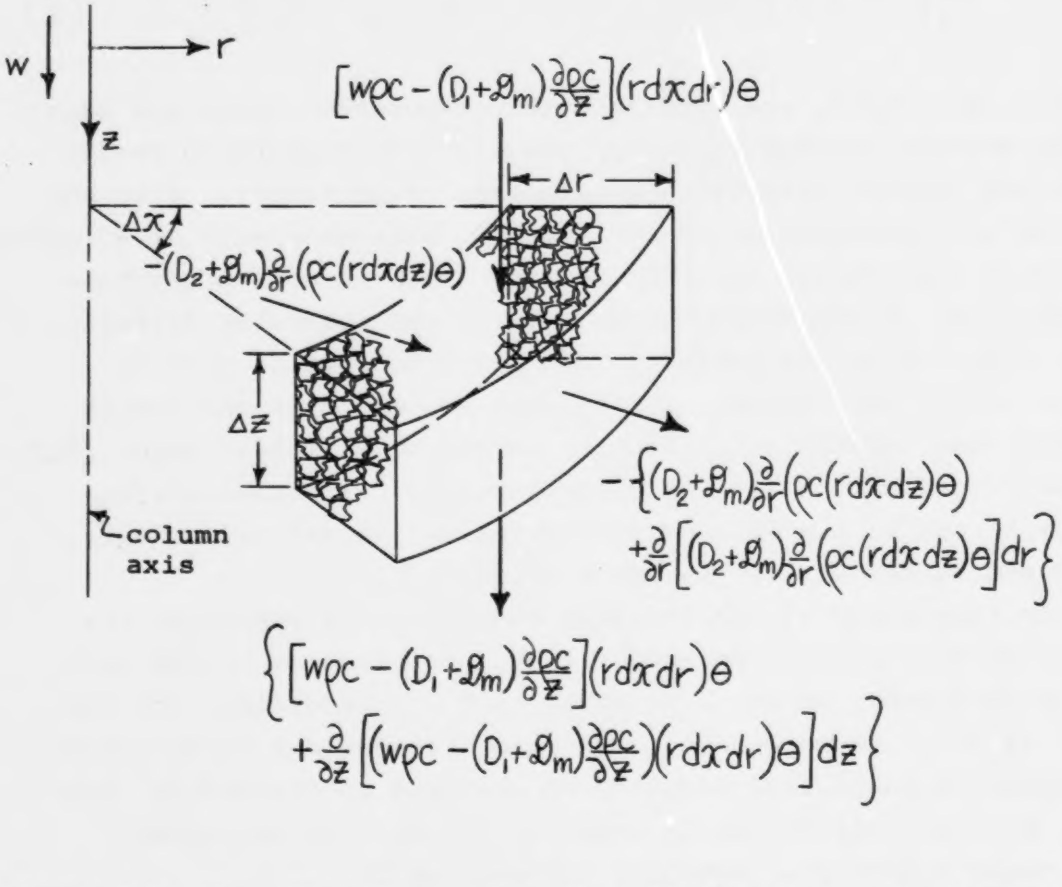

w
r
z
$\left[w\rho c - (D_1+\mathcal{D}_m)\frac{\partial \rho c}{\partial z}\right](r\,dx\,dr)\theta$
Δr
Δx
$-(D_2+\mathcal{D}_m)\frac{\partial}{\partial r}\left(\rho c(r\,dx\,dz)\theta\right)$
Δz
column axis
$-\left\{(D_2+\mathcal{D}_m)\frac{\partial}{\partial r}\left(\rho c(r\,dx\,dz)\theta\right) + \frac{\partial}{\partial r}\left[(D_2+\mathcal{D}_m)\frac{\partial}{\partial r}\left(\rho c(r\,dx\,dz)\theta\right)\right]dr\right\}$
$\left\{\left[w\rho c - (D_1+\mathcal{D}_m)\frac{\partial \rho c}{\partial z}\right](r\,dx\,dr)\theta + \frac{\partial}{\partial z}\left[\left(w\rho c - (D_1+\mathcal{D}_m)\frac{\partial \rho c}{\partial z}\right)(r\,dx\,dr)\theta\right]dz\right\}$

Figure 3-1 Mass Flux Components in a Small Volume of a Packed Sand Column

3.1.2 Longitudinal Dispersion

Consider now a flow through a sand column with the concentration of tracer maintained uniform across the column and constant in time at z = 0 (see Fig. 3-2).

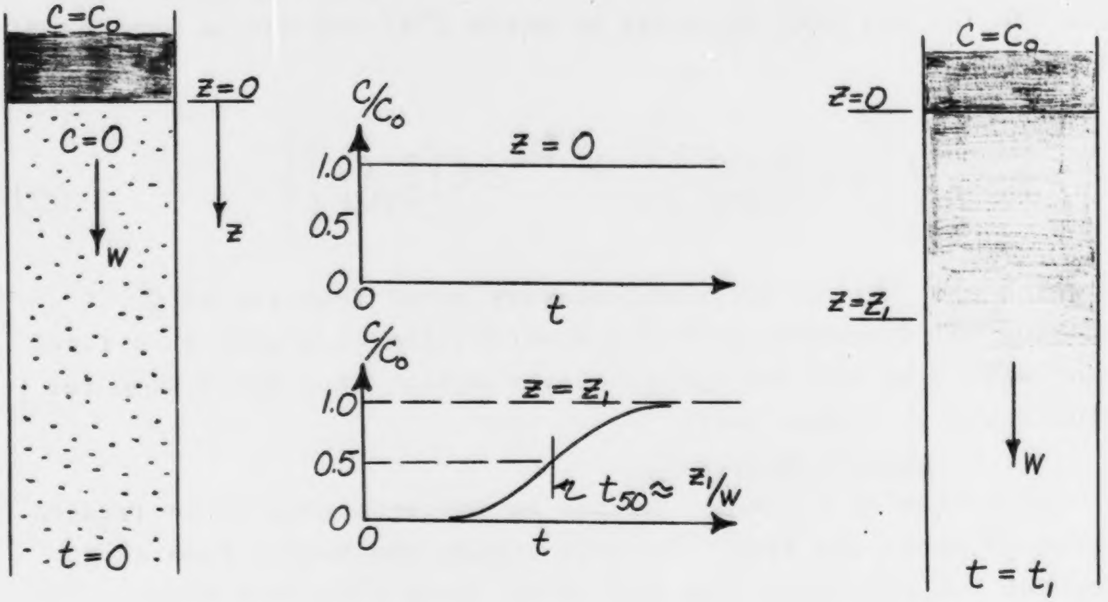

C=C₀
z=0
C=0
W
z
t=0
C/C₀
1.0
0.5
0
0
z = 0
t
C/C₀
1.0
0.5
0
0
z = z₁
t₅₀ ≈ z₁/w
t
C=C₀
z=0
z=z₁
W
t = t₁

Figure 3-2 Schematic Longitudinal Dispersion Column Setup and Typical Measurement

For this set of boundary conditions, there are no radial concentration gradients and equation (2) reduces to

$$\frac{\partial c}{\partial t} + w\frac{\partial c}{\partial z} = D_1\frac{\partial^2 c}{\partial z^2} \qquad (3)$$

with boundary and initial conditions

$$\begin{aligned} C(z=0, t>0) &= C_0 \\ C(z=\infty, t) &= 0 \\ C(z, t=0) &= 0 \end{aligned} \tag{4}$$

The solution to equation (3) with the conditions specified by equation (4) has been obtained by Ogata [78] and can be expressed as

$$\frac{C}{C_0} = \frac{1}{2}\left\{ erf_c\left[\frac{z-wt}{2\sqrt{D_1 t}}\right] + e^{wz/D_1} erf_c\left[\frac{z+wt}{2\sqrt{D_1 t}}\right] \right\}, \tag{5}$$

in which $erf_c(\phi)$ is the complementary error function of ϕ. Equation (5) describes both the distribution of tracer at a fixed point with time and the spatial distribution at a fixed time (as illustrated in Figure 3-2).

3.1.3 Lateral Dispersion

Injection of a tracer, either an instantaneous pulse (finite amount of mass, see Fig. 3-3) or a steady continuous feed at a constant concentration (see Fig. 3-4), into a uniform flow through a sand column results in both longitudinal and lateral concentration gradients. For either type of injection, equation (2) may be solved and combined with experimental measurements to determine D_2, the lateral dispersion coefficient.

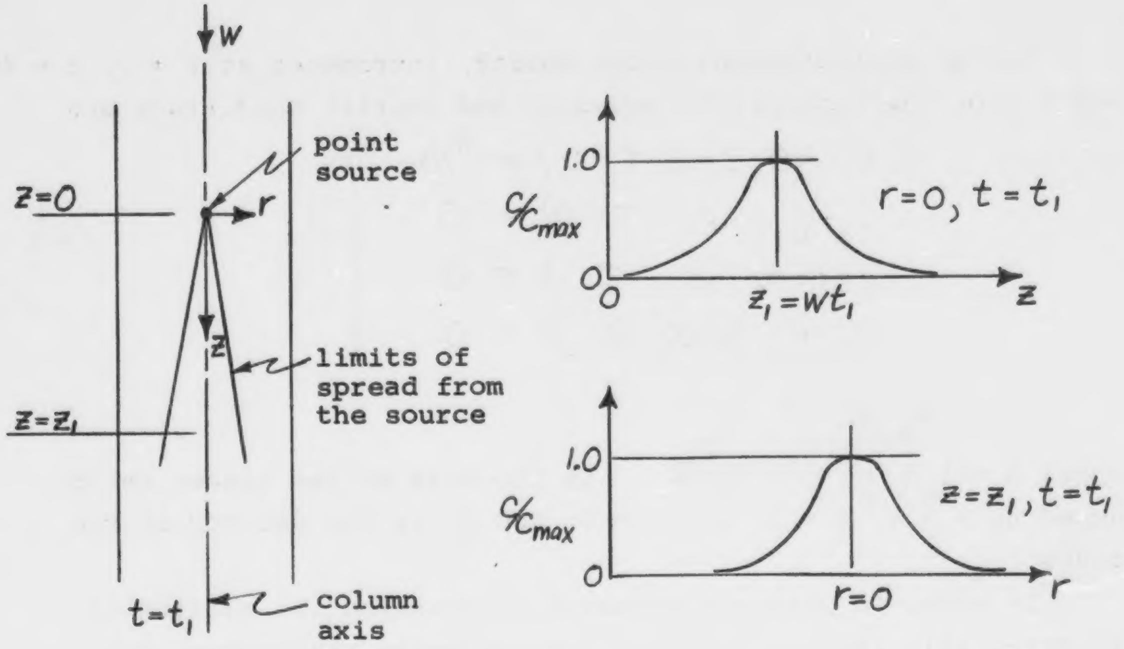
w
point source
z=0
r
z
limits of spread from the source
z=z₁
t=t₁
column axis
1.0
C/Cmax
0
0
z₁ =wt₁
z
r=0, t = t₁
1.0
C/Cmax
0
r=0
r
z=z₁, t=t₁

Figure 3-3 Schematic Column Setup and Typical Measurement for an Instantaneous Point Source Injection

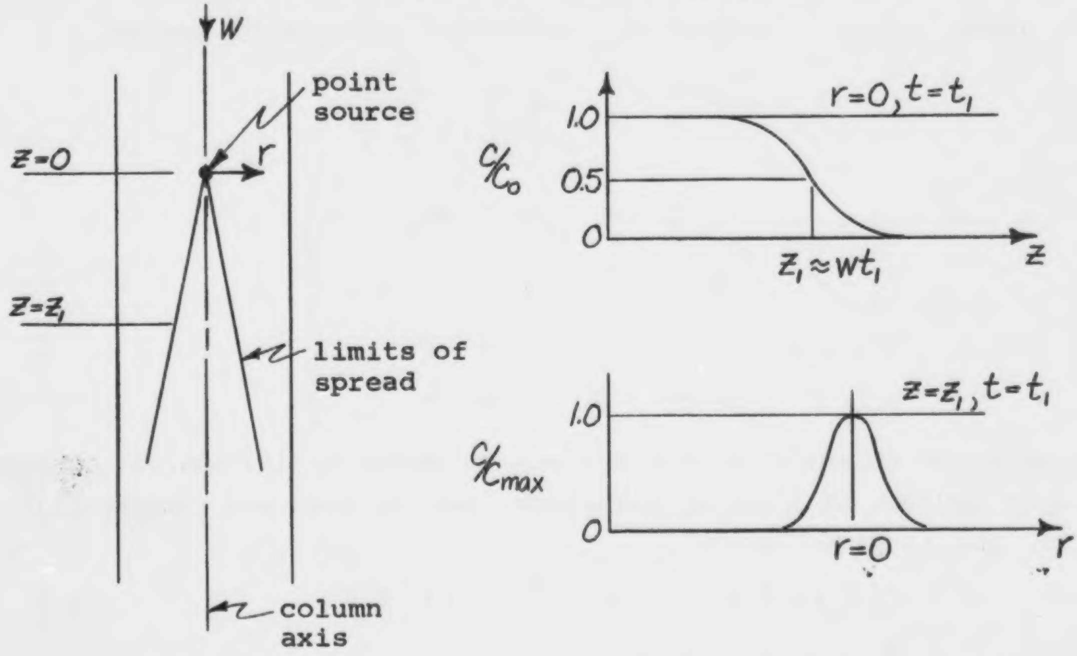
w
point source
z=0
r
z=z₁
limits of spread
column axis
1.0
0.5
0
C/Co
r=0, t=t₁
z₁≈wt₁
z
1.0
C/Cmax
0
r=0
r
z=z₁, t=t₁

Figure 3-4 Schematic Column Setup and Typical Measurement for a Continuous Point Source Injection

For an instantaneous point source, introduced at r = 0, z = 0, and t = 0, the appropriate boundary and initial conditions are

$$\left.\begin{aligned} c(r=0, z=0, t=0) &= M/\rho \\ c(r, z, t<0) &= 0 \\ c(r=\infty, z, t) &= 0 \\ c(r, z=\infty, t) &= 0 \end{aligned}\right\} \tag{6}$$

where $M = \int_{-\infty}^{\infty}\left(\int_{0}^{\infty}\rho c 2\pi r dr\right)dz$ is the mass of the tracer introduced at r = 0, z = 0, and t = 0; and ρ is the density of the tracer.

In order to obtain a solution to equation (2) subject to equation (6), let us introduce the following transformations:

$$\begin{aligned} \xi &= t \\ \mu &= z - wt \end{aligned} \tag{7}$$

With these change of variables, equations (2) and (6) become

$$\frac{\partial c}{\partial \xi} = D_1 \frac{\partial^2 c}{\partial \mu^2} + \frac{D_2}{r}\frac{\partial}{\partial r}\left(r\frac{\partial c}{\partial r}\right) \tag{8}$$

and

$$\left.\begin{aligned} c(r=0, \mu=0, \xi=0) &= M/\rho \\ c(r, \mu, \xi<0) &= 0 \\ c(r=\infty, \mu, \xi) &= 0 \\ c(r, \mu=\infty, \xi) &= 0 \end{aligned}\right\} \tag{9}$$

The solution to equation (8) subject to equation (9) can be expressed as a product of simpler solutions, see Carslaw and Jaegar [25] p. 33, and is given by

$$c(r,\mu,\xi) = c_1(\mu,\xi)c_2(r,\xi) \tag{10}$$

where $c_1(\mu, \xi)$ is a solution of

$$\frac{\partial c_1}{\partial \xi} = D_1\frac{\partial^2 c_1}{\partial \mu^2} \tag{11}$$

and $c_2(r, \xi)$ is a solution of

$$\frac{\partial c_2}{\partial \xi} = \frac{D_2}{r}\frac{\partial}{\partial r}\left(r\frac{\partial c}{\partial r}\right) . \qquad (12)$$

Solutions to equations (11) and (12) satisfying the requirement of an instantaneous point source at $\mu = r = \xi = 0$ are given by

$$c_1(\mu, \xi) = \frac{M_1/\rho}{2\sqrt{\pi D_1 \xi}}\, e^{-\mu^2/4D_1\xi} \qquad (13)$$

and

$$c_2(r, \xi) = \frac{M_2/\rho}{4\pi D_2 \xi}\, e^{-r^2/4D_2\xi} . \qquad (14)$$

Using equations (13) and (14) in equation (10) gives

$$c(\mu, r, \xi) = \frac{M/\rho}{8(\pi\xi)^{3/2} D_1^{1/2} D_2}\, e^{-\left[\mu^2/4D_1\xi + r^2/4D_2\xi\right]} \qquad (15)$$

as the solution to equation (8) with $M = M_1M_2$. Introducing the transformations, equation (7), into equation (15) gives

$$c = \frac{M/\rho}{8(\pi t)^{3/2} D_1^{1/2} D_2}\, e^{-\left[(z-wt)^2/4D_1t + r^2/4D_2t\right]} . \qquad (16)$$

Equation (16) is the solution to equation (2) for the case of an instantaneous injection of an amount of mass M at $r = z = 0$ at time $t = 0$.

Suppose that instead of an instantaneous injection of a finite amount of mass, mass is introduced at a constant rate, Q, at $z = 0$, $r = 0$ from time $t = 0$ to time $t = t$. Thus, in a time $\Delta\tau$ an amount of mass

$$\Delta M = \rho c_0 Q \Delta\tau \qquad (17)$$

will be introduced, where c_0 is the concentration of the injected fluid. The change in concentration, Δc, at a point r and z due to an increment of mass, ΔM , introduced at time τ is

$$\Delta C = \frac{\Delta M/\rho}{(4\pi(t-\tau))^{3/2} D_1^{1/2} D_2} e^{-\left[r^2 + D_2/D_1 (z - w(t-\tau))^2\right]/4D_2(t-\tau)} \quad . \qquad (18)$$

The concentration of tracer at a point r and z at time t due to a continuous injection at the constant rate, Q, can be found by integrating equation (18). Combining equations (17) and (18), the concentration of tracer is

$$C = \frac{C_0 Q}{(4\pi) D_1^{1/2} D_2} \int_0^t \left[e^{-\left[r^2 + D_2/D_1 (z - w(t-\tau))^2\right]/4D_2(t-\tau)} \right] \frac{d\tau}{(t-\tau)^{3/2}} \quad . \qquad (19)$$

Letting $\eta = \sqrt{r^2 + \frac{D_2}{D_1} z^2}$, equation (19) becomes

$$C = \frac{C_0 Q e^{wz/2D_1}}{(4\pi)^{3/2} D^{1/2} D_2} \int_0^t \left[e^{-\left[\eta^2/4D_2(t-\tau) + \left(w^2/4D_1\right)(t-\tau)\right]} \right] \frac{d\tau}{(t-\tau)^{3/2}} \quad . \qquad (20)$$

Now, letting $\theta = \eta/\sqrt{4D_2(t-\tau)}$, equation (20) becomes

$$C = \frac{C_0 Q e^{wz/2D_1}}{2(\pi)^{3/2}(D_1 D_2)^{1/2}\eta} \int_{\eta/\sqrt{4D_2 t}}^{\infty} e^{-\left[\theta^2 + \left(\frac{w^2\eta^2}{16 D_1 D_2}\right)\frac{1}{\theta^2}\right]} d\theta \quad . \qquad (21)$$

Equation (21) can be rearranged to give

$$C = \frac{C_0 Q e^{wz/2D_1}}{2\pi^{3/2}(D_1D_2)^{1/2}\eta} \left\{ \frac{e^{w\eta/2\sqrt{D_1D_2}}}{2} \int_{\eta/\sqrt{4D_2t}}^{\infty} \left(1 - \left[\frac{w\eta}{4\sqrt{D_1D_2}}\right]\frac{1}{\theta^2}\right) e^{-\left[\theta + \left(\frac{w\eta}{4\sqrt{D_1D_2}}\right)\frac{1}{\theta}\right]^2} d\theta \right.$$

$$\left. + \frac{e^{-w\eta/2\sqrt{D_1D_2}}}{2} \int_{\eta/\sqrt{4D_2t}}^{\infty} \left(1 + \left[\frac{w\eta}{4\sqrt{D_1D_2}}\right]\frac{1}{\theta^2}\right) e^{-\left[\theta - \left(\frac{w\eta}{4\sqrt{D_1D_2}}\right)\frac{1}{\theta}\right]^2} d\theta \right\} . \qquad (22)$$

Letting

$$\gamma = \theta + \left(\frac{w\eta}{4\sqrt{D_1D_2}}\right)\frac{1}{\theta}$$
$$\xi = \theta - \left(\frac{w\eta}{4\sqrt{D_1D_2}}\right)\frac{1}{\theta} \qquad (23)$$

equation (22) becomes

$$C = \frac{C_0 Q e^{wz/2D_1}}{2\pi^{3/2}(D_1D_2)^{1/2}\eta} \left\{ \frac{e^{w\eta/2\sqrt{D_1D_2}}}{2} \int_{\left(\frac{\eta}{\sqrt{4D_2t}} + \frac{wt}{\sqrt{4D_1t}}\right)}^{\infty} e^{-\gamma^2} d\gamma + \frac{e^{-w\eta/2\sqrt{D_1D_2}}}{2} \int_{\left(\frac{\eta}{\sqrt{4D_2t}} - \frac{wt}{\sqrt{4D_1t}}\right)}^{\infty} e^{-\xi^2} d\xi \right\} . \qquad (24)$$

Using the definition of the complementary error function, equation (24) becomes

$$C = \frac{C_0 Q e^{\left[wz/2D_1 - w\eta/2\sqrt{D_1D_2}\right]}}{8\pi(D_1D_2)^{1/2}\eta} \left\{ erf_c\left[\frac{\eta}{\sqrt{4D_2t}} - \frac{wt}{\sqrt{4D_1t}}\right] + e^{w\eta/\sqrt{D_1D_2}}\, erf_c\left[\frac{\eta}{\sqrt{4D_2t}} + \frac{wt}{\sqrt{4D_1t}}\right] \right\} \qquad (25)$$

in which $\eta = -\sqrt{r^2 + (D_2/D_1)z^2}$.

Equation (25) is the solution to equation (2) for the case of a continuous injection of mass at a constant rate, Q, from time t = 0 to time t = t. If mass is supplied at this constant rate for a long period of time, a steady-state distribution will be reached. This distribution can be found by letting $t \rightarrow \infty$ in equation (25). Thus, under steady-state conditions, equation (25) becomes

$$c = \frac{c_0 Q}{4\pi D_2 \eta} e^{\left[wz/2D_1 - w\eta/2\sqrt{D_1 D_2}\right]} \quad . \qquad (26)$$

Equation (26) has also been obtained by Klinkenberg _et_ _al_, [59]. Equation (26) satisfies equation (2) with $\partial c/\partial t$ = 0 (since steady state has been reached). Thus, equation (26) is the solution of

$$w\frac{\partial c}{\partial z} = D_1 \frac{\partial^2 c}{\partial z^2} + \frac{D_2}{r}\frac{\partial}{\partial r}\left(r\frac{\partial c}{\partial r}\right) \quad . \qquad (27)$$

Equations (16), (25), or (26) describe the instantaneous, continuous, and steady-state distributions of tracer concentration arising from a point source under the combined influences of convection and longitudinal and lateral dispersion.

Though concentration gradients exist both longitudinally and laterally, the longitudinal concentration gradients are usually small, and hence, the flux of mass due to longitudinal dispersion is small compared to the flux of mass due to lateral dispersion. For a steady-state distribution of tracer, the net flux of mass due to longitudinal and lateral dispersion can be calculated from equation (26). The net flux of mass due to longitudinal dispersion is $D_1 \partial^2 c/\partial z^2$. Evaluating the second derivative from equation (26) gives

$$D_1\frac{\partial^2 c}{\partial z^2} = \frac{C_0 Q}{4\pi}\frac{D_1}{D_2}\, e^{\left[\frac{Wz}{2D_1} - \frac{W\eta}{2\sqrt{D_1 D_2}}\right]}\left\{-\frac{1}{\eta^3}\left(\frac{D_2}{D_1}\right) + \frac{1}{\eta}\left[\frac{W}{2D_1} - \frac{W}{2\sqrt{D_1 D_2}}\left(\frac{D_2}{D_1}\frac{z}{\eta}\right)\right]^2\right.$$

$$+ 3\left(\frac{D_2}{D_1}\right)^2\frac{z^2}{\eta^5} - \left(\frac{W}{2D_1}\right)\left(\frac{D_2}{D_1}\right)\frac{z}{\eta^3} - \frac{W}{2\sqrt{D_1 D_2}}\left(\frac{D_2}{D_1}\right)\frac{1}{\eta^2} + \frac{W}{\sqrt{D_1 D_2}}\left(\frac{D_2}{D_1}\right)^2\frac{z^2}{\eta^4}$$

$$\left. - \left(\frac{D_2}{D_1}\right)\frac{z}{\eta^3}\left[\frac{W}{2D_1} - \frac{W}{2\sqrt{D_1 D_2}}\left(\frac{D_2}{D_1}\frac{z}{\eta}\right)\right]\right\} \quad . \qquad (28)$$

Similarly, the net flux of mass due to lateral dispersion is $D_2/r\,\partial/\partial r\,(r\,\partial c/\partial r)$. Evaluating the derivatives from equation (26) gives

$$\frac{D_2}{r}\frac{\partial}{\partial r}\left(r\frac{\partial c}{\partial r}\right) = \frac{C_0 Q}{4\pi}\, e^{\left[\frac{Wz}{2D_1} - \frac{W\eta}{2\sqrt{D_1 D_2}}\right]}\left\{-\frac{2}{\eta^3} + \frac{3r^2}{\eta^5} - \frac{W}{2\sqrt{D_1 D_2}}\frac{2}{\eta^2} + \frac{W}{\sqrt{D_1 D_2}}\frac{r^2}{\eta^4}\right\}. \qquad (29)$$

In order to compare the magnitudes of these two fluxes of mass, let us consider their variation with z for r = 0. Substituting r = 0 into equations (28) and (29), and noting that $\eta = \sqrt{D_2/D_1}\, z$, leads to

$$D_1\frac{\partial^2 c}{\partial z^2} = \frac{C_0 Q}{4\pi}\left(\frac{D_1}{D_2}\right)^{3/2}\left(\frac{2}{z^3}\right) \qquad (30)$$

for the net mass flux due to longitudinal dispersion and

$$\frac{D_2}{r}\frac{\partial}{\partial r}\left(r\frac{\partial c}{\partial r}\right) = -\frac{C_0 Q}{4\pi}\left(\frac{D_1}{D_2}\right)^{3/2}\left(\frac{2}{z^3}\right)\left[1+ {}^{wz}/_{2D_1}\right] \qquad (31)$$

for the net mass flux due to lateral dispersion. The positive sign in equation (30) and the negative sign in equation (31) can be explained by referring to Figure 3-5.

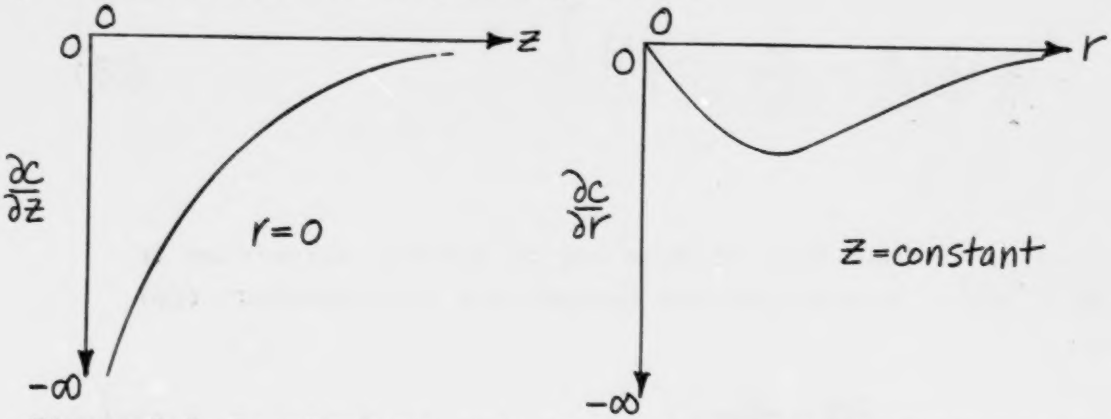

Figure 3-5 Longitudinal and Lateral Concentration Gradients for a Continuous Point Source Injection

From Figure 3-5, it is evident that since $\partial c/\partial z$ increases as z increases, that $\partial^2 c/\partial z^2$ will be positive. Also, $\partial c/\partial r$ is equal to 0 at r = 0, and $\partial c/\partial r$ decreases as r increases; therefore, $1/r\,\partial/\partial r(r\,\partial c/\partial r)$ will be negative. However, even though $1/r\,\partial/\partial r(r\,\partial c/\partial r)$ is negative, there will be a positive flux of mass laterally (radially) due to lateral dispersion.

Disregarding the negative sign, the ratio of the net lateral to longitudinal flux of mass due to dispersion at r = 0 becomes

$$\frac{\frac{D_2}{r}\frac{\partial}{\partial r}\left(r\frac{\partial c}{\partial r}\right)}{D_1\,\partial^2 c/\partial z^2} = 1 + {}^{wz}/_{2D_1} \quad . \qquad (32)$$

The ratio of the lateral to the longitudinal dispersion mass transfer at any other r and z will be of the same order of magnitude as at r = 0. Thus, when ${}^{wz}/_{2D_1}$, is a large number, (i.e., for points far away from the point of injection) the flux of mass due to longitudinal dispersion will be very much smaller than that due to longitudinal dispersion. To estimate the magnitude of $wz/2D_1$, consider the experimental results of Figure 3-15. Assuming $n_1 = 1$, we have that $D_1/\nu \approx \mathbb{R} = wd_{50}/\nu$. Thus, $D_1 \approx wd_{50}$ and $\frac{wz}{2D_1} \approx z/2d_{50}$. Now, if $z = 100\ d_{50}$ (i.e., 100 particle diameters from the source), then $wz/2D_1 \approx 50$, and the ratio of lateral to longitudinal mass transfer is $1 + wz/2D_1 \approx 51$. Under these conditions, it would appear that the net flux of mass due to longitudinal dispersion, $D_1 \partial^2 c/\partial z^2$, in equation (27) can be neglected; however, since the elimination of $D_1 \partial^2 c/\partial z^2$ from equation (27) causes a reduction in the order of the equation with respect to z, let us consider an alternate criteria based upon the solution, equation (26), to equation (27), for which the term can be neglected.

η in equation (26) can be expressed as

$$\eta = z\sqrt{\frac{D_2}{D_1}}\sqrt{1 + (D_1/D_2)(r/z)^2} \quad . \tag{33}$$

Now, for $\left(D_1/D_2\, r^2/z^2\right)^2 <$ 1, equation (33) can be expanded in a series to give

$$\eta = \sqrt{D_2/D_1}\, z \left\{ 1 + \frac{1}{2}\left(\frac{D_1}{D_2}\frac{r^2}{z^2}\right) - \frac{1}{8}\left(\frac{D_1}{D_2}\frac{r^2}{z^2}\right) + \cdots \right\} \quad . \tag{34}$$

If $\left(D_1/D_2\, r^2/z^2\right)^2 << 1$ and $\left(D_1/D_2\, r^2/z^2\right) < 1$. then equation (33) can be approximated by

$$\eta = \sqrt{D_2/D_1}\, z \left\{ 1 + \frac{1}{2}\left(D_1/D_2\, r^2/z^2\right) \right\} \quad . \tag{35}$$

Using equation (35) and the fact that ($D_1/D_2\, r^2/z^2$) < 1 in equation (26) gives

$$c = \frac{c_0 Q}{4\pi D_2 z}\, e^{-r^2/4D_2 z/w} \quad . \qquad (36)$$

Equation (36) can be shown by direct substitution to be the solution of

$$w\frac{\partial c}{\partial z} = \frac{D_2}{r}\frac{\partial}{\partial r}\left(r\frac{\partial c}{\partial r}\right) \qquad (37)$$

in which longitudinal dispersion has no influence on the tracer distribution. Thus, for longitudinal dispersion to have no influence on the tracer distribution, and for equations (26) and (27) to reduce to (36) and (37), respectively, $\frac{D_1}{D_2}\frac{r^2}{z^2} \ll 1$.

3.2 Experimental Equipment and Procedure

3.2.1 Experimental Equipment

In order to determine the magnitude of the longitudinal and lateral dispersion coefficients and to verify the theoretical predictions of the tracer distribution, it was decided to carry out some experimental tests. For the tests, a uniform flow through a porous medium was required; in addition, a means of introducing either a continuous supply of a tracer at a point or a uniform distribution of tracer across the medium would be needed.

To achieve a uniform flow through a sand medium, it was decided to use a column for the test section. This section was

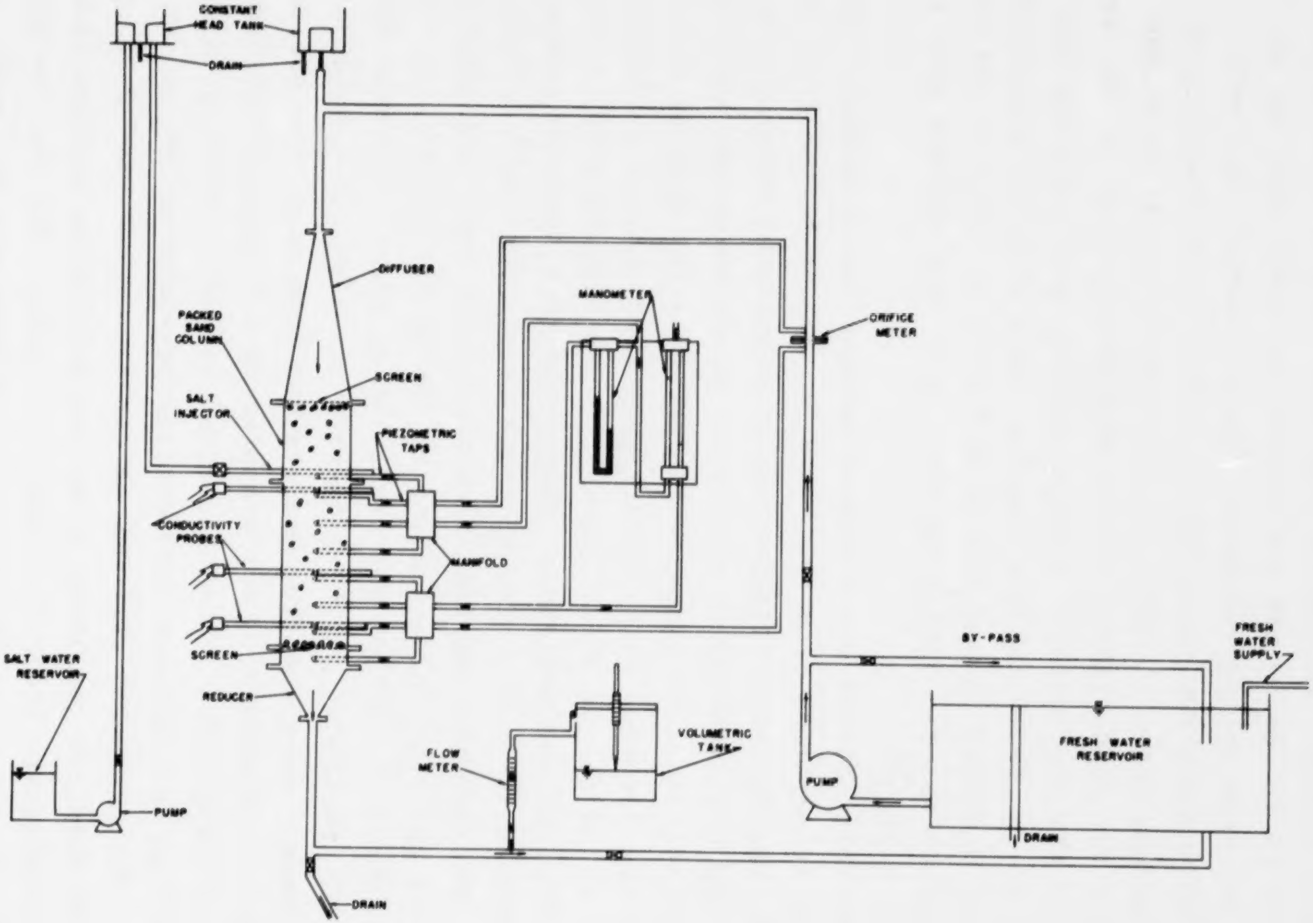
CONSTANT HEAD TANK
DRAIN
DIFFUSER
PACKED SAND COLUMN
SCREEN
SALT INJECTOR
PIEZOMETRIC TAPS
MANOMETER
ORIFICE METER
CONDUCTIVITY PROBES
MANIFOLD
SCREEN
SALT WATER RESERVOIR
REDUCER
BY-PASS
FRESH WATER SUPPLY
FLOW METER
VOLUMETRIC TANK
FRESH WATER RESERVOIR
PUMP
PUMP
DRAIN
DRAIN

FIGURE 3-6 SCHEMATIC LAYOUT FOR LONGITUDINAL AND LATERAL DISPERSION COLUMN TESTS

made from a lucite column, 4 ft. long, with an inside diameter of 8 1/4 in. and a 1/4 in. wall thickness (see Fig. 3-6). Stainless steel screens at the top and bottom of the column contained the porous medium. Piezometer taps were located on 6 in. centers beginning 14 in. below the top screen (an additional tap was located 10 in. from the top screen). The piezometer taps were connected through two manifolds to either a water-mercury or an air-water manometer on which the piezometric heads were read. Locations for conductivity probes were provided at 14, 32, and 44 in. below the top screen. A point source, salt injector was located 10 in. below the top screen. This injector consisted of a 1/4 in. diameter copper tube with a 1/32 in. hole in the center. The injector was fed from a constant head tank and the flow regulated by a valve.

The test section was situated between two diffusers. Both acted as transitions from the 8 1/4 in. column to the 2 in. pipe; however, the upstream diffuser was also designed to minimize energy losses and disturbances in the flow. Fresh water was supplied to the test section from a reservoir through 2 in. pipe by means of a 1 1/2 HP, Ingersol Rand, Centrifugal Pump, having a rating of 60 cfs. at 76 ft. of head. With this capacity of pump, a wide range of flows was available, ranging up to a Reynolds number of 1000, depending on the size of media used. For tests at small flows, the flow was supplied from a constant head tank mounted on top of the 2 in. pipe leading to the upstream diffuser. The flow in the test section was regulated by valves upstream and downstream of the column and by a by-pass valve on the discharge side of the pump. When the flow was started from rest, the period of buildup to a steady flow was measured by a Schaevitz differential pressure transducer. This transducer varied linearly with applied pressure up to a maximum differential pressure of 300 in. of water. The frequency response of the transducer was 70-80 cps.. The flow rate for the large flows was metered by orifice plates of various sizes, mounted in the 2 in. pipe. For the low flows, Reynolds numbers less than about 40, a rotameter was used.

In order to study dispersion over a wide Reynolds number range, particularly at large Reynolds numbers, two different media were used in the tests. One was a coarse New Jersey beach sand, called a No. 2 sand, with a mean size (d_{50}) of 0.167 cm., and a uniformity coefficient of 1.35 (d_{60}/d_{10}). The other, also a coarse New Jersey beach sand, called a No. 4 sand, had a mean diameter (d_{50}) of 0.345 cm., and a uniformity coefficient of 1.17 (d_{60}/d_{10}). The column was packed with sand by filling it in layers about 1 inch thick and then rodding each layer to insure a dense, uniform packing.

For the tests, a solution of approximately 0.1% NaCl was used as a tracer. A dilute solution of NaCl was used in order to minimize density and viscosity differences between the fresh water and tracer solution. In addition, at this low concentration, conductivity is nearly linear with concentration for a ten-fold change in concentration. This fact greatly simplified the data taking and analysis.

In order to detect the tracer, conductivity probes, having the same design as those used by Rumer [45] were constructed. In fact, several of the probes used in this study had been used by Rumer [45]. The probes were made from 1/4 in. phenolic resin rod with two platinum wires, acting as electrodes, wrapped around the rod (see Fig. 3-7). Several spacings of the electrode wires were tried, including 3/32, 3/16, 3/8, and 5/8 inch, in order to determine what effects the spacing of electrodes and the size of the particles had on the tracer measurements. As the electrode spacing increased, the width of the electrode wires were increased from 1/64, 3/64, 3/32, to 1/8 inch. The effect of particle size and electrode spacing is discussed in Section 3.4.1. The platinum electrodes were set into the rod so that they were flush with its surface. Grooves along the rod provided a channel to embed leads from these electrodes to an amphenol connector mounted at one end of the rod. The design of the probes made their response nearly insensitive to rotation. The probes were calibrated in place, and their response, as measured by the deflection of the pen on the Sanborn recorder, varied linearly with concentration for a ten-fold change in concentration.

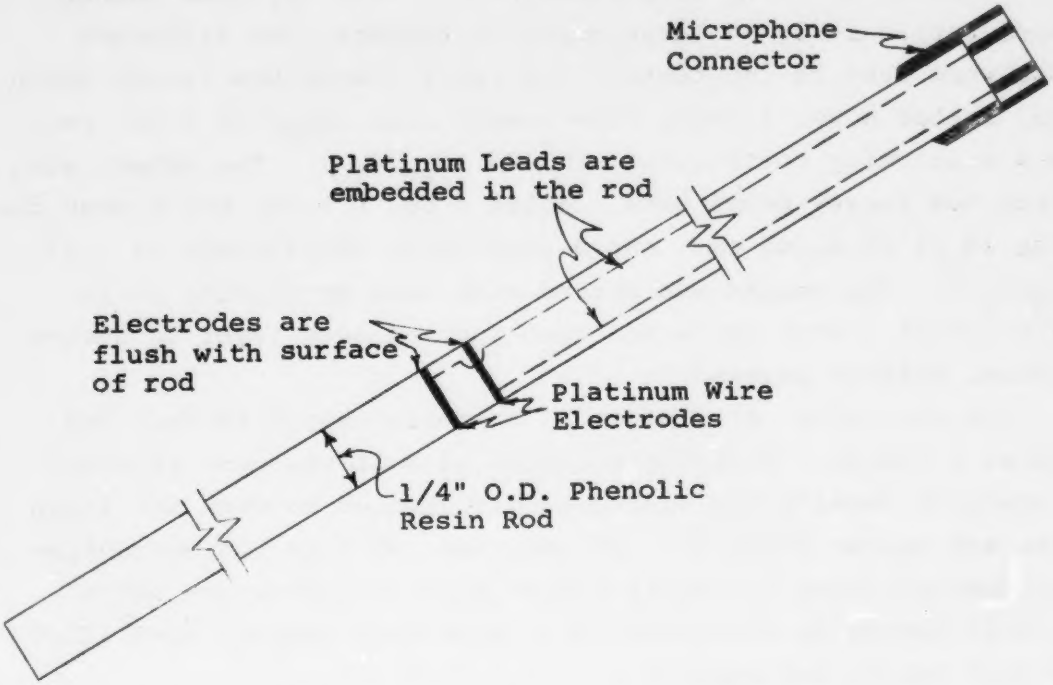
Microphone Connector
Platinum Leads are embedded in the rod
Electrodes are flush with surface of rod
Platinum Wire Electrodes
1/4" O.D. Phenolic Resin Rod

Figure 3-7 Conductivity Probe

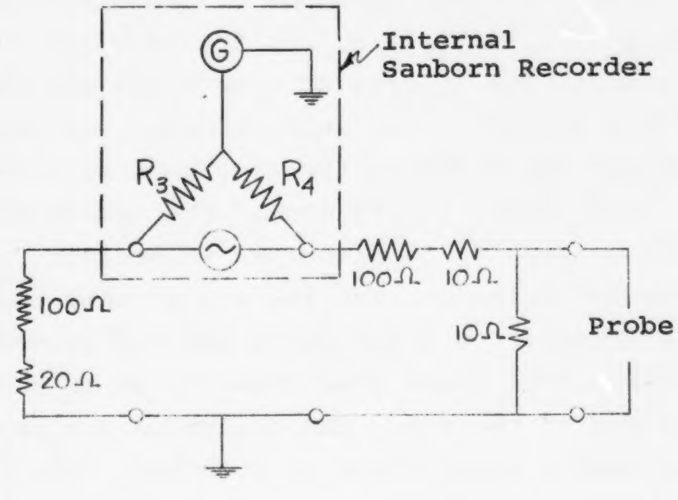
G
Internal Sanborn Recorder
R3
R4
100Ω
10Ω
100Ω
20Ω
10Ω
Probe

Figure 3-8 Wheatstone Bridge Circuit for Conductivity Probe

The conductivity probes were excited by a high frequency (2400/cps) low voltage (4.5 volts) signal from a 4-channel Sanborn Recorder, "150" Series. The exciting singal was fed to the probe through a Wheatstone Bridge. Two legs of this bridge are adjustable and internal to the Sanborn, and the other two legs are external, fixed, 120 ohm resistors. The probe, having a large resistance, compared with the 120 ohm fixed resistors, was placed parallel for greater sensitivity, with one of the fixed 120 ohm legs. The changes in concentration of the tracer solution at the probe, induce changes in resistance in the arm of the bridge with the probe. This unbalance causes a flow of current in the other bridge legs which is amplified by the Sanborn and fed to a recording pen which traces a deflection proportional to the amount of current or resistance change at the probe. The sensitivity of the Sanborn Recorder is 8 microvolts of voltage unbalance per mm. of pen stylus deflection.

3.2.2 Longitudinal Dispersion Testing Procedure

Because of difficulties in instantaneously stopping and starting the flow, particularly at the higher flow rates, it was decided to measure the time distribution of a tracer in a steady, uniform flow through the column test section. Electrical interference of conductivity probes measuring simultaneously within the column, allowed only two probes (one near the top and the other near the bottom of the column) to be used for any one test. Probes at 14 in. and 44 in. below the top screen were far enough apart to minimize or eliminate interference.

Before beginning a test, the column was thoroughly flushed with fresh water; the upstream and downstream control valves were adjusted to give the desired velocity for the test. After setting these valves, the flow of fresh water was shut off by closing a quick opening valve, actuated by hand or solenoid. Having shut off the fresh water pump, a dilute salt solution (approximately 0.1%) was slowly pumped into the column from the bottom. The fresh water was displaced upwards and flowed out of the column through the constant head tank on top of the diffuser. The salt solution was pumped into the column until a uniform concentration existed throughout the column. The mixed region of salt solution and fresh water was drained off near the top of the column until an abrupt interface between the salt solution and fresh water was formed. After establishing this condition, the quick opening valve at the bottom was closed. With the tracer solution in place, the conductivity-probes were balanced and set at the desired sensitivity. The fresh water pump was turned on, and for the low flows the constant head tank was allowed to overflow. Then, with everything in readiness, the quick opening valve was opened, and, at the same time, the timing mechanism on the Sanborn Recorder was started. A record of the initial interface position was also made so that the $z = 0$ position and $t = 0$ time would be known for the analysis. Before and after each test, the temperature of the fresh water and tracer solutions were measured. In order to eliminate temperature differences between both fluids, they were allowed to come to equilibrium with the air before the test was begun.

For the tests at the larger velocities, Reynolds numbers greater than 5-10, a time lag existed between the time of valve opening and the time of steady flow. This time lag was due to the readjustment of head in the column, from a constant head with the valve closed, to a linear head variation when the valve was opened. The time lag was measured by placing a pressure transducer across the piezometer taps in the column and recording the time for this transducer to reach a steady reading when the quick opening valve was opened. For tests at the high velocities, data could be taken only with conductivity probes placed at 32 in. or 44 in. below the top screen, since the flow was unsteady as it passed the top probe.

To determine the permeability of the packing, the piezometric head distribution and average velocity were measured for several low velocities (Reynolds numbers less than 1).

3.2.3 Lateral Dispersion Testing Procedure

These experiments were designed to measure the steady-state distribution of a tracer (salt solution) injected on the centerline of the column in a steady, uniform flow.

To begin these tests, fresh water flow was started in the column at the desired velocity. At the center of the column, 10 in. below the upper screen (see Fig. 3-6), a flow of 1% NaCl solution was introduced into the fresh water flow through a 1/32 in. diameter hole and regulated by a small needle valve. The rate of salt flow was adjusted to give a minimum of initial mixing with the fresh water. The flow was maintained steady by means of a constant head tank. A 1% salt solution was used because of the dilution as the point source was dispersed. At this initial concentration, the output signal from the probes was very good. As soon as the salt flow was begun, the buildup to a steady-state tracer distribution was measured at the column centerline for each probe. From these measurements, the seepage velocity could be determined. When a steady-state tracer distribution was established at each probe, the probes were moved across the column in small increments to measure the radial distribution of concentration at each probe location. Increments as small as 1/16 in. were needed near the center of the column where radial changes in concentration were the greatest. These increments were increased to 1/4 and 1/2 in. away from the center of the column where the radial changes were not large. Over the full column length, no tracer was detected within 1 in. of the wall at the maximum fresh water velocity.

3.3 Analysis of Data

3.3.1 Longitudinal Dispersion

To determine the coefficient of longitudinal dispersion, D_1, equation (5) was simplified and applied to the experimental measurements of the time variation of concentration at a point z. When the parameter, D_1/wz, is small, the second term in equation (5),

$e^{wz/D_1} \operatorname{erf_c}\left[\frac{z+wt}{2\sqrt{D_1 t}}\right]$ is very much less than the first term, $\operatorname{erf_c}\left[\frac{z-wt}{2\sqrt{D_1 t}}\right]$, except for very short times. Under these conditions, equation (5) becomes

$$c/c_0 = \frac{1}{2} \operatorname{erf_c}\left[\frac{z-wt}{2\sqrt{D_1 t}}\right] . \tag{38}$$

Letting $\xi = wt/z$ and $\eta = D_1/wz$, equation (38) can be rewritten as

$$c/c_0 = \frac{1}{2} \operatorname{erf_c}\left[\frac{1-\xi}{2\sqrt{\xi\eta}}\right] \tag{39}$$

For any z, η is a constant. Thus, as η is a constant for any z and since the $\operatorname{erf_c}(\ )$ is the integral of the Gaussian probability distribution, a plot of c/c_0 in percent versus $1-\xi/2\sqrt{\xi}$ results in a straight line on arithmetic-probability paper with a standard deviation of concentration, $\sigma = \sqrt{\eta/2}$. Substituting for η , the longitudinal dispersion coefficient is

$$D_1 = wz\eta = 2\sigma^2 wz \tag{40}$$

Equations (39) and (40) can be used to determine dispersion coefficients for η values up to 0.010 even though the second term in equation (5) is not negligible. A plot on arithmetic probability paper, (see Fig. 3-9) of equation (5), expressed in terms of ξ and η , and equation (39), with $\eta = 0.010$, show that the lines of best fit through equations (5) and (39) have the same slope and standard deviation. Thus, although the experimental data is correctly described by equation (5), the method of analysis, outlined for small η values, can be applied to determine longitudinal dispersion coefficients for η values up to 0.010.

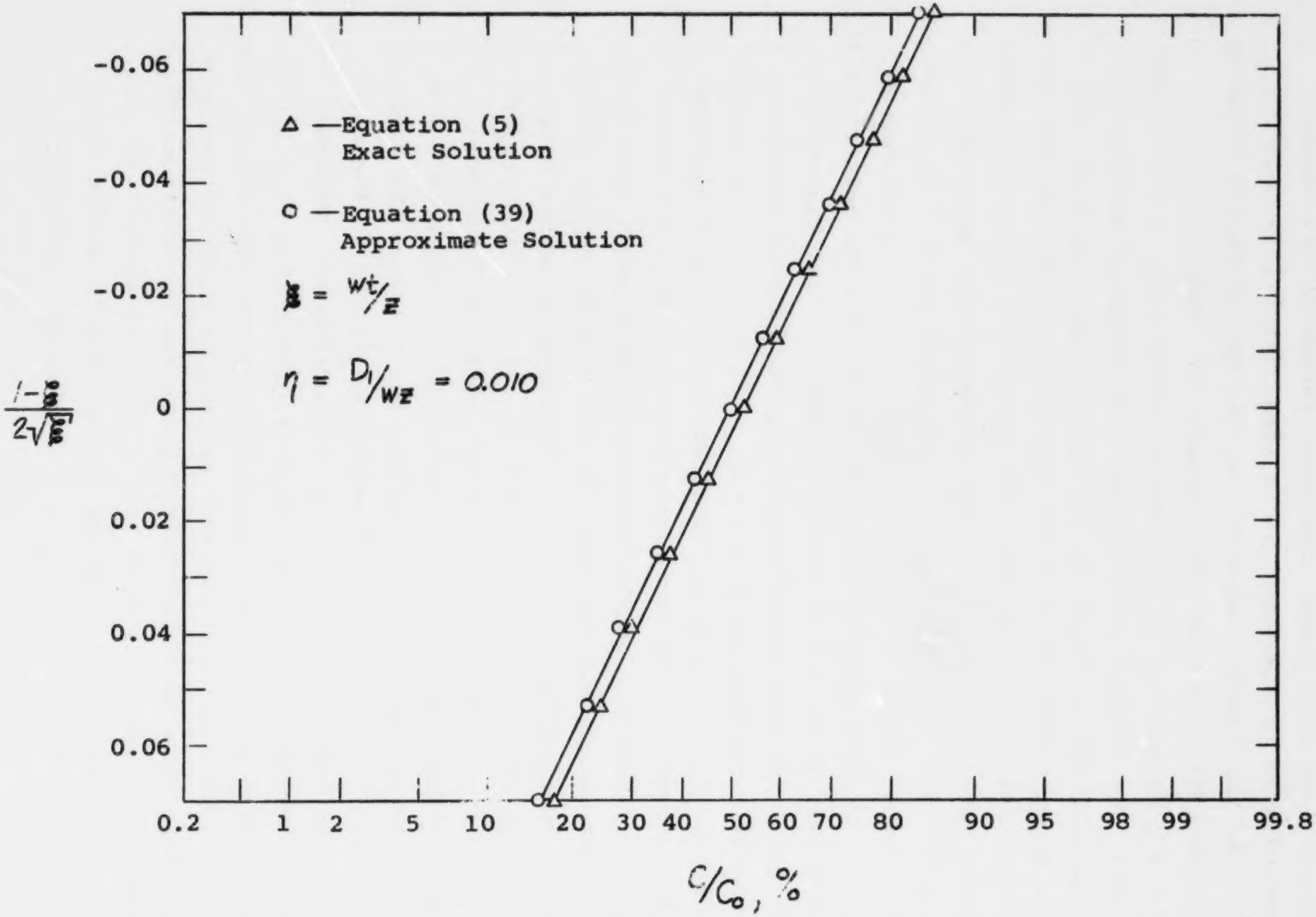

Figure 3-9 Plot of Exact and Approximate Concentration Distributions for Longitudinal Dispersion

For η values less than 0.002, the error caused by the neglect of the second term in equation (5) is less than 2-1/2% when $c/c_o = 1/2$. Hence, the seepage velocity, w, can be determined directly from equation (39), for when c/c_o equals 1/2, then ξ equals 1 and w equals z/t_{50} (where t_{50} is the time at which $c/c_o = 1/2$ at any position z). The seepage velocity was also computed knowing the average velocity and porosity of the sand column. In fact, for η values greater than about 0.002, the seepage velocity was determined from the average velocity and porosity. Ogata [78] plots equation (5) versus η when $\xi = 1$ and shows how the error due to the neglect of $e^{wz/D_1} \operatorname{erf}_c\left[\frac{z+wt}{2\sqrt{D_1 t}}\right]$ increases as $\eta = D_1/wz$ increases. He indicates that since $e^{wz/D_1} \operatorname{erf}_c\left[\frac{z+wt}{2\sqrt{D_1 t}}\right]$ is a maximum at $\xi = 1$, the maximum error in equation (5) due to the neglect of this term also occurs at $\xi = 1$ or $t = z/w$; however, from Figure 3-9, it can be seen that the error is greatest for $\xi < 1$ or $t < z/w$ and approaches a maximum for $\xi = t = 0$.

The above analysis requires that at t = 0, a step function change in concentration be introduced at the point z = 0 into a steady flow. However, as the experiments were begun from rest, a certain time period was required for the flow to become steady. For Reynolds numbers less than about 20 (Reynolds number based upon seepage velocity and mean particle size), the time period for the buildup to a steady velocity was very small compared to the mean travel time to a probe. Hence, the choice of z = 0 as the position of the initial interface and t = 0 as the time when the flow started, introduced negligible errors in the calculation of the longitudinal dispersion coefficient. However, for Reynolds Numbers greater than 20, the time period of buildup to steady flow was not small compared with the mean travel time to the probe. As a result, the measured tracer distribution gave a smaller dispersion coefficient than predicted by equation (39), which assumes a steady flow from time t = 0. To account for the reduced mixing (dispersion) during the buildup to steady flow, the true time scale was replaced by a shorter but equivalent time scale for which the velocity remains constant at the steady-state velocity. The equivalent time scale was determined by requiring that the spread of the tracer distribution occurring during the unsteady flow period be equal to the spread occurring during an equivalent time period of steady flow at the steady-state velocity. By defining an equivalent time scale in this manner, the influence of the reduced mixing during the unsteady flow period on the tracer distribution was taken into consideration; in addition, it was possible to analyze the experimental results using equations (39) and (40) with the true time scale replaced by the equivalent time scale.

For a random process of particle displacement, it is well-known that

$$D_1 = \frac{1}{2}\frac{d(\sigma^2)}{dt} \qquad (41)$$

where σ^2 is the variance of the resulting distribution. Here we assume that the salt tracer is composed of many particles undergoing random displacements. Rearranging equation (41) and integrating, gives

$$\sigma^2 = 2\int_0^t D_1\, dt \qquad (42)$$

Equating equation (42) to the variance arising from a steady flow for a different time period gives

$$\sigma^2 = 2D_{1_0}t' = 2\int_0^t D_1\, dt \qquad (43)$$

since D_{1_0} is a constant. If we further assume that $D_1 = \alpha_1 W$ and $D_{1_0} = \alpha_1 W_0$ (a good approximation at large velocities), equation (43) becomes

$$t' = \int_0^t \left(\frac{W}{W_0}\right) dt \qquad (44)$$

which defines the equivalent time scale, t'. When $t = t_c$ (see Fig. 3-10), $t' = t_c'$ and the flow is steady. Letting

$\Delta t = t_c - t_c'$, equation (38) becomes

$$\frac{C}{C_o} = \frac{1}{2}\,\mathrm{erf_c}\left[\frac{z' - w_o t'}{2\sqrt{D_{1_o} t'}}\right] \tag{45}$$

with $t' = t - \Delta t$ and $z' = z - w_o \Delta t$.

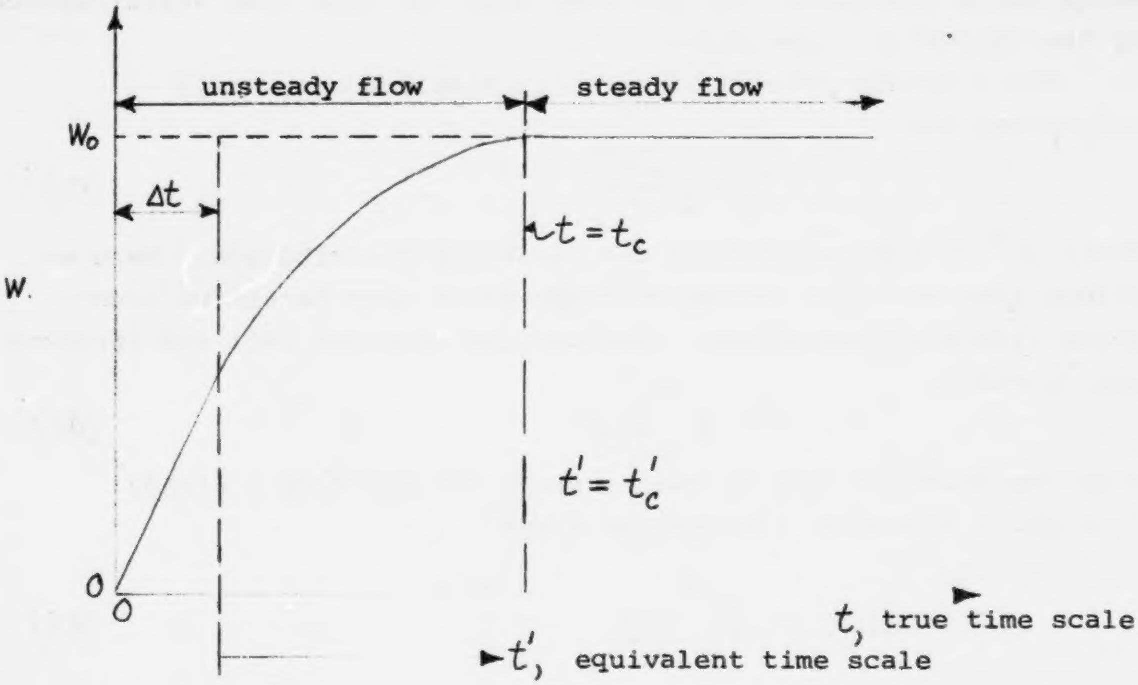

Figure 3-10 Buildup to Steady Flow for Axial Flow through a Packed Sand Column

Bear [10] has obtained a result similar to equation (45) starting from equation (3) and assuming that w and D_1 (where $D_1 = \alpha_1 w$) are functions of time.

To determine t' in equation (44), the transient seepage velocity, w, was calculated based upon a derived relationship between the transient head gradient and the seepage velocity and upon measurements of the former. Irmay [53] has shown by a volume integration of the Navier-Stokes equations in a small region of a porous medium, that the relationship between the average head gradient and the seepage velocity is

$$\frac{\partial h}{\partial z} = Aw + Bw^2 + C\frac{\partial w}{\partial t} \qquad (46)$$

where z is the direction of flow, w is the average seepage velocity, A = θ/K (porosity/Darcy permeability), B = $\beta\theta^2/gd_{50}$ (where β = a packing factor and d_{50} is the mean grain diameter), and C = 1/g. The term $C\,\partial w/\partial t$ in equation (46) was neglected since, after the first tenth of a second, it contributed less than 3% of the total head gradient. Introducing the quantities, w_0 = steady flow velocity and dh/dz_{max} = steady flow head gradient, into equation (46), neglecting $C\frac{\partial w}{\partial t}$, and solving for w/w_0 gives

$$w' = \frac{w}{w_0} = -\frac{a}{2b} + \sqrt{\left(\frac{a}{2b}\right)^2 + \left(\frac{1}{b}\right)\Delta h'} \qquad (47)$$

where $\Delta h' = \frac{\partial h}{\partial z}\Big/\left(\frac{dh}{dz}\right)_{max}$ a = $Aw_0\Big/\left(\frac{dh}{dz}\right)_{max}$ and b = $Bw_0^2\Big/\left(\frac{dh}{dz}\right)_{max}$
Equation (47) was introduced into equation (44) and integrated graphically from t = 0 to t = t_c for each run to determine t_c'. The quantities A and B were determined from measurements of headloss over a wide range of seepage velocities under conditions of steady flow. Knowing t_c', Δt and t' are known, and equation (45) was applied in the same manner as for the steady flow tests to determine D_1.

To illustrate the procedure for analyzing the experimental data, consider Test 9, No. 2 Sand. A plot of the relative concentration, c/c_0, (where c_0 = 0.104% was the initial concentration in the column) with time, is given in Figure 3-11 at the probe in the media near the bottom of the column (about 31 in. below the initial interface). To account for the unsteady flow after the valve was opened, equation (44) was graphically integrated using equation (47) with t_c = 2.52 sec., A = 0.434 sec/cm , B = 0.048 sec^2/cm^2, a = 0.592, b = 0.427, and dh/dz_{max} = 4.786. $\Delta h'$ as a function of time was obtained from measurements of the buildup to a steady-state head gradient. Performing the integration gave t_c' = 1.97 sec.; hence, Δt = 2.52 - 1.97 = 0.55 sec. and t' = t - 0.55 sec.. Correcting all the measured times by 0.55 sec., the quantity $\frac{1-\xi'}{2\sqrt{\xi'}}$ (where $\xi' = w_o t'/z'$ and w_o = 6.522 cm/sec and z' = 72.63 cm) was calculated and plotted against c/c_o as shown in Figure 3-12. From Figure 3-12, the standard deviation, σ , is 0.063, η = 0.00794, and D_1 = 3.82 cm^2/sec.

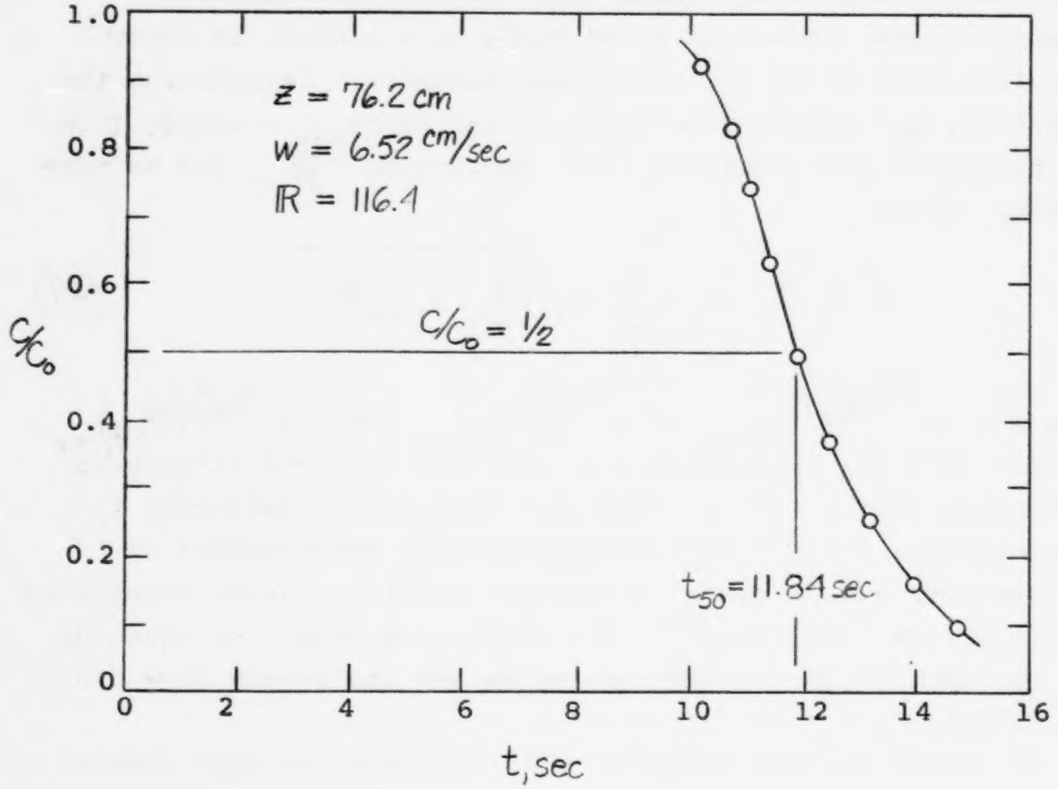

Figure 3-11 Time Variation of Tracer Concentration at a Point during Longitudinal Dispersion Test 9, No. 2 Sand

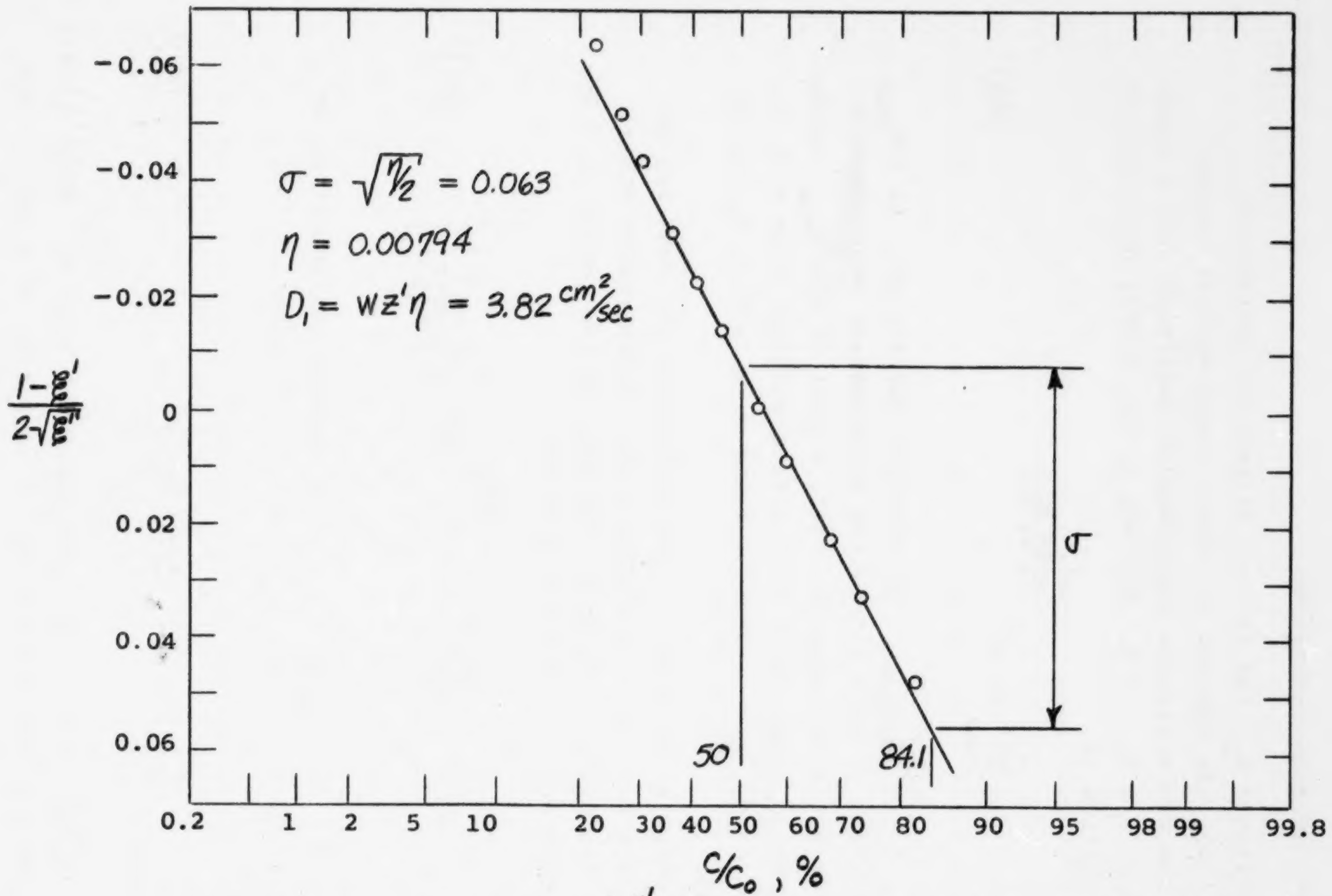

Figure 3-12 c/c_o versus $\frac{1-\xi'}{2\sqrt{\xi'}}$ for Longitudinal Dispersion Test 9, No. 2 Sand

3.3.2 Lateral Dispersion

To evaluate D_2, the lateral dispersion coefficient, equation (36), was applied to steady-state, spatial measurements of the concentration distribution resulting from a point injection at $r = 0$, $z = 0$. For any z, the radial distribution of concentration is

$$\frac{c}{c_{max}} = e^{-r^2/(4D_2 z/w)} \tag{48}$$

where $c_{max} = C_o Q / 4\pi D_2 z$ (a constant for any z). As c/c_{max} and r are known at each z from the experimental measurements, if the data satisfies equation (48), a plot of $\sqrt{\ln c/c_{max}}$ versus r on arithmetic graph paper will give a straight line with a slope of $m = \sqrt{4D_2 z/w}$. Then, knowing m, z, and w, D_2 may be determined.

The seepage velocity, w, was determined for each run by measuring the buildup to a steady-state concentration distribution at two probes located on the axis of the column ($r = 0$). Applying equation (20) for $r = 0$ gives

$$\frac{c}{c_{max}} = \frac{1}{2}\left\{ erf_c\left[\frac{z - wt}{2\sqrt{D_1 t}}\right] + e^{wz/D_1} erf_c\left[\frac{z + wt}{2\sqrt{D_1 t}}\right]\right\} \tag{49}$$

where $c_{max} = C_o Q / 4\pi D_2 z$ (the maximum concentration at any z occurring at $t = \infty$). When $z = wt$, equation (49) reduces to

$$\frac{c}{c_{max}} = \frac{1}{2}\left\{1 + e^{1/\eta^2} erf_c(1/\eta)\right\} \tag{50}$$

where $\eta = \sqrt{D_1/wz}$. Now, as η decreases, the term $e^{1/\eta^2} erf_c(1/\eta) \rightarrow 0$ and $c/c_{max} \longrightarrow 1/2$ $\left[\text{for } \eta < 1/3,\ e^{1/\eta^2} erf_c(1/\eta) < 0.002\right]$. Now, knowing the t_{50} (time at which $c/c_{max} = 1/2$) at each probe, the average velocity was found from

$$w = \frac{\Delta z}{\Delta t_{50}} \qquad (51)$$

where Δz = distance between the probes and Δt_{50} = difference in time between the t_{50} at one probe and the t_{50} at the other probe. The seepage velocity, computed from equation (51), was checked by calculating it using the average or Darcy velocity and the porosity.

Due to the initial mixing of the salt tracer (caused from its discharge from the injector) with the surrounding fresh water, the injector could not be considered as a point source at $z = 0$, $r = 0$. Thus, the distance between each probe and the injector was not equal to z and an equivalent $z = 0$ had to be determined. As previously indicated, the slope m at each probe was determined from the radial distribution of concentration at each of the two probes. As D_2 and w are constants for each run,

$$\frac{m_1}{m_2} = \sqrt{\frac{z_1}{z_2}} = \sqrt{\frac{z_1}{z_1 + \Delta z}} \qquad (52)$$

where Δz is the distance between the two probes. Thus, from (52), z_1 and z_2 were found, and knowing m, z, and w, D_2 was determined from

$$D_2 = \frac{wm^2}{4z} \qquad (53)$$

A typical run (Run 3, Lateral Dispersion) and its analysis are presented below to illustrate the method of data reduction. Figure 3-13 is a plot of c/c_{max} versus r for two probes located at 4 inches and 34 inches below the injector. The values of c/c_{max} were determined directly from the deflections of the Sanborn pen, since, in calibration, Sanborn deflection was found to be linear with concentration. Figure 3-14 shows a plot of $\sqrt{\ln C/C_{max}}$ versus r in inches for both probes (the subscript 1 refers to the probe 4 in. below the injector; whereas the subscript 2 refers to the probe 34 in. below the injector). The slopes, m, determined from Figure 3-14, are m_1 = 0.460 in. and m_2 = 0.877 in.. Applying equation (52) to determine z_1 and z_2 gives

$$z_1 = \frac{\Delta z}{[(m_2/m_1)^2 - 1]} = \frac{30}{[(1.907)^2 - 1]} = 11.37 \text{ in.} = 28.88 \text{ cm.}$$

and $z_2 = z_1 + \Delta z$ = 41.37 in. = 105.00 cm.. From the measurements of the buildup to a steady-state concentration distribution Δt_{50} = 295 sec.; thus, the seepage velocity is $w = \frac{\Delta z}{\Delta t_{50}} = \frac{(30)(2.54)}{295}$ =0.258 cm/sec.. Using the seepage velocity and the distance z_1 in equation (53) gives

$$D_2 = \frac{(.460)^2(2.54)^2(.258)}{4(28.88)} = 0.00304 \text{ cm}^2/\text{sec}$$

$$\text{and} \quad \frac{D_2}{\nu} = \frac{0.304 \times 10^{-2}}{0.975 \times 10^{-2}} = 0.312 \quad .$$

The Reynolds number for this test is

$$\mathbb{R} = \frac{w d_{50}}{\nu} = \frac{(.258)(.167)}{.975 \times 10^{-2}} = 4.42 \quad .$$

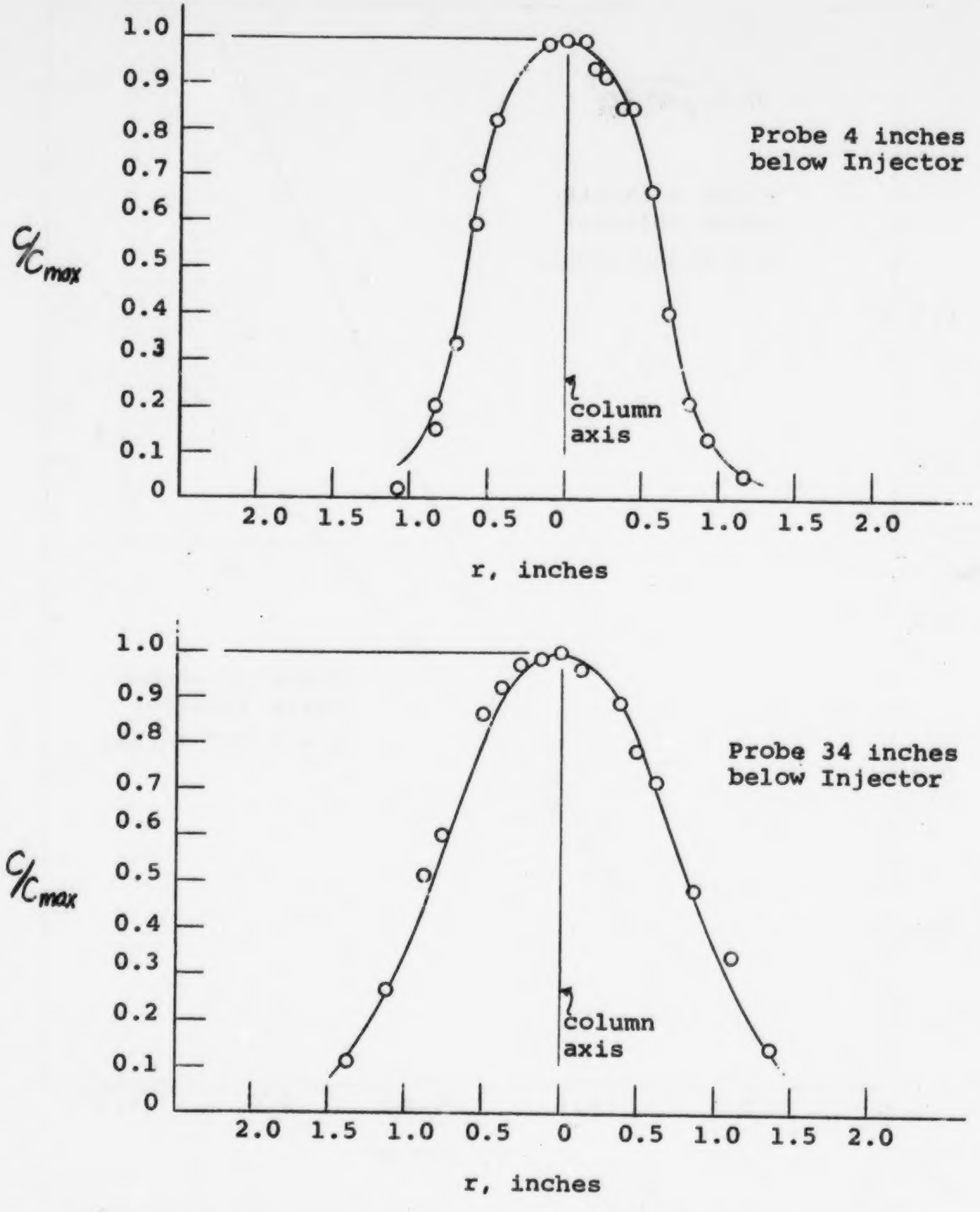

Figure 3-13 c/cmax versus r for Lateral Dispersion Run 3

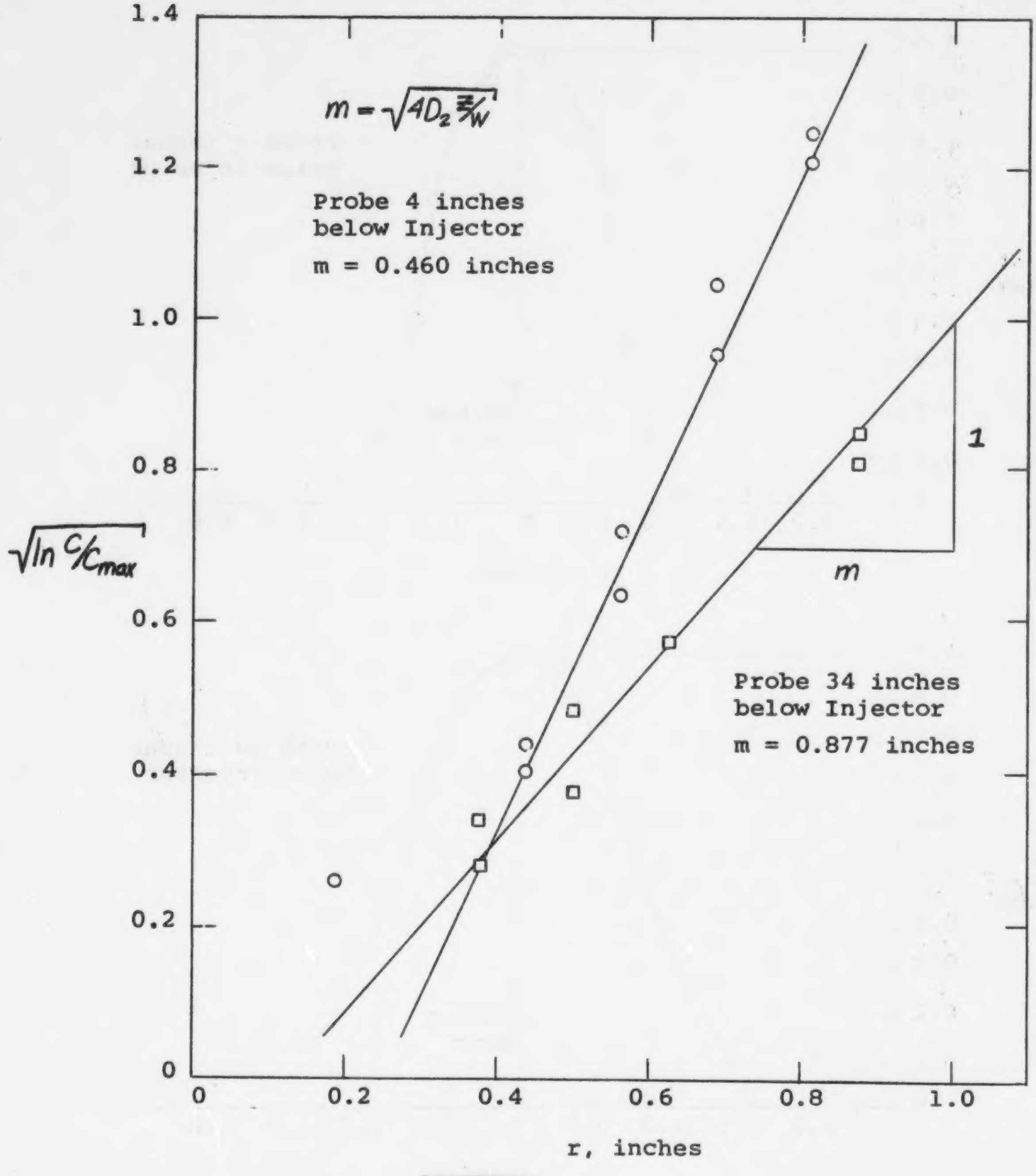

Figure 3-14 $\sqrt{\ln C/C_{max}}$ versus r for Lateral Dispersion
Run 3

3.4 Presentation and Discussion of Results

3.4.1 Longitudinal Dispersion

The ratio of the longitudinal dispersion coefficient to the kinematic viscosity, D_l/ν, from experimental measurements on the No. 2 sand (d_{50} = 0,167 cm) and the No. 4 sand (d_{50} = 0.345 cm) is plotted in Fig. 3-15 against the Reynolds number, $\mathbb{R} = wd_{50}/\nu$. The results of the individual tests are also tabulated in Table I. The ratio, D_l/ν, is also plotted against the permeability Reynolds number, $\mathbb{R}_k = w\sqrt{k}/\nu$, in Figures 3-16 (k = intrinsic permeability of the media). The lines of best fit for the experimental data are

$$D/\nu = 1.70 \left(\frac{wd_{50}}{\nu} \right)^{1.20} \tag{54}$$

and

$$D/\nu = 223 \left(\frac{w\sqrt{k}}{\nu} \right)^{1.20} \tag{55}$$

The experimental results presented in Fig. 3-15 indicate that the correlation expressed by equation (54) is valid over a Reynolds number range of 0.2 to about 10. Above a Reynolds number of 10, the exponent 1.2 on the Reynolds number decreases approaching a value of 1.0 near a Reynolds number of 50. The exponent on the Reynolds number in equation (54) remains constant at 1.0 for Reynolds numbers from 50 to 100. The experimental correlation given in equation (55) holds for the permeability Reynolds number range 0.004 to about 0.1. In the permeability Reynolds number range 0.1 to about 0.5, the exponent on the Reynolds number decreases from 1.2 to 1.0. For the permeability Reynolds number range 0.5 to 2.0, the exponent on the Reynolds number in equation (55) remains constant at 1.0.

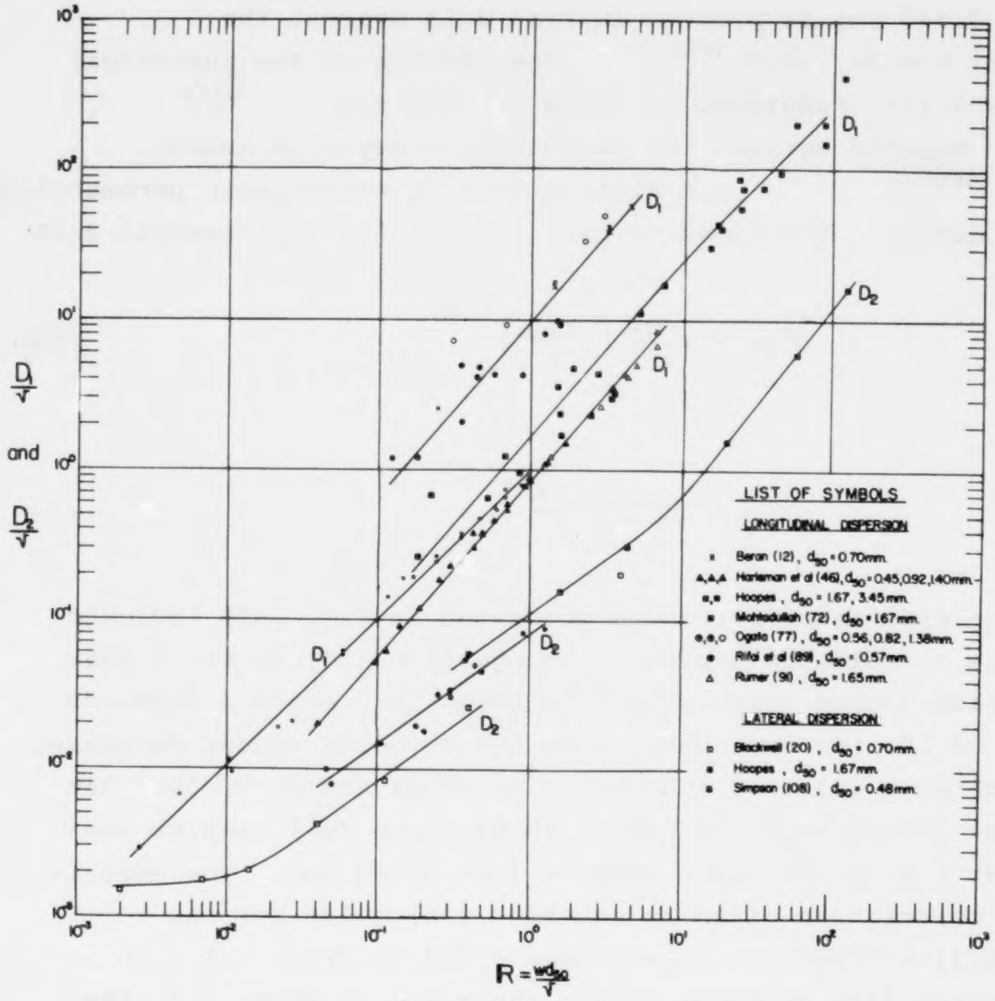

FIGURE 3-15 CORRELATION OF D_1/ν AND D_2/ν WITH $\mathbb{R} = wd_{50}/\nu$

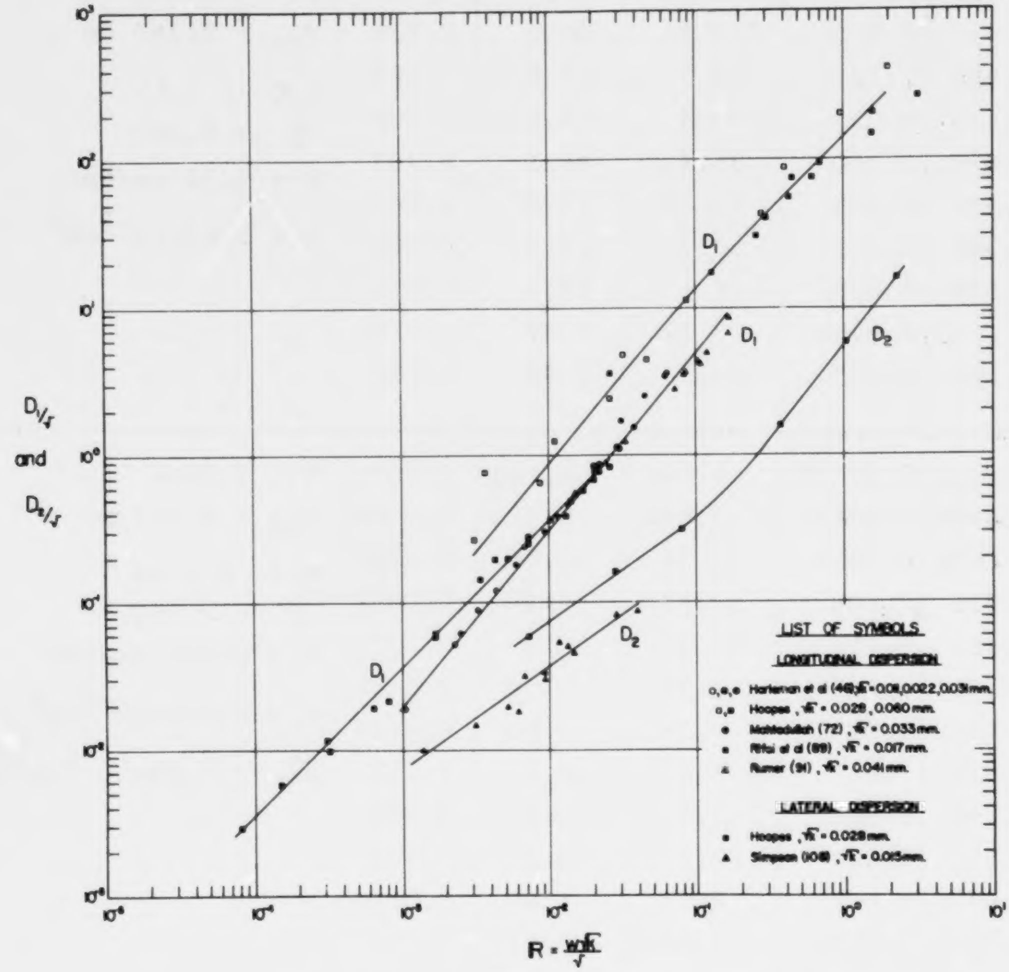

FIGURE 3-16 CORRELATION OF D_1/ν AND D_2/ν WITH $\mathbb{R} = w\sqrt{k}/\nu$

Table I - Summary of Longitudinal Dispersion Tests

Run No.	w, cm/sec	D_1 cm^2/sec	$\frac{D_l}{\nu}$	$\mathbb{R} = \frac{wd_{50}}{\nu}$	$\mathbb{R}_k = \frac{w\sqrt{k}}{\nu}$	Media and its Characteristics
17	0.809	0.608	75.6	34.7	0.606	No. 4 Sand d_{50} = 0.345 cm U.C. = 1.17 θ = 0.357 K = 4.76 cm/sec k = $3.63\text{x}10^{-5}\text{cm}^2$
20	1.97	1.570	203.4	88.0	1.536	
27	1.918	1.121	148.3	87.6	1.529	
28	0.315	0.223	30.4	14.8	0.258	
29	0.959	0.700	95.4	45.1	0.787	
30	0.550	0.559	75.4	25.6	0.447	
31	0.383	0.311	40.7	17.3	0.302	
32	0.559	0.426	55.1	24.9	0.435	
33	0.0315	0.0256	3.52	1.49	0.026	
34	0.160	0.127	17.1	7.46	0.130	
1*	0.0105	0.00254	0.264	0.182	0.0031	No. 2 Sand d_{50} = 0.167 cm U.C. = 1.35 θ = 0.360 K = 0.829 cm/sec k = $0.791\text{x}10^{-5}\text{cm}^2$ $\mathcal{D}_m$ = $0.95\text{x}10^{-5}\text{cm}^2/\text{sec}$
2*	0.0301	0.00623	0.648	0.522	0.0088	
3*	0.0896	0.0227	2.36	1.56	0.0263	
4*	0.316	0.108	11.21	5.24	0.0882	
6*	0.961	0.418	43.4	16.7	0.281	
7	0.151	0.0401	4.36	2.74	0.0461	
8*	0.0378	0.0115	1.24	0.68	0.0114	
9	6.522	3.82	408.0	116.4	1.959	
10	3.188	1.90	203.0	56.9	0.958	
11	1.344	0.82	87.7	24.0	0.404	
12	0.0991	0.041	4.72	1.90	0.0320	
13	0.0111	0.0058	0.677	0.22	0.0037	

* - average of D_1 from two probes

The choice of variables, w, d_{50}, ν, and $\sqrt{k}$, with which D_1 and D_2 have been correlated is based upon a model of the dispersion process coupled with dimensional considerations and experimental evidence. Scheidegger [102] concludes that for no lateral mixing (due to molecular diffusion) $D_1 = \alpha_1 w$ (where α_1 is a geometrical constant of the porous medium). Scheidegger [102] also found that $D_1 = \beta_1 w^2$ when molecular diffusion was important. De Josselin De Jong [32] and Saffman [92] have also found that the dispersion coefficient is linearly related to the velocity. The dispersion coefficients obtained in the development of the convective-dispersion equation (see Rumer [45]), were shown to depend upon the spatial variation of the seepage velocity in a small region of the porous media from the average seepage velocity in that region. These spatial variations resulted from the tortuous streamline pattern through the pores, from the velocity distribution within each pore, and from turbulence within the pores (important at large flow rates). Thus, the dispersion coefficients should depend upon the Reynolds Number, which characterizes the state of flow (laminar, non-linear laminar [106], or turbulent), the viscosity, which effects the pore velocity distribution, the average seepage velocity, and the average particle size, which is related to the average pore size. The molecular diffusion coefficient will indirectly effect the dispersion coefficients since the radial transport of tracer due to diffusion within each pore will tend to reduce the tracer gradients in the direction of flow, and hence, reduce the dispersion coefficient in the flow direction, see Taylor [112]. Experiments [45] and [51] indicate that molecular diffusion is important only at small flow rates, $\mathbb{R} < 10^{-3} - 10^{-2}$. Thus, for the region of flows where molecular diffusion is not important, one would expect that

$$D_1 \sim \alpha_1 w \quad . \tag{56}$$

Dividing both sides of equation (56) by the kinematic viscosity gives

$$\frac{D_1}{\nu} \sim \left(\frac{\alpha_1}{d_{50}}\right)\left(\frac{w d_{50}}{\nu}\right) = \left(\frac{\alpha_1}{d_{50}}\right)\mathbb{R} \quad . \tag{57}$$

Experimental evidence, see Harleman and Rumer [45], Harleman *et al* [46], and Mohtadullah [72], indicates that equation (57) should be

$$\frac{D_1}{\nu} = \psi_1\left(\frac{W d_{50}}{\nu}\right)^{n_1} = \psi_1 \mathbb{R}^{n_1} \qquad (58)$$

in which n_1 is a constant, slightly greater than 1, and ψ_1 is a constant, dependent upon the physical properties of the porous medium.

The constant α_1 in equation (57) or ψ_1 in equation (58) are functions of the media properties; hence,

$$\alpha_1 \text{ or } \psi_1 = f(d_{50}, \text{U.C.}, \theta, \beta, \gamma) \qquad (59)$$

where d_{50} is the mean particle size; U.C. is the uniformity coefficient of the medium; θ is the porosity of the packed medium; and β and γ are shape and roughness factors of the individual particles. For uniform media, d_{50} is a characteristic length of the pore structure; however, for non-uniform media, Mohtadullah [72] and Rumer *et al* [46] have introduced $\sqrt{k}$ (where k is the intrinsic permeability) as the characteristic length of the pore structure since it reflects the influence of not only the particle size but also the distribution of particle sizes on the flow through the media. For uniform media, either $\sqrt{k}$ or d_{50} may be used as a characteristic length, for there is a linear relationship between and d_{50}, see Raimondi *et al* [85].

Using $\sqrt{k}$ in place of d_{50} as the characteristic length, equation (58) becomes

$$\frac{D_1}{\nu} = \phi_1\left(\frac{W\sqrt{k}}{\nu}\right)^{n_1} = \phi_1 \mathbb{R}_k^{\,n_1}$$

where $\mathbb{R}_k$ is the permeability Reynolds number. Mohtadullah [72] from some experiments with non-uniform media, found a linear correlation between ϕ_1 and U.C., the uniformity coefficient; however, there was no correlation between ψ_1 and U.C.. In addition, he found that n_1 in equations (58) and (60) was independent of particle size and shape; however, for non-uniform media, n_1 decreased, approaching 1.0 for very non-uniform media.

The plot, Figure 3-15, of D_1/ν versus $\mathbb{R}$ indicates large differences in dispersion coefficients obtained by different investigators at the same Reynolds number. The principal reasons for these differences lie in the experimental setups and techniques used to measure the tracer distributions by the different investigators. Beran [12] introduced a slug of radioactive tracer into a steady flow through a 1 in. diameter column and measured the subsequent time variation in tracer concentration as the laminar flow passed through a small tube, 0.079 in. diameter, leading from the column. Taylor's work [112] on laminar flow through a tube shows that the dispersion coefficient is directly proportional to the velocity squared and inversely proportional to the molecular diffusion coefficient. No information is given on the molecular diffusion coefficient of the tracer; however, since the tube velocity is about 55 times greater than the column seepage velocity, and since the tracer travels 12 in. in the tube before being measured, an appreciable increase in the spread of the tracer slug, and hence the dispersion coefficient, may occur. Another factor tending to increase the spread of the tracer is the non-uniform flow pattern from the column to the tube. Since no provision was made for a gradual change in area from the column to the tube. the velocities near the column center will be greater and the velocities near the column walls will be less than the average column velocity. As a result of this velocity distribution, the spread of the tracer distribution, and hence the dispersion coefficient, will be increased. Thus, the measured dispersion coefficients, reported by Beran [12], are too large due to the location of the measurement point and the flow pattern out of the column.

Ogata [77] in his column experiments measured tracer distributions by sampling and photometer measurements of the column effluent in the region just below the bottom screen supporting the sand bed. The tracer was introduced at the top of the column through a tube much smaller in diameter than the column (which was 4 1/2 in. in diameter) into a 1/4 in. space between the top of the sand and the top of the column. It was assumed that the jet action of the tracer inlet into the space above the sand would rapidly distribute the tracer uniformly across the column. However, during the buildup to a uniform tracer concentration across the top of the column, some tracer would enter the media. As a result, the slope of the tracer distribution (and hence the dispersion coefficient), measured at the column base, would be greater than for the distribution resulting from an initially uniform tracer concentration at the column top. In addition, the measured dispersion coefficients were also increased due to the additional mixing between the bottom of the media and the measuring point.

Rifai [89] in his column experiments measured the concentration distribution of a dilute NaCl tracer by sampling at a point on the axis of the column just below the supporting screen of the sand packing. The nature of his inlet device for the tracer at the top of the column is not known. Also, it is not known if, in his sampling, the velocity into the sampler was the same as the column effluent velocity. Any difference between the velocity into the sampler and out of the column would distort the measured tracer distribution. In addition, if the mixing characteristics of the bottom screen and block were different from the media, the spread of the tracer distribution entering the sampling tube would be altered.

Rumer [45], Mehlhorn [46], and Mohtadullah [72] used a technique similar to that of this study for introducing a dilute salt tracer and measuring the resulting dispersed pattern. To detect the tracer, a conductivity probe (consisting of two platinum electrodes aligned parallel to each other and to the direction of flow) was mounted within and on the axis of the sand column. Thus, the probe responded to average changes in tracer concentration over the pore volume between the electrodes. The electrode spacing was about 1/8 of an inch, which allowed from 2 to 6 particles between the plates. No different spacings were used so that the influence of electrode spacing on the measurements is not known; however, for all particle sizes, the same dispersion coefficients were obtained at the same Reynolds number.

The experimental results of this investigation were obtained in a manner similar to that of Rumer [45], Mehlhorn [46], and Mohtadullah [72], except that a different type of conductivity probe was used. The probe used has been described in section 3.2; however, its main features are indicated in Figure 3-17 below. In the case of the ringed electrodes, the electric field of the probe is all external to the probe (as indicated by the lines of current flow). Whereas, for the parallel plate probe, the electric field is confined between the two plates. Thus, the ringed electrode probe will respond to NaCl tracer before the tracer actually reaches the probe and after it passes the probe. Consequently, the ringed electrode probe will indicate a tracer distribution which is flatter or more spread out than the parallel plate probe which responds only during the time when the tracer is between the plates. And, since the dispersion coefficient is directly proportional to the slope of the tracer distribution, the ringed electrode probe will give a larger dispersion coefficient than the parallel plate probe. The results of the measurements with the

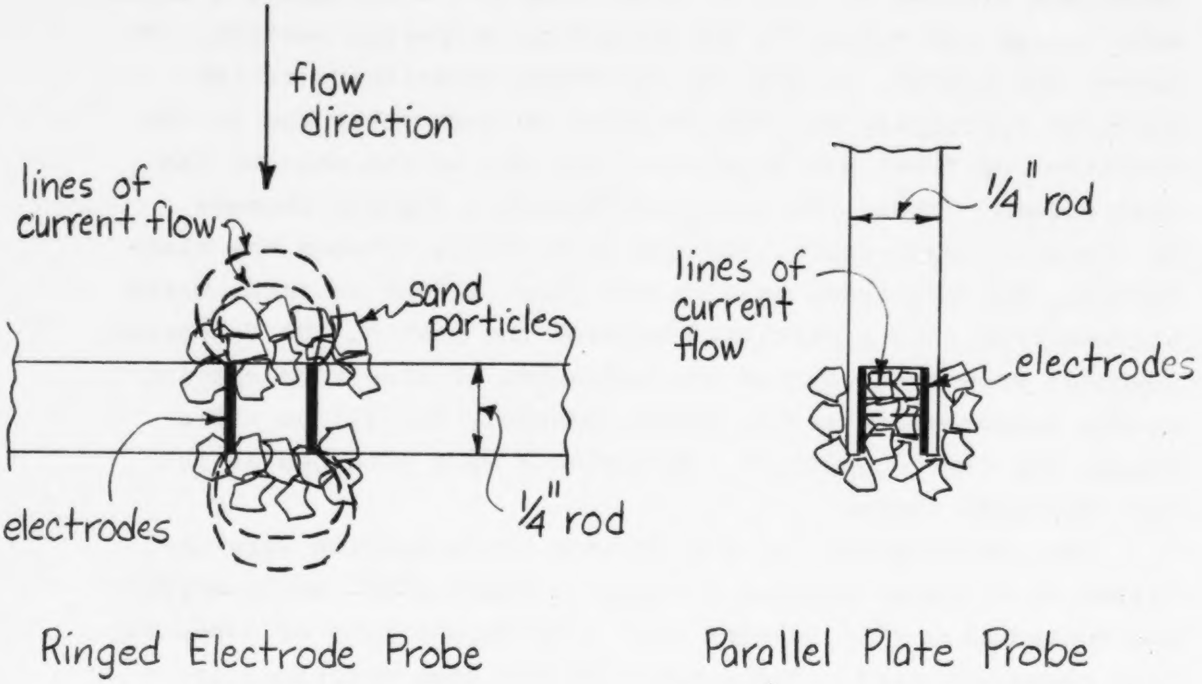
flow direction
lines of current flow
sand particles
electrodes
1/4" rod
Ringed Electrode Probe
1/4" rod
lines of current flow
electrodes
Parallel Plate Probe

Figure 3-17 Comparison of the Characteristics of the Ringed Electrode and Parallel Plate Probes

ringed electrode probe (see Fig. 3-15) indicate that the dispersion coefficients measured with the ringed electrode probe are twice as large as the dispersion coefficients measured with the parallel electrode probe for the same Reynolds number.

The spacings of the electrodes on the ringed probes varied from 3/32 of an inch to about 5/8 of an inch. There appeared to be no influence of the electrode spacing on the measurements of the longitudinal dispersion coefficients in either the No. 2 or the No. 4 sand, except at Reynolds numbers greater than 50. At these Reynolds numbers, the 3/32 of an inch electrode spacing in the No. 2 sand gave larger dispersion coefficients than the larger electrode spacings in the No. 4 sand.

From this discussion of the results of different investigators, it is apparent that, while different methods of tracer introduction (step function, slug, and sinusoidal [37]) and different tracers may be used to determine the longitudinal dispersion coefficient, the technique for measuring the tracer distribution and the location of the measuring station can make a significant difference in the measured dispersion coefficients. Thus, to eliminate the influence on the tracer distribution of mixing conditions outside the media, measurements should be made within the media with a probe or sampler, designed to respond only to concentration changes in a small region. Finally, this comparison of the experimental results and techniques of several investigators in Figure 3-15 has also shown that only the experimental measurements of Harleman *et al* [46], Mohtadullah [72], and Rumer [91] have truly reflected the dispersive characteristics of the porous medium. Thus, their results for the longitudinal dispersion coefficient (see Fig. 3-15) may be used in the study of miscible fluid displacement problems in uniform sands.

3.4.2 Lateral Dispersion

The ratio, D_2/ν , of the lateral dispersion coefficient to the kinematic viscosity (obtained from experimental measurements on the No. 2 sand (d_{50} = 0.167 cm) has been plotted in Figures 3-15 and 3-16 against the particle size Reynolds number, $\mathbb{R} = \frac{W d_{50}}{\nu}$, and the permeability Reynolds number, $\mathbb{R}_k = \frac{W\sqrt{k}}{\nu}$, respectively. The experimental results are tabulated in Table II. Though more experimental data at different Reynolds numbers is needed to completely define a correlation, the work of Blackwell [20], Simpson [108], Bischoff [19], Rumer [45], and Grane [42] suggest that over the Reynolds number range, 0.01-5.0, a straight line correlation exists between

D_2/ν and $\mathbb{R}$. Fitting a straight line (by eye) to the experimental data gives

$$D_2/\nu = 0.11\left(\frac{wd_{50}}{\nu}\right)^{0.70} \qquad (61)$$

and

$$D_2/\nu = 1.86\left(\frac{w\sqrt{k}}{\nu}\right)^{0.70} \qquad (62)$$

Table II - Summary of Lateral Dispersion Tests

Run No.	w, cm/sec	D_2, cm²/sec	D_2/ν	$\mathbb{R}=\frac{wd_{50}}{\nu}$	$\mathbb{R}_k=\frac{w\sqrt{k}}{\nu}$	Media and its Characteristics
3	0.258	0.00304	0.312	4.42	0.079	No. 2 Sand
5	0.0779	0.00133	0.160	1.57	0.028	d_{50}= 0.167 cm
6	0.0211	0.00052	0.059	0.402	0.0072	U.C. = 1.35
7	3.256	0.054	5.84	58.8	1.049	θ = 0.360
8	1.11	0.0140	1.56	20.7	0.369	K = 0.829 cm/sec
9	7.02	0.149	16.1	126.5	2.256	$k = 0.791\times10^{-5}$ cm²
						$\mathcal{D}_m=0.95\times10^{-5}$ cm²/sec

Above a Reynolds number of 5 in Figure 3-15 or 0.1 in Figure 3-16, the slope of the D_2/ν versus $\mathbb{R}$ correlation increases and becomes approximately parallel to the D_1/ν versus $\mathbb{R}$ correlation for Reynolds numbers greater than 20 in Figure 3-15 and 0.4 in Figure 3-16. This change in slope of the D_2/ν versus $\mathbb{R}$ correlation indicates a large increase in the lateral mixing as the flow changes from laminar to laminar nonlinear [106] (i.e., as inertial influences on the flow pattern become important). Another indication of the increased lateral mixing can be seen by the decrease in the slope of the

D_1/ν versus $\mathbb{R}$ correlation at the same Reynolds number as the D_2/ν versus $\mathbb{R}$ correlation shows an increase in slope. Similar observations of these slope changes in the D_1/ν and D_2/ν versus $\mathbb{R}$ correlations at the limit of the laminar flow range have been reported by Bischoff and Levenspiel [19] in tests on spheres.

It should be pointed out that, although the above correlations are based upon a limited amount of experimental data, the intent of this phase of the study was to obtain some information on the magnitude of the lateral dispersion coefficient over a wide Reynolds number range, and to use this information to determine the influence of lateral dispersion on the concentration distribution for flow between two wells, see section 4.4.2.

In section 3.1.3 it was shown that the mass transfer due to longitudinal dispersion had a negligible influence on the measured tracer distribution and equation (36) could be used to determine D_2 provided that $D_1/D_2(r/z)^2 \ll 1$. Consider run 3, discussed previously in section 3.3.2: using the calculated values of D_2 = 0.00304 cm^2/sec and z_1 = 28.88 cm along with D_1 = 0.0490 cm^2/sec (determined from the results of Harleman et al in Fig. 3-15 at a $\mathbb{R}$ = 4.42) in the above requirement gives $r_1 \ll 7$ cm = 2.8 inches. Thus, all c/c_{max} values used in the analysis of the tracer distribution using equation (48) must be less than 2.8 inches. From Figures 3-13 and 3-14 it can be seen that all of the values of c/c_{max} used in the analysis of the tracer distribution were for $r_1 < 0.9$ in. and c/c_{max} is less that 0.1 for $r_1 > 1.0$ inches. Thus, the use of equation (36) to determine D_2 appears reasonable.

The experimental concentration distributions were obtained using the ringed electrode probes with an electrode spacing of 0.094 inches. As the longitudinal concentration gradients are very small, any measurement errors introduced in the direction of flow by the electric field of the probe (see section 3.1) will be very small. However, in the plane perpendicular to the column axis, the electric field of the probe is not aligned with the lines of constant concentration (see Fig. 3-18), and thus, the probe will indicate a smaller concentration at any radius than is actually present. This error in the probe response will be large at small radii and decrease as the radius from the center of the concentration distribution increases.

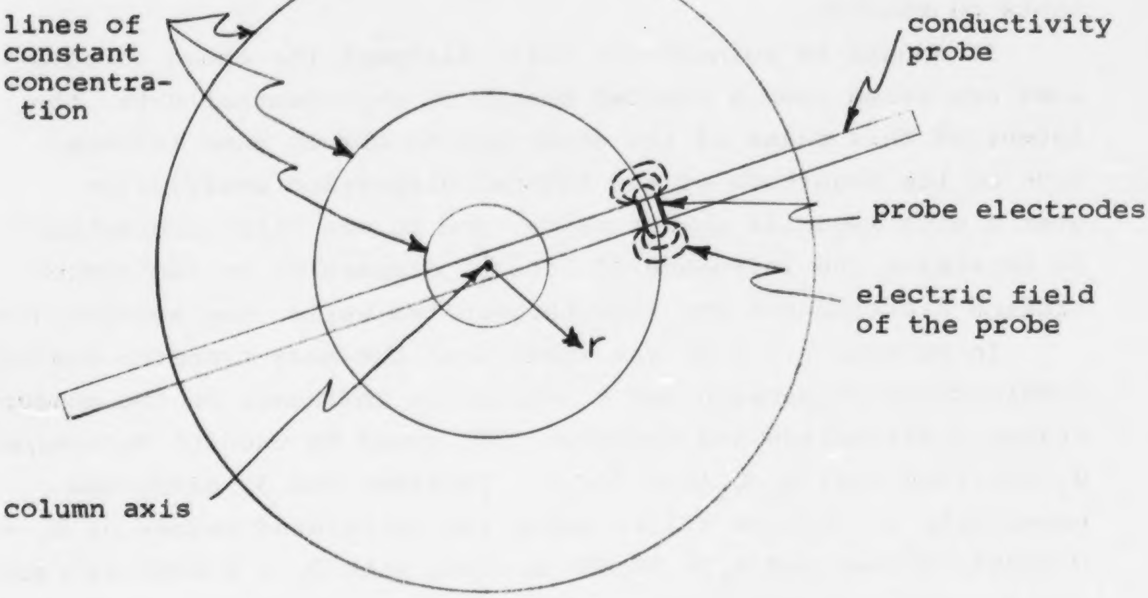
lines of constant concentration
conductivity probe
probe electrodes
electric field of the probe
r
column axis

Figure 3-18 Measurement of Radial Tracer Variation with the Conductivity Probe

Hence, the slope, m, of the measured concentration distributions will be too large. In addition, the error in the slope, m, will be greater for the probe at 4 in. below the injector than for the probe at 34 in. below, because the principal variations in concentration at the probe 4 in. below the injector occur at smaller radii than at the probe 34 in. below. The net result of this measurement error will be to give lateral dispersion coefficients which are too large.

Comparing the results of these experiments with the work of Blackwell [20] on unconsolidated sand (see Fig. 3-15) indicates that the D_2 values obtained in this study are larger by a factor of 2 for Reynolds numbers less than 5. The lateral dispersion coefficients obtained from this investigation appear to agree with the work of Simpson [108] (see Fig. 3-15); however, Simpson's measurements were made in an artificial sandstone which has a pore structure that is different from the unconsolidated sand.

In addition to the comparison of the results of this study with those of Blackwell [20] and Simpson [108], it is interesting to compare the experimental setups used in these three investigations. Simpson [108] measured the steady-state lateral spread of a line source in a two-dimensional (or plane) flow. (This method has also been used by Grane [42] and Rumer [45]). In this study and in the work of Blackwell [20], the steady-state radial spread of a tracer in one-dimensional flow through a column was measured. Blackwell [20] introduced the tracer at the top of the column over an annular area at the column wall, while in this study, the tracer was injected at a point on the column axis. Although different dispersion coefficients have been obtained in the three setups, these differences are due to the consolidated media used by Simpson [108] and the error in probe measurements of this study. Thus, either of these methods may be used to determine lateral dispersion coefficients.

From Figure 3-15, it is apparent that for Reynolds numbers less than about 0.01, the coefficients of lateral and longitudinal dispersion are almost equal and approach the molecular diffusion coefficient of the tracer in the sand medium. In the Reynolds number range, 0.01 to about 5.00, the dispersion coefficients vary with the Reynolds number as given by equations (54), (55), (61), and (62); and the ratio of longitudinal to the lateral dispersion coefficient is

$$\frac{D_1}{D_2} = 15.5\left(\frac{wd_{50}}{\nu}\right)^{0.50} \qquad (63)$$

and

$$\frac{D_1}{D_2} = 120\left(\frac{w\sqrt{k}}{\nu}\right)^{0.50} \qquad (64)$$

Harleman and Rumer [48] for the same Reynolds number range obtained the relationship, $D_1/D_2 = 18.3\left(\frac{wd_{50}}{\nu}\right)^{0.5}$, from tests on spheres. For Reynolds numbers greater than 5.0, however, the ratio of longitudinal to lateral dispersion coefficients will vary with the Reynolds number.

IV. DISPERSION IN RADIAL FLOW AND FLOW BETWEEN TWO WELLS

4.1 Theoretical Developments

4.1.1 General Convective - Dispersion Equation for Two-Dimensional Flows

A tracer introduced into a flow, over an area or at a point, will be moved away from its point of introduction by the combined mechanisms of convection, dispersion, and diffusion. For any two-dimensional flow or flow in a plane, the resulting time and spatial distribution of this tracer can be obtained from the condition that the tracer must be conserved.

Consider a two-dimensional, laminar flow through a porous medium with part of its streamline and equipotential line pattern as shown in Figure 4-1.

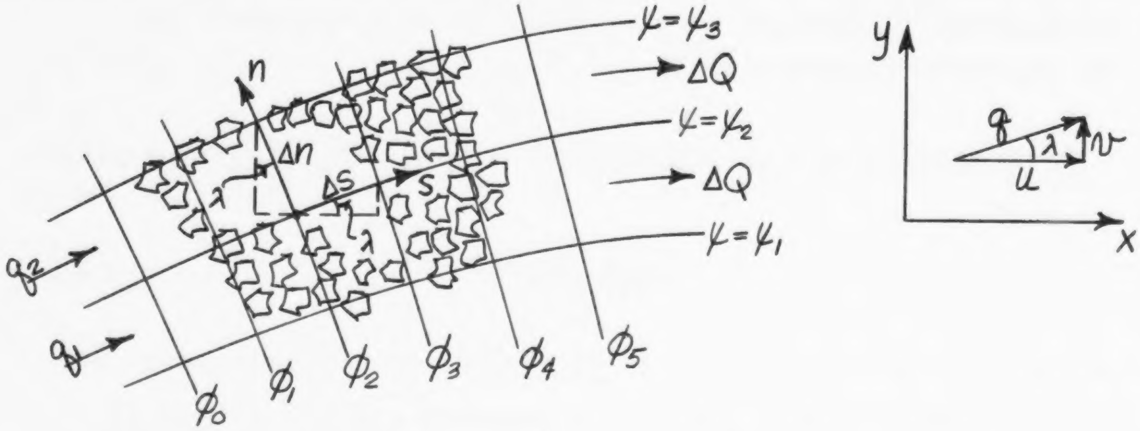
$\psi=\psi_3$
ΔQ
n
$\psi=\psi_2$
Δn
ΔS
S
λ
L
λ
ΔQ
$\psi=\psi_1$
q_2
q_1
ϕ_0
ϕ_1
ϕ_2
ϕ_3
ϕ_4
ϕ_5
y
q
λ
v
u
x

Figure 4-1 Streamline and Equipotential Line Pattern for a Steady, Two-Dimensional Flow

The streamlines, in Figure 4-1, are denoted by ψ = constant, and the equipotential lines are denoted by ϕ = constant. The q_1 and q_2 refer to the average seepage velocity between any two streamlines; the "1" and "2" indicate that the seepage velocity may vary from streamtube to streamtube. The seepage velocity is used in this development since fluid particles move at this velocity rather than the superficial or Darcy velocity. The ΔQ refers to the discharge in any streamtube which is a constant from streamtube to streamtube. Darcy's Law is assumed to govern the flow; hence, the flow satisfies Laplace's equation ($\nabla^2\phi = 0$ and $\nabla^2\psi = 0$), and ϕ and ψ form an orthogonal, curvilinear co-ordinate system. s and n are the orthogonal co-ordinates along the streamlines and equipotential lines, respectively.

For any small volume of thickness Δz, bounded by two streamlines and two equipotential lines, the mass conservation of tracer requirement leads to an equation expressing the balance between the time rate of change of mass within this volume and the net efflux of mass out of the volume due to convection, dispersion, and diffusion. This statement can be expressed mathematically as

$$\frac{\partial}{\partial t}\left(\rho c\, \Delta s \Delta n \Delta z\, \theta\right) + \frac{\partial}{\partial s}\left(\rho c q\, \Delta n \Delta z\, \theta\right) = \frac{\partial}{\partial s}\left[\left(D_1' + \mathcal{D}_m\right)\frac{\partial}{\partial s}(\rho c)\, \Delta n \Delta z\, \theta\right]\Delta s$$
$$+ \frac{\partial}{\partial n}\left[\left(D_2' + \mathcal{D}_m\right)\frac{\partial}{\partial n}(\rho c)\, \Delta s \Delta z\, \theta\right]\Delta n \;+ S \qquad (65)$$

where ρ = density$\left(\frac{\text{mass of solution}}{\text{volume of solution}}\right)$, c = concentration of tracer$\left(\frac{\text{mass of tracer}}{\text{mass of solution}}\right)$, θ = porosity, D_1', D_2', and $\mathcal{D}_m$ are coefficients of longitudinal and lateral dispersion and molecular diffusion, respectively, and S is the rate of gain of tracer within the volume. The fluxes of mass across the area $\Delta n \Delta z \theta$ due to convection and longitudinal dispersion and molecular diffusion along the streamlines are $\rho c q$ and $-(D_1' + \mathcal{D}_m)\frac{\partial}{\partial s}(\rho c)$, respectively. The flux of mass due to lateral dispersion and molecular diffusion transverse to the streamlines is $-(D_2' + \mathcal{D}_m)\frac{\partial}{\partial n}(\rho c)$ across the area $\Delta s \Delta z \theta$. The negative sign in front of the terms expressing the flux of mass due to dispersion and diffusion accounts for the fact that mass is dispersed in the direction of decreasing concentration (negative concentration gradients).

In this study, the tracer is conservative, and S is equal to 0. Also, molecular diffusion is small in conparison to the mechanical mixing of dispersion, and it will be neglected. However, as molecular diffusion may be important in field situations, its influence on the tracer distribution will be treated after the effects of dispersion are considered. If it is assumed that the longitudinal and lateral dispersion coefficients vary linearly with the local seepage velocity, then

$$\begin{aligned} D_1' &= \alpha_1' q \\ D_2' &= \alpha_2' q \end{aligned} \qquad (66)$$

in which α_1' and α_2' are constants and functions of the media structure only. Equation (66), while introduced primarily for analytical convenience, is a good approximation, provided there are not large velocity or Reynolds number variations throughout the flow field (see Fig. 3-15).

Introducing equation (66) into equation (65), setting $S = 0$, and neglecting $\mathcal{D}_m$, gives

$$\frac{\partial(\rho c)}{\partial t}\Delta s \Delta n + \frac{\partial}{\partial s}(\rho c q \Delta n)\Delta s = \frac{\partial}{\partial s}\left(\alpha_1' q \frac{\partial}{\partial s}(\rho c)\Delta n\right)\Delta s + \frac{\partial}{\partial n}\left(\alpha_2' q \frac{\partial}{\partial n}(\rho c)\Delta s\right)\Delta n . \qquad (67)$$

Now, since the streamlines and equipotential lines are solutions of Laplace's equation, their pattern will approximate squares in the x-y plane (i.e., their intersections will be at right angles and the lengths along their sides will be approximately the same). Thus, we have that

$$\Delta s \cong \Delta n \qquad (68)$$

Noting also that $q\Delta n$ = flow through a streamtube, leads to

$$\Delta\psi = \Delta Q = q\Delta n \cong q\Delta s = \text{constant} \qquad (69)$$

for all streamtubes, independent of Δs or Δn. Using equation (69) in equation (67) and replacing the approximately equal sign with an equal sign gives

$$\frac{\partial}{\partial t}(\rho c) + q\frac{\partial}{\partial s}(\rho c) = \alpha_1' q\frac{\partial^2}{\partial s^2}(\rho c) + \alpha_2' q\frac{\partial^2}{\partial n^2}(\rho c) \quad . \qquad (70)$$

Finally, assuming that the density of the fluid and the tracer are both equal and constant, allows equation (70) to be written as

$$\frac{\partial c}{\partial t} + q\frac{\partial c}{\partial s} = \alpha_1' q\frac{\partial^2 c}{\partial s^2} + \alpha_2' q\frac{\partial^2 c}{\partial n^2} \quad . \qquad (71)$$

Equation (71) is the general convective-dispersion equation for plane laminar flows with s and n the co-ordinates along the streamlines and equipotential lines, respectively.

Equation (71) can also be expressed in terms of the streamline and equipotential line functions, ψ and ϕ, directly with the help of the fact that

$$q = \frac{d\phi}{ds} = \frac{d\psi}{dn} \qquad (72)$$

Now,

$$\frac{\partial}{\partial s} = \frac{\partial}{\partial \phi}\cdot\frac{d\phi}{ds} = q\frac{\partial}{\partial \phi}$$

and

$$\frac{\partial}{\partial n} = \frac{\partial}{\partial \psi} \cdot \frac{d\psi}{dn} = q\frac{\partial}{\partial \psi} \qquad (73)$$

Since $d\psi/ds = d\phi/dn = 0$.

Using equation (73) in equation (71) leads to

$$\frac{\partial c}{\partial t} + q^2\frac{\partial c}{\partial \phi} = q^2\frac{\partial}{\partial \phi}\left(\alpha_1' q\frac{\partial c}{\partial \phi}\right) + q^2\frac{\partial}{\partial \psi}\left(\alpha_2' q\frac{\partial c}{\partial \psi}\right) . \qquad (74)$$

Equation (74) is the general convective-dispersion equation for steady, plane flows in terms of the equipotential and stream functions, ϕ and ψ . Equations (71) and (74) have also been given by Bachmat and Bear [3]. They arrived at these equations by first expressing the conservation of mass equation in a general tensorial form, suitable for any co-ordinate system; in the case of plane flows, it reduces to equations (71) and (74). Rumer [45] has given the general convective-dispersion equation for 1,2, and 3 dimensional flows in terms of a cartesion co-ordinate system.

4.1.2 Dispersion in Steady, Radial Flow from a Line Source

4.1.2.1 Description of the Flow Field

The flow field, to be studied here, is generated by a line source, along the z-axis at r = 0, which discharges fluid at a constant rate, Q, into an infinite, homogeneous, and isotropic aquifer. The aquifer is confined by two parallel planes, perpendicular to the z-axis and spaced a distance, b, apart (see Fig. 4-2).

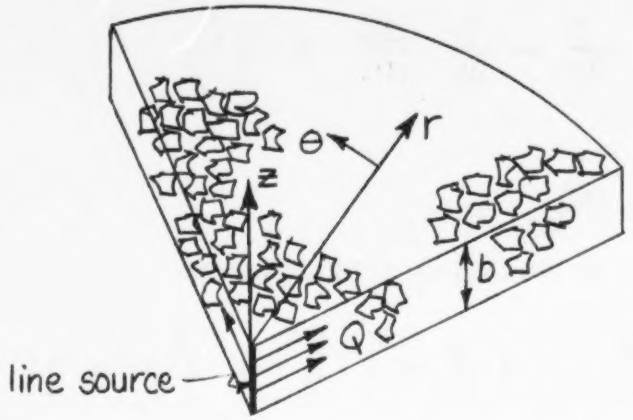

Figure 4-2 Flow Field and Co-ordinate System for Dispersion in Radial Flow from a Line Source

The superficial velocity at any radius, obtained from the continuity equation, is

$$\bar{v} = \frac{Q}{2\pi b r} \quad . \tag{75}$$

Away from the immediate vicinity of the source, the flow will be laminar and governed by Darcy's Law which states that

$$\bar{v} = -K \frac{\partial h}{\partial r} \tag{76}$$

where K is the permeability of the media, h is the piezometric head at any radius, r, and the minus sign accounts for the fact that $\partial h/\partial r$ is negative. Equating equations (75) and (76) gives

$$h_1 - h_2 = \frac{Q}{2\pi b K} \ln \frac{r_2}{r_1} \tag{77}$$

as the head distribution in the aquifer where h_1 and h_2 are the piezometric heads at r_1 and r_2. The seepage velocity (i.e., the average velocity within the pores of the media) is equal to $\bar{V}/\theta$ and from equation (75) we have

$$q_r = \frac{Q}{2\pi b\theta r} = \frac{A}{r} \qquad (78)$$

where q_r is the seepage velocity and $A = Q/2\pi b\theta$. From equation (78) and the definition of a velocity potential and stream function,

$$q_r = \frac{\partial\phi}{\partial r} = \frac{1}{r}\frac{\partial\psi}{\partial\theta} \qquad (79)$$

the expressions for the velocity potential and stream function, based on the seepage velocity, are

$$\begin{aligned} \phi &= A \ln r \\ \psi &= A\theta \end{aligned} \qquad (80)$$

where θ is the angular co-ordinate with limits of 0 to 2π.

4.1.2.2 Convective-Dispersion Equation

The general equation describing the spatial and time distribution of a tracer introduced at the line source (or any other point) is given by equations (71) or (74). These equations can be simplified by expressing them in terms of the r and θ co-ordinates. Letting $s = r$ and $n = r\theta$ in equation (71) and remembering that $q_r = A/r$, gives

$$\frac{\partial c}{\partial t} + \frac{A}{r}\frac{\partial c}{\partial r} = \alpha_1' \frac{A}{r}\frac{\partial^2 c}{\partial r^2} + \alpha_2' \frac{A}{r}\frac{1}{r^2}\frac{\partial^2 c}{\partial \theta^2} \qquad (81)$$

as the convective-dispersion equation for steady, radial flow from a line source. If we assume that the concentration distribution is symmetrical with respect to θ so that no lateral concentration gradients develop, then equation (81) reduces to

$$\frac{\partial c}{\partial t} + \frac{A}{r}\frac{\partial c}{\partial r} = \alpha_1' \frac{A}{r}\frac{\partial^2 c}{\partial r^2} \qquad (82)$$

Equation (82) describes the time and radial distribution of a tracer introduced into a steady, plane flow from a line source. Ogata [71] has obtained a solution to equation (82) in integral form for the case where the tracer is introduced when $t = 0$ at $r = r_w$ (r_w is the well radius), and the concentration of tracer at $r = r_w$ is maintained constant for $t > 0$. This integral solution is too complicated to evaluate analytically and a numerical integration of the integral would be required. For the case of $r_w = 0$ (i.e., a line source), Ogata's result reduces to a simpler integral expression; however, no analytical method was found with which to evaluate the integral. A numerical evaluation of this integral for one value of r (by hand) showed that for very large times, the integral could be simplified; however, for times up to the mean travel time of the tracer to the radius where the distribution was calculated, neither the limits of the integral nor the integral itself could be simplified. Thus, as no way was found to analytically evaluate the integral solutions to equation (82), a numerical solution of equation (82) and several other analytical approaches to solving equation (82) were tried.

Equation (82) was solved numerically using standard finite difference techniques (see Carslaw and Jaegar [25] and Ritchmeyer [88]) and the help of an IBM 7090-4 computer. In order to generalize the results of the numerical solution, equation (82) was first expressed in dimensionless form as

$$\frac{\partial G}{\partial \tau} + \frac{1}{\rho}\frac{\partial G}{\partial \rho} = \frac{1}{\rho}\frac{\partial^2 G}{\partial \rho^2} \qquad (83)$$

where $G = C/C_0$, $\rho = r/\alpha_1'$, and $\tau = At/\alpha_1'^2$. C_0 is the concentration of tracer at the point r = 0 and is assumed to be constant for all time. Though other boundary conditions are possible, the requirement of a constant concentration at r = 0 was relatively simple to accomplish experimentally. To carry out a numerical solution of equation (83), the continuous (ρ, τ) plane is replaced by a grid or mesh of points, spaced $\Delta\rho$ and $\Delta\tau$ apart. At each mesh point, the continuous derivatives in equation (83) are replaced by finite approximations, derived from Taylor series expansions of the relative concentration G about the mesh point (ρ, τ). In this way, the continuous spatial derivatives at a point are expressed in terms of the values of G at that point and its neighboring mesh points for the same time, while the temporal derivative at a point is expressed in terms of the value of G at the point at one time and one time increment later.

Letting the space and time mesh sizes be constants and equal to $\Delta\rho$ and $\Delta\tau$ respectively, then any point in the grid is defined by

$$\begin{aligned} \rho &= m\Delta\rho \\ \tau &= n\Delta\tau \end{aligned} \qquad (84)$$

where m and n are the integers 1,2,3, ...
Thus, the Taylor expansions of G about any mesh point (ρ, τ), become

$$G(\rho+\Delta\rho,\tau) = G_{m+1,n} = G_{m,n} + \left(\frac{\partial G}{\partial \rho}\right)_{m,n}(\Delta\rho) + \frac{1}{2}\left(\frac{\partial^2 G}{\partial \rho^2}\right)_{m,n}(\Delta\rho)^2 + \cdots$$

$$G(\rho-\Delta\rho,\tau) = G_{m-1,n} = G_{m,n} - \left(\frac{\partial G}{\partial \rho}\right)_{m,n}(\Delta\rho) + \frac{1}{2}\left(\frac{\partial^2 G}{\partial \rho^2}\right)_{m,n}(\Delta\rho)^2 - \cdots \tag{85}$$

and

$$G(\rho,\tau+\Delta\tau) = G_{m,n+1} = G_{m,n} + \left(\frac{\partial G}{\partial \tau}\right)_{m,n}(\Delta\tau) + \frac{1}{2}\left(\frac{\partial^2 G}{\partial \tau^2}\right)_{m,n}(\Delta\tau)^2 + \cdots$$

Solving the equations in (85) for the space and time derivatives at the point (ρ,τ) or (m,n), using central differences for the space derivatives and a forward difference for the time derivative, gives

$$\left(\frac{\partial G}{\partial \rho}\right)_{m,n} = \frac{G_{m+1,n} - G_{m-1,n}}{2\Delta\rho}$$

$$\left(\frac{\partial^2 G}{\partial \rho^2}\right)_{m,n} = \frac{G_{m+1,n} + G_{m-1,n} - 2G_{m,n}}{(\Delta\rho)^2} \tag{86}$$

and

$$\left(\frac{\partial G}{\partial \tau}\right)_{m,n} = \frac{G_{m,n+1} - G_{m,n}}{\Delta\tau}$$

Substituting equation (86) into equation(83) and solving for $G_{m,n+1}$ leads to

$$G_{m,n+1} = G_{m,n}\left(1 - \frac{2\Delta\tau}{m(\Delta\rho)^3}\right) + G_{m+1,n}\left(\frac{\Delta\tau}{m(\Delta\rho)^3} - \frac{\Delta\tau}{2m(\Delta\rho)^2}\right) + G_{m-1,n}\left(\frac{\Delta\tau}{m(\Delta\rho)^3} + \frac{\Delta\tau}{2m(\Delta\rho)^2}\right) . \tag{87}$$

Thus, knowing the values of G at all the spatial mesh points, m, for one time, n, the time history of relative tracer concentration, G, can be determined at each mesh point, m, using equation (87). The boundary and initial conditions applied in the computations were

$$\begin{aligned} G(m=0,n=0) &= \tfrac{1}{2} \\ G(m=0,n\geq 1) &= 1 \\ G(m\geq 1,n=0) &= 0 \end{aligned} \qquad . \tag{88}$$

The conditions expressed by equation (88) correspond to a step function being introduced at $\rho = 0$ and $\tau = 0$. Since a step function introduces a discontinuity at $\rho = 0$ and $\tau = 0$, the value of G at $\rho = \tau = 0$ was set equal to 1/2 (a well-known procedure in Fourier Series approximations of discontinuous functions, Crandall [28]). In order for equation (87) to predict the tracer concentration distribution described by equation (83), the mesh size, $\Delta\rho$ and $\Delta\tau$, must be chosen in such a way that equation (87) will be stable (i.e., no oscillations in the numerical solution) and converge to the exact solution of equation (83) (i.e., the difference between the solutions of equations (83) and (87) should be a minimum). Richtmyer [88] has shown that these requirements can be met provided that the coefficients of each of the terms in equation (87) are positive and that their sum is equal to 1. Application of these conditions require that

$$1 - \frac{2\Delta\tau}{m(\Delta\rho)^3} \geq 0$$

and

$$\frac{\Delta\tau}{m(\Delta\rho)^2}\left(\frac{1}{\Delta\rho} - \frac{1}{2}\right) \geq 0 \qquad . \tag{89}$$

The second inequality requires that the space mesh size be

$$\Delta\rho \leq 2 \qquad . \tag{90}$$

Using equation (90) in equation (89) and noting that the worst case occurs when m = 1 (when m = 0, G = 1.0), leads to the condition that the time mesh size must be

$$\Delta\tau \leqslant \frac{(\Delta\rho)^3}{2} \leqslant 4 \quad . \tag{91}$$

Hence, to insure stability and convergence, conditions (90) and (91) must be satisfied by the grid or mesh. As $\Delta\rho$ and $\Delta\tau$ approach 0, the approximations, given by equation (86), become better and the numerical solution approaches the exact solution. However, for very small $\Delta\rho$ and $\Delta\tau$, a great many computations are required to extend the numerical solution to large ρ and τ. To test the influence of mesh size, two numerical solutions of equation (87) were carried out using the conditions of equations (90) and (91). In the first case, $\Delta\rho$ and $\Delta\tau$ were set equal to 1 and 1/4, respectively, while in the second case, $\Delta\rho$ and $\Delta\tau$ were set equal to 2 and 4, respectively.

The results for the first case are plotted in Figure 4-3 for τ = 0, 225, 450, 900, and 1800. For the second case, the numerical solution is plotted in Figure 4-4 for τ = 1856 and 8040. The numerical solution at τ = 1856 with $\Delta\rho$ = 1 and $\Delta\tau$ = 1/4 is also plotted in Figure 4-4. Comparing the two numerical solutions at τ = 1856 shows that the tracer distributions computed with the two different mesh sizes are in close agreement. Thus, for $\tau >$ 2000, the coarser mesh size will give a good approximation to the exact solution of equation (83).

However, for values of $\tau <$ 2000, the differences in shape and time of occurrence of the two numerical solutions become very pronounced. Hence, for $\tau <$ 2000, the smaller mesh size ($\Delta\rho = 1$ and $\Delta\tau = \frac{1}{4}$) must be used to approximate the solution of equation (83). Numerical errors in the computations were kept at a minimum by rounding off values of G in the tenth decimal place and by continuing the calculations for each τ until the values of G at any ρ were less than 10^{-10}. For very small values of ρ, a mesh smaller than $\Delta\rho$ = 1 and $\Delta\tau$ = 1/4 should be used in order to insure a good approximation of

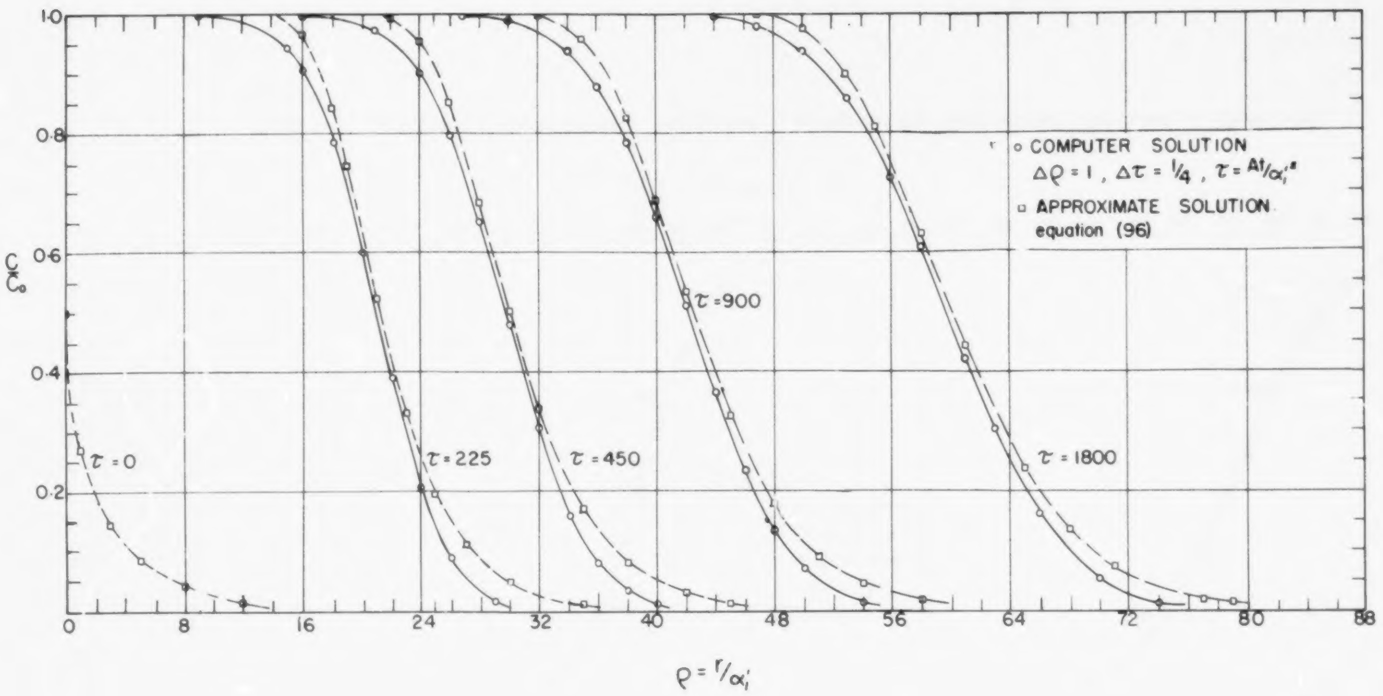

Figure 4-3 Comparison of Numerical and Approximate Solutions for the Concentration Distribution in Radial Flow

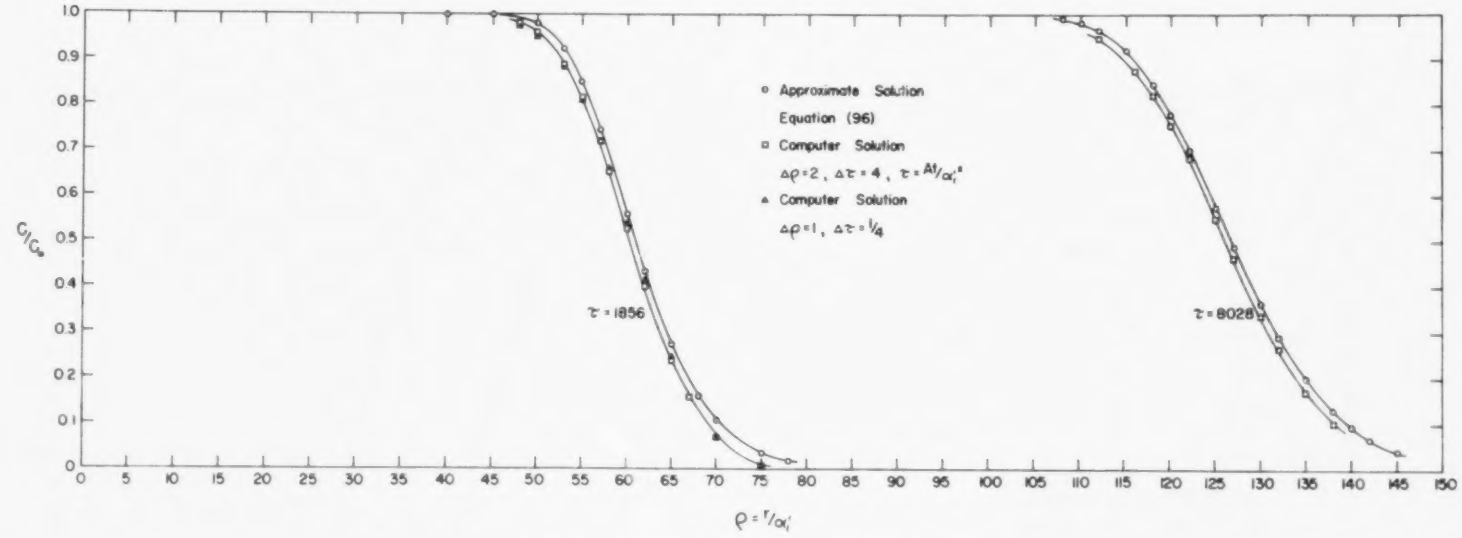

Figure 4-4 Comparison of Numerical and Approximate Solutions for the Concentration Distribution in Radial Flow

equation (83); however, as the errors in the actual tracer concentrations introduced at any τ by the mesh size will be damped within a few time steps (since the numerical solution is stable), and since the tracer distribution very close to the source (r = 0) was not needed in the experimental work, no calculations with a finer mesh size were carried out.

Ogata [77] has also carried out a numerical solution to equation (83) using a finite difference scheme similar to the one used here. However, he makes the assumption that the parameter $\Delta\tau/\rho(\Delta\rho)^2$ or $\Delta\tau/m(\Delta\rho)^3$ (see equation (87)) is equal to a constant. And since he chooses $\Delta\rho$ to be a constant, then $\Delta\tau/\rho$ or $\Delta\tau/m\Delta\rho$ must be constant; thus, as his solution progresses to larger and larger ρ values, $\Delta\tau$ must increase. But, he apparently assumes that $\Delta\tau$ is a constant, since no provision is made for interpolation between successive τ values in his numerical solution. In addition, a comparison of the results of Ogata's numerical calculations with the experimental results of this study and those from Lau's work [65] revealed that Ogata's numerical solution at the same radial co-ordinate as the experimental results, lagged by 50-100% in time and gave more dispersion (i.e., had a flatter slope) than the experimental findings

In addition to the numerical solution of equation (82), several other analytical approaches were investigated; however, only one of these approaches gave a solution which agreed with the experimental findings. This method is based upon a differential equation proposed by Raimondi _et al_ [85] and yields an approximate solution to equation (82). This approach is based upon the assumption that the influence of dispersion (i.e., the term on the right hand side of equation (82)) on the tracer distribution, becomes small in comparison to the local convective effect as the tracer moves away from the source. When the dispersion term in equation (82) is small,

$$\frac{\partial c}{\partial t} \cong -\frac{A}{r}\frac{\partial c}{\partial r}$$

and

$$\frac{\partial}{\partial r} \cong -\frac{r}{A}\frac{\partial}{\partial t} \qquad (92)$$

Now, introducing equation (92) into the dispersion term, $\alpha_1' \frac{A}{r}\frac{\partial^2 c}{\partial r^2}$, in equation (82), changes the spatial gradients to temporal gradients and leads to the expression

$$\frac{\partial c}{\partial t} + \frac{A}{r}\frac{\partial c}{\partial r} = \alpha_1' \frac{r}{A}\frac{\partial^2 c}{\partial t^2} \qquad (93)$$

where the approximately equal sign in equation (92) has been replaced by an equal sign. Raimondi et al [85] give a solution to equation (93) for the case when a tracer is injected at r = 0 for a finite time period. For the continuous injection of a tracer of constant concentration, C_o , at r = 0, their solution can be modified to give

$$\frac{C}{C_o} = \frac{1}{2}\,\mathrm{erf}_c\left[\frac{r^2/2 - At}{\sqrt{4/3\,\alpha_1' r^3}}\right] \qquad (94)$$

for the tracer distribution, where erf_c is an abbreviation for the complementary error function of the quantity in brackets.

The influence of molecular diffusion on the tracer distribution (this becomes important at large distances from the well where the velocities are small) can be accounted for by adding the term $\frac{\mathcal{D}_m}{A^2} r^2 \frac{\partial^2 c}{\partial t^2}$ to equation (93) in which $\mathcal{D}_m$ is the coefficient of molecular diffusion. The solution to the convective-dispersion equation (93), including the influence of molecular diffusion, is given by

$$\frac{c}{c_o} = \frac{1}{2}\,\mathrm{erf}_c\left[\frac{r^2/2 - At}{\sqrt{\frac{4}{3}\alpha_1' r^3 + \frac{\mathcal{D}_m}{A} r^4}}\right] \qquad (95)$$

However, as molecular diffusion has a negligible influence on the tracer distribution in this study (see section 4.4.1.), equation (94) will be used to describe the tracer distributions.

Equation (94) satisfies the boundary conditions (i.e., $c(r = 0,\ t > 0) = c_o$ and $c\ (r = \infty\ ,\ t \geq 0) = 0$; however, it does not satisfy the initial condition, $c(r,\ t = 0) = 0$. When the spatial gradients were changed to temporal gradients in the dispersion term of equation (82), an additional initial condition on $\partial c/\partial t$ was required. In obtaining equation (94), $\partial c/\partial t$ was set equal to zero at $t = 0$. This is true away from the immediate vicinity of the source; however, it is not true very close to the source (within 10 - 20 particle diameters). Thus, the approximate solution predicts a finite amount of mass in the media at $t = 0$. In order to generalize the application of equation (94) to any media and flow rate, equation (94) can be expressed in the dimensionless form

$$\frac{c}{c_o} = \frac{1}{2}\,\mathrm{erf}_c\left[\frac{\rho^2/2 - \tau}{\sqrt{\frac{4}{3}\rho^3}}\right] \qquad (96)$$

where $\rho = r/\alpha_1'$ and $\tau = At/\alpha_1'^2$. Equation (96) has been plotted in Figures 4-3 and 4-4 at the same times or τ values as the numerical solution, discussed previously. From a comparison of equation (96) with the numerical solution, a number of observations and conclusions can be made. In the first place, the approximate solution (96) at any τ predicts that the tracer has moved further into the media than is predicted from the numerical solution. The difference in area, however, between these two solutions is a constant for all τ and is equal to the amount of mass (predicted by the approximate solution (96); see Figure 4-3) present in the media at $\tau = 0$. Also, the slopes (between ± one standard deviation of concentration) of the tracer distributions, predicted by the two solutions at the same τ, are the same. Hence, as the slopes of the two solutions are the same for the same τ and since any error in time between the two solutions decreases as τ increases, the approximate solution (94) or (96) will give a good approximation of the tracer distribution at large τ (for $\tau = 1000$, the time error between the approximate and numerical solutions is 1%; for $\rho = 45$ also).

Lau et al [65], while not obtaining an explicit solution to equation (82), suggested an approximate method by which the spread or standard deviation of the tracer distribution could be estimated. Their approach is based upon the assumptions that (a) the tracer distribution is nearly a normal distribution, and (b) the tracer distribution is the linear sum of two effects - one due to longitudinal dispersion and the other due to the divergence of the streamlines. For a tracer undergoing longitudinal dispersion in uniform flow and for a tracer experiencing steepening concentration gradients in diverging flow with no dispersion, expressions for the change in standard deviation of tracer distribution with radial distance were obtained. These two expressions, when added and integrated, gave

$$\sigma = \sqrt{\frac{2}{3}\alpha_1\left(r - \frac{r_w^3}{r^2}\right)} \qquad (97)$$

as the standard deviation for a tracer in radial, diverging flow with dispersion (r_w is the radius of the well). Comparing equation (97) for the case where $r_w = 0$ with the standard deviation obtained from the approximate solution (94), shows that the two standard deviations have the same value

$$\sigma = \sqrt{\frac{2}{3}\alpha_1 r} \tag{98}$$

provided the dispersion coefficient, α_1', along the radial streamlines is equal to α_1, the longitudinal dispersion coefficient. The relationship of α_1 and α_1' is discussed in section 4.4.1 in connection with the experimental results for radial flow dispersion.

4.1.3 Convective Dispersion Equation for Steady Flow Between a Recharging Well and a Pumping Well in a Confined Aquifer

4.1.3.1 Description of the Flow Field

This flow field can be represented analytically by superposition of the flow fields of a line source and a line sink, discharging at the same rate, Q. In this approach, the wells are assumed to have a zero radius; however, the results are also valid for finite radii wells (see Fig. 4-7 ; for well diameter to well spacing ratios of less than 0.04, the difference in arrival time at the pumping well between a fluid particle leaving the center of the well and the well circumference is less than 0.5%). The line source and sink are located on the x - axis and are spaced a distance $2x_0$ apart (see Fig. 4-5). The flow is assumed to take place in an infinite, homogeneous, and isotropic aquifer. The aquifer is confined by two planes perpendicular to the z - axis and spaced a distance, b, apart. The streamlines, ψ , for this flow [11] are circles of radius $x_0 \operatorname{cosec}(\psi/A)$ with centers on the y - axis at $(0, -x_0 \cot(\psi/A))$. A is called the source or sink strength and is defined as $Q/2\pi b\theta$, where θ is the porosity of the aquifer. The equation for a streamline is

$$\psi/A = \tan^{-1}\left(\frac{2x_0 y}{x_0^2-[x^2+y^2]}\right) . \tag{99}$$

The equipotential lines, ϕ/A, are also circles [117] with radii $x_0 \operatorname{cosech}(\phi/A)$ and centers on the x - axis at ($x_0 \coth(\phi/A)$, 0). The equipotential lines satisfy the equation

$$\phi/A = \tanh^{-1}\left(\frac{2 x x_0}{x_0^2+[x^2+y^2]}\right) . \tag{100}$$

The streamlines and equipotential lines for this flow have been defined in terms of the seepage velocity.

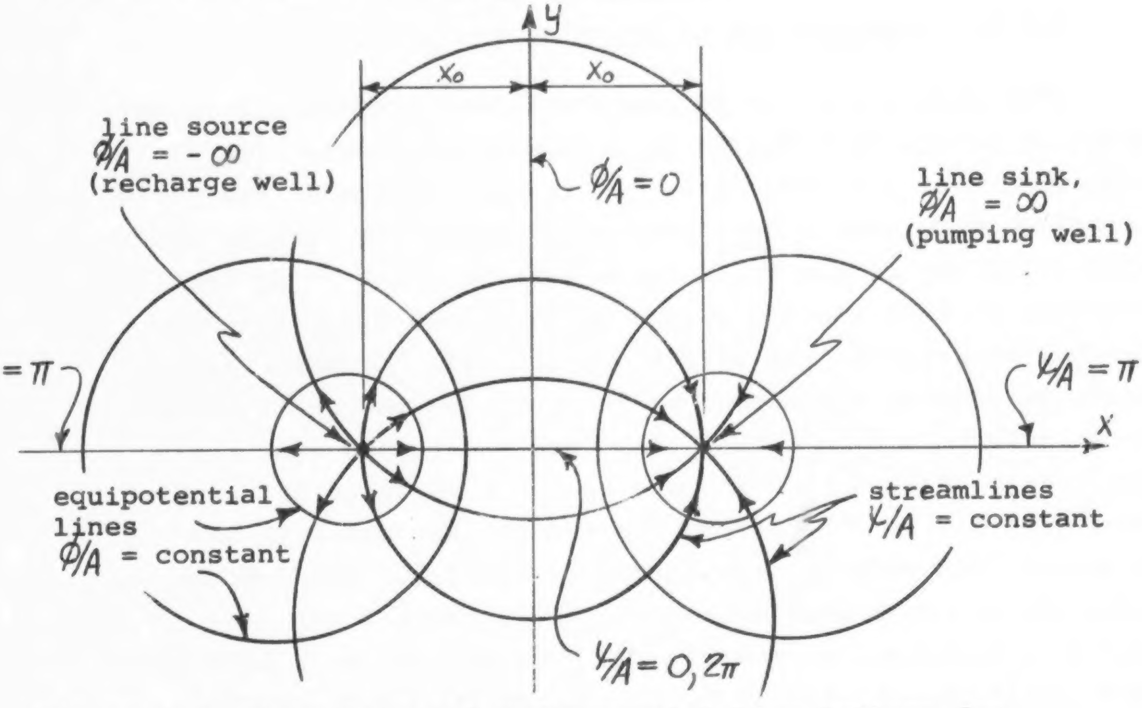
y
x_0
x_0
line source
$\phi/A = -\infty$
(recharge well)
$\phi/A = 0$
line sink,
$\phi/A = \infty$
(pumping well)
$\psi/A = \pi$
$\psi/A = \pi$
x
equipotential lines
ϕ/A = constant
streamlines
ψ/A = constant
$\psi/A = 0, 2\pi$

Figure 4-5 Streamline and Equipotential Line Pattern for Flow between a Line Source and a Line Sink

The flow field produced by the line source and line sink will be assumed laminar except in a small region very close to the source and sink. Thus, the flow throughout most of the aquifer will satisfy Darcy's Law which states that

$$\bar{v} = \theta q = -K \frac{\partial h}{\partial s} \qquad (101)$$

where s is a distance along a streamline, $\bar{v}$ is the average or superficial velocity along a streamline, q is the seepage velocity along a streamline, K is the permeability (a constant throughout the aquifer), and h is the piezometric head at any s. Applying the definition of a velocity potential, $q =$ to equations (101) and (100), we have that

$$\phi = -\frac{Kh}{\theta} = A \tanh^{-1}\left[\frac{2xx_0}{x_0^2 + (x^2 + y^2)}\right] \qquad (102)$$

Thus, by rearranging equation (102), the piezometric head distribution throughout the aquifer is given by

$$h = -\frac{\phi\theta}{K} = \frac{A\theta}{K} \tanh^{-1}\left[\frac{2xx_0}{x_0^2 + (x^2 + y^2)}\right] \qquad (103)$$

The seepage velocity components, u and v, obtained by differentiating the expression for the velocity potential, equation (100), at any point in the flow field, are

$$u = -2Ax_0\left[\frac{(x^2 - x_0^2 - y^2)}{(x^2 - x_0^2 - y^2)^2 + (2xy)^2}\right] \qquad (104)$$

$$v = -2Ax_0\left[\frac{(2xy)}{(x^2 - x_0^2 - y^2)^2 + (2xy)^2}\right] \qquad (105)$$

where u and v are the components in the x and y directions, respectively. Combining equations (104) and (105), the seepage velocity at any point in the flow is

$$q = 2Ax_0\left[\frac{1}{(x^2-x_0^2-y^2)^2+(2xy)^2}\right]^{1/2} . \qquad (106)$$

Using the definitions of the velocity potential, equation (100), and the streamfunction equation (99), the seepage velocity, expressed in terms of ϕ and ψ is

$$q = \frac{A}{x_0}\left(\cosh(\phi/A) + \cos(\psi/A)\right) . \qquad (107)$$

4.1.3.2 Convective - Dispersion Equation

Introducing a tracer at the recharging well or line source gives rise to both longitudinal gradients (along a streamline) and lateral gradients (transverse to a streamline) of tracer concentration. Hence, the general convective-dispersion equation, obtained in section 4.1.1, must be used to describe the spatial and temporal distribution of tracer. This equation can be expressed in terms of two different co-ordinate systems as

$$\frac{\partial c}{\partial t} + q\frac{\partial c}{\partial s} = \alpha_1' q\frac{\partial^2 c}{\partial s^2} + \alpha_2' q\frac{\partial^2 c}{\partial n'^2} \qquad (108)$$

and

$$\frac{\partial c}{\partial t} + q^2\frac{\partial c}{\partial \phi} = q^2\frac{\partial}{\partial \phi}\left(\alpha_1' q\frac{\partial c}{\partial \phi}\right) + q^2\frac{\partial}{\partial \psi}\left(\alpha_2' q\frac{\partial c}{\partial \psi}\right) \qquad (109)$$

where q in equation (108) is a function of s and n' (distances along a streamline and normal to a streamline, respectively) and q in equation (109) is given by equation (107). s and n' can be determined by integrating the velocity, equation (72), along a streamline and along an equipotential line. Thus,

$$s = \int_{-\infty}^{\phi} \frac{d\phi}{q} \bigg|_{\psi=\text{const.}} = \frac{x_o}{\sin(\psi/A)} \left\{ -\sin^{-1}(\cos(\psi/A)) + \sin^{-1}\left[\frac{\cosh(\phi/A)\cos(\psi/A)+1}{\cosh(\phi/A)+\cos(\psi/A)} \right] \right\} \tag{110}$$

$$= \frac{x_o}{\sin(\psi/A)} \left\{ (\psi/A) + 2\tan^{-1}\left[\tan(\psi/2A)\tanh(\phi/2A) \right] \right\} \tag{111}$$

for $0 < \psi/A < 2\pi$,

$$s = \int_{-\infty}^{\phi} \frac{d\phi}{q} \bigg|_{\psi=\text{const.}} = x_o(1 + \tanh(\phi/2A)) \tag{112}$$

for $\psi/A = 0, 2\pi$, and

$$n' = n - m = \int_{\psi_o}^{\psi} \frac{d\psi}{q} \bigg|_{\phi=\text{const.}} = \frac{2}{\sinh(\phi/A)} \left\{ \tan^{-1}\left[\tan(\psi/2A)\tanh(\phi/2A) \right] - \tan^{-1}\left[\tan(\psi_o/2A)\tanh(\phi/2A) \right] \right\} \tag{113}$$

where ψ_o is the streamline along which s is measured and n and m are distances, measured from the $\psi = 0$ streamline to the streamlines ψ and ψ_o.

A complete, analytical solution to the convective-dispersion equation, either equations (108) or (109), was not obtained due to the nature of the variable coefficients in the equations. However, a numerical solution of equation (109) was carried out using finite difference techniques. Limitations on the mesh size (in order to assure convergence of the numerical solution to the actual solution) and interpolation between mesh points, required a large amount of computation time in order to move the tracer only a short distance away from the recharge well. Thus, due to the slow propagation of the tracer distribution in the flow field using finite difference techniques, the numerical solution of the convective-dispersion equation (109) was not carried to completion. However, by neglecting either one or both of the dispersion terms in equations (108) and (109), three very interesting and useful analytical solutions of the convective-dispersion equation were obtained for the following conditions: (a) no dispersion along or transverse to the streamlines (i.e., $\alpha_1' = \alpha_2' = 0$); (b) dispersion along the streamlines but no dispersion across the streamlines (i.e., $\alpha_1' \neq 0$ but $\alpha_2' = 0$); and (c) dispersion transverse to the streamlines but no dispersion along the streamlines (i.e., $\alpha_2' \neq 0$ but $\alpha_1' = 0$). From these three solutions, the relative importance of convection and the two dispersion terms in equations (108) and (109) on the tracer distribution at different times and locations in the flow field can be determined.

(a) Tracer Distribution with No Dispersion

Setting the dispersion terms in equation (109) equal to zero, reduces the convective-dispersion equation to

$$\frac{\partial c}{\partial t} + q^2 \frac{\partial c}{\partial \phi} = 0 \qquad (114)$$

where q is given by equation (107). Equation (114) will be solved for the tracer distribution along any streamline, ψ/A = constant, and for the temporal variation of the tracer distribution at the pumping well. The tracer is introduced at the recharging well as a step function change in concentration; however, the tracer does not disturb the steady-state flow pattern in the aquifer. For these conditions, the tracer distribution, described by equation (114), will satisfy the following boundary and initial conditions:

$$\begin{aligned} &c\left(\phi/A = -\infty,\ 0 \leq \psi/A < 2\pi,\ t > 0\right) = C_0 \\ &c\left(-\infty \leq \phi/A \leq \infty,\ 0 \leq \psi/A < 2\pi,\ t = 0\right) = 0 \quad . \end{aligned} \tag{115}$$

Letting $\tau = At/x_0^2$, $\eta = \phi/A$, and $\xi = \psi/A$, equations (114) and (115) become

$$\frac{\partial c}{\partial \tau} + q'^2 \frac{\partial c}{\partial \eta} = 0 \tag{116}$$

where $q' = x_0 q/A$ and

$$\begin{aligned} &c\left(\eta = -\infty,\ 0 \leq \xi < 2\pi,\ \tau > 0\right) = C_0 \\ &c\left(-\infty \leq \eta \leq \infty,\ 0 \leq \xi < 2\pi,\ \tau = 0\right) = 0 \quad . \end{aligned} \tag{117}$$

Taking the Laplace Transform, defined by

$$\bar{c} = \int_0^\infty c(\eta, \xi = \text{const.}, \tau)\, e^{-p\tau}\, d\tau \tag{118}$$

of equations (116) and (117) gives

$$\frac{d\bar{c}}{d\eta} + \frac{p}{q'^2}\bar{c} = 0 \tag{119}$$

and

$$\bar{c}\left(\eta = -\infty,\ 0 \leq \xi < 2\pi\right) = C_0/p \quad . \tag{120}$$

The complete solution to equation (119), subject to the boundary conditions of equation (120), is given by

$$\bar{c} = \frac{c_0}{p} e^{-\int \frac{p\,d\eta}{q'^2}} = \frac{c_0}{p} e^{-\left[p\csc^2\xi\left(1 + \frac{\sinh\eta}{\cosh\eta + \cos\xi} - \cot\xi \sin^{-1}(\cos\xi) + \cot\xi \sin^{-1}\left[\frac{\cosh\eta\cos\xi + 1}{\cosh\eta + \cos\xi}\right]\right)\right]} \qquad (121)$$

for $0 < \xi < 2\pi$.

For $\xi = 0,\ 2\pi$, the complete solution to equation (119) is

$$\bar{c} = \frac{c_0}{p} e^{-\int \frac{p}{q'^2} d\eta} = \frac{c_0}{p} e^{-\left[\frac{p}{3}\left(1 + (\tanh \eta/2)\left[1 + \frac{1}{\cosh\eta + 1}\right]\right)\right]} \qquad (122)$$

The inverse Laplace Transforms of $\bar{c}$ in equations (121) and (122) can be obtained from Laplace Transform Tables, see [52], in the form

$$\begin{aligned} c &= 0 \quad \text{for } 0 < \tau < a \\ c &= c_0 \quad \text{for } a < \tau \end{aligned} \qquad (123)$$

where

$$a = \csc^2\xi \left\{1 + \frac{\sinh\eta}{\cosh\eta + \cos\xi} - \cot\xi \sin^{-1}(\cos\xi) + \cot\xi \sin^{-1}\left[\frac{\cosh\eta\cos\xi + 1}{\cosh\eta + \cos\xi}\right]\right\} \qquad (124)$$

for $0 < \xi < 2\pi$, and

$$a = \frac{1}{3}\left\{1 + (\tanh \eta/2)\left[1 + \frac{1}{\cosh\eta + 1}\right]\right\} \qquad (125)$$

for $\xi = 0,\ 2\pi$. Equation (123) is the solution to equation (114) for the boundary and initial conditions given by equation (115). This solution predicts that the tracer distribution moves along streamlines, $\xi = \psi/A$ = constant, as a square wave or step function. The front of this step function moves at the mean seepage velocity along the streamline. Thus, a, in equations (123), (124), and (125) is the time required for the tracer, introduced at the recharging well and travelling along a streamline at the seepage velocity, to arrive at any other point along that streamline. The temporal distribution of tracer at the pumping well will not, however, be a step function, since the tracer travel time from the recharge well to the pumping well is different for each streamline. The concentration of tracer in the pumping well at any time, τ , is the average taken over all the streamlines of the tracer concentrations arriving at the well at time, τ ; hence, the pumping well concentration is given by

$$C_p(\tau) = \frac{2\xi(a)}{2\pi} C_o = \frac{\xi(a)}{\pi} C_o \qquad (126)$$

where ξ (a) refers to the streamline with a travel time to the pumping well, a, equal to τ . The travel time, a, from the recharge well to the pumping well, obtained from equations (124) and (125), is

$$a = 2\csc^2\xi\left[1 - \xi\cot\xi\right] \qquad (127)$$

for $0 < \xi < 2\pi$ and

$$a = 2/3 \qquad (128)$$

for $\xi = 0, 2\pi$. Using equations (127) and (128) in equation (126), the tracer distribution at the pumping well for the case of no dispersion was determined; this distribution has been plotted in Figure 4-6.

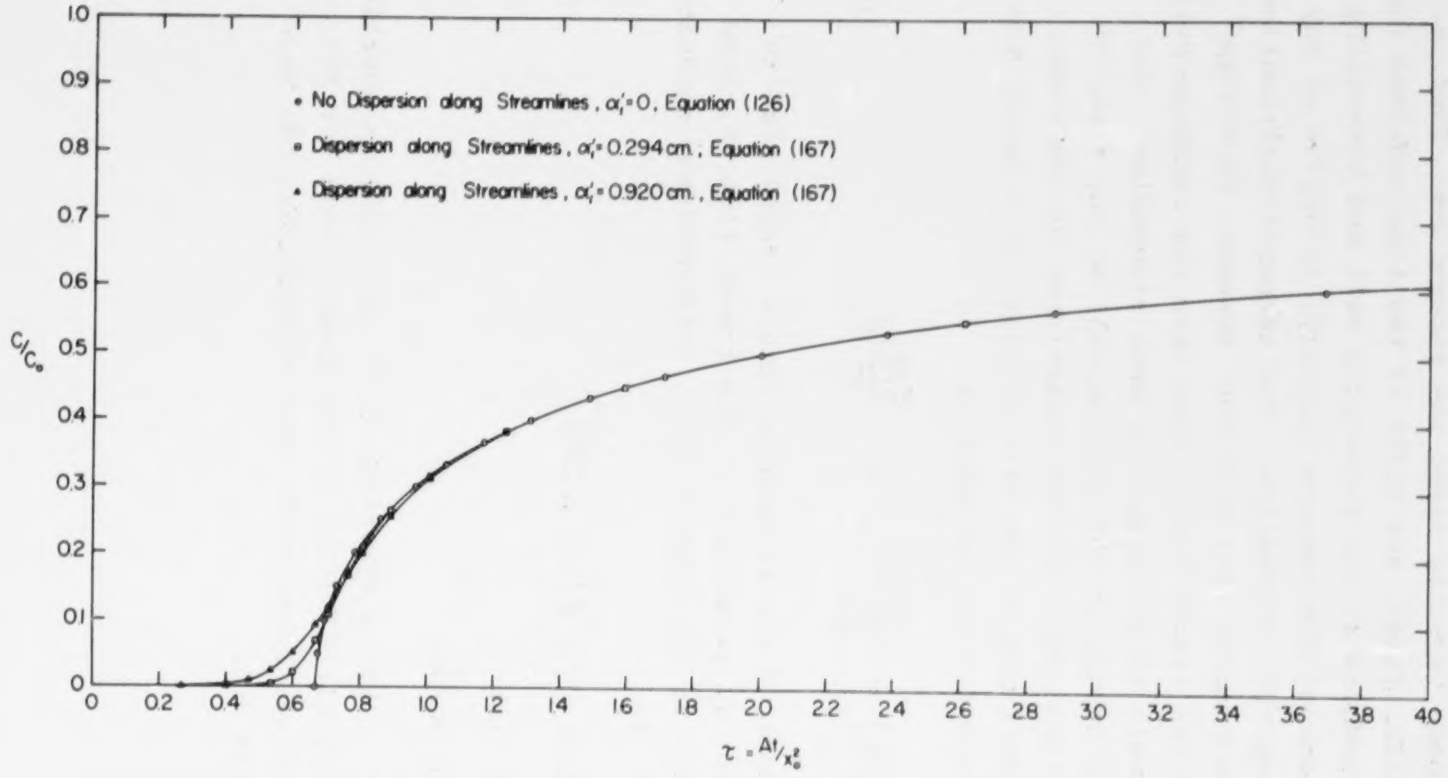

Figure 4-6 Concentration Distribution at Pumping Well with and without Dispersion along Streamlines

(b) Tracer Distribution with Longitudinal Dispersion along the Streamlines

In this case, transverse dispersion across the streamlines is neglected; hence, setting $\alpha_2' = 0$ in equation (109), the convective-dispersion equation reduces to

$$\frac{\partial c}{\partial t} + q^2 \frac{\partial c}{\partial \phi} = q^2 \frac{\partial}{\partial \phi}\left(\alpha_1' q \frac{\partial c}{\partial \phi}\right) \qquad (129)$$

with q = $\frac{A}{x_0}\left(\cosh(\phi/A) + \cos(\psi/A)\right)$. A solution to equation (129) was attempted using the Laplace Transform technique; although a solution to the transformed equation was obtained, no inverse transform for this solution could be found.

Then, since an exact solution to equation (129) was not obtained, a solution of (129) with a modified dispersion term was sought. This approach, used by Raimondi et al [85] to solve the radial dispersion equation (see Section 4.1.2), is based upon the assumption that as the tracer distribution moves away from the vicinity of the recharge well, the influence of dispersion on the tracer distribution becomes small in comparison with the local convective effect. Introducing this assumption into equation (129) gives

$$\frac{\partial c}{\partial t} \cong -q^2 \frac{\partial c}{\partial \phi} \qquad (130)$$

or

$$\frac{\partial}{\partial \phi} \cong -\frac{1}{q^2}\frac{\partial}{\partial t} \qquad (131)$$

Changing the spatial gradients to temporal gradients in the dispersion term, $q^2 \frac{\partial}{\partial \phi}\left(\alpha_1' q \frac{\partial c}{\partial \phi}\right)$, of equation (129), using the assumption of equation (131) leads to

$$\frac{\partial c}{\partial t} + q^2 \frac{\partial c}{\partial \phi} \cong \frac{\partial}{\partial t}\left(\frac{\alpha_1'}{q}\frac{\partial c}{\partial t}\right) \qquad (132)$$

Replacing the approximately equal sign in equation (132) with an equal sign, and using the fact that the flow is steady (i.e., $q = q(t)$), allows equation (132) to be simplified to

$$\frac{\partial c}{\partial t} + q^2 \frac{\partial c}{\partial \phi} = \frac{\alpha_1'}{q} \frac{\partial^2 c}{\partial t^2} \quad . \tag{133}$$

Equation (133) describes the spatial and temporal distribution of the tracer in the flow field, subject to the limitations of the assumption in equation (131). If the tracer is introduced into the steady-state flow as a step function change in concentration at the recharge well, then the tracer distribution must satisfy the following boundary and initial conditions:

$$\begin{aligned} c(\phi/A = -\infty,\ 0 \leq \psi/A < 2\pi,\ t > 0) &= C_0 \\ c(-\infty \leq \phi/A \leq \infty,\ 0 \leq \psi/A < 2\pi,\ t = 0) &= 0 \end{aligned} \tag{134}$$

Applying the Laplace transformation, defined by

$$\bar{c}(\phi, p) = \int_0^\infty c(\phi, t)\, e^{-pt}\, dt \tag{135}$$

to equations (133) and (134) gives

$$p\bar{c} + q^2 \frac{d\bar{c}}{d\phi} = \frac{\alpha_1'}{q} p^2 \bar{c} \tag{136}$$

and

$$\bar{c}(\phi/A = -\infty,\ 0 \leq \psi/A < 2\pi) = \frac{C_0}{p} \tag{137}$$

Equation (136) can be rearranged as

$$\frac{d\bar{c}}{d\phi} + \left[\frac{p}{q^2} - \frac{\alpha_1' p^2}{q^3} \right] \bar{c} = 0 \tag{138}$$

which has a solution

$$\bar{c} = Be^{-ap+bp^2} \tag{139}$$

The quantities a and b in equation (139) are given by

$$a = \int_{-\infty}^{\phi} \frac{1}{q^2}\,d\phi = \frac{x_o^2}{A\sin^2\xi}\left\{1 + \frac{\sinh\eta}{(\cosh\eta+\cos\xi)} - \cot\xi\sin^{-1}(\cos\xi) + \right.$$
$$\left. + \cot\xi\sin^{-1}\left[\frac{\cosh\eta\cos\xi+1}{\cosh\eta+\cos\xi}\right]\right\} \tag{140}$$

and

$$b = \int_{-\infty}^{\phi} \frac{\alpha_1'}{q^3}\,d\phi = \frac{\alpha_1' x_o^3}{2A^2\sin^2\xi}\left\{\frac{\sinh\eta}{(\cosh\eta+\cos\xi)^2} - \frac{3\cos\xi}{\sin^2\xi}\left[1 - \cot\xi\sin^{-1}(\cos\xi)\right] - \right.$$
$$\left. - \frac{3\cos\xi}{\sin^2\xi}\left[\frac{\sinh\eta}{\cosh\eta+\cos\xi} + \cot\xi\sin^{-1}\left(\frac{\cosh\eta\cos\xi+1}{\cosh\eta+\cos\xi}\right)\right] + \frac{1}{\sin\xi}\left[\sin^{-1}(\cos\xi) - \sin^{-1}\left(\frac{\cosh\eta\cos\xi+1}{\cosh\eta+\cos\xi}\right)\right]\right\} \tag{141}$$

for $0 < \xi < 2\pi$ where $\xi = \psi/A$ and $\eta = \phi/A$.
For $\xi = 0, 2\pi$

$$a = \frac{x_o^2}{3A}\left(1 + \frac{\sinh\eta}{(\cosh\eta+1)}\left[1 + \frac{1}{(\cosh\eta+1)}\right]\right) \tag{142}$$

and

$$b = \frac{\alpha_1' x_o^3}{5A^2}\left\{\frac{2}{3} + \frac{\sinh\eta}{(\cosh\eta+1)}\left[\frac{1}{(\cosh\eta+1)^2} + \frac{2}{3(\cosh\eta+1)} + \frac{2}{3}\right]\right\} \tag{143}$$

In order to satisfy the boundary condition of equation (137), the constant B in equation (139) is equal to C_o/p.
Thus, the transformed solution to equation (138) is given by

$$\bar{c} = \frac{C_o}{p}\,e^{-ap+bp^2} \tag{144}$$

with a and b defined by equations (140), (141), (142), and (143).

Rewriting equation (144) as

$$\bar{c} = \frac{c_0}{p}\, e^{-a^2/4b + b(p - a/2b)^2} \qquad (145)$$

and defining a new transform variable r = $p - a/2b$, allows equation (145) to be written as

$$\bar{c} = c_0 e^{-a^2/4b + at/2b}\left(\frac{e^{br^2}}{r + a/2b}\right) \quad . \qquad (146)$$

The inverse transform of equation (146) can be found using the convolution theorem

$$\mathcal{L}^{-1}\left(f_1(r) f_2(r)\right) = \int_0^t F_1(t-\tau) F_2(\tau)\, d\tau \quad . \qquad (147)$$

Letting

$$\left.\begin{aligned} & f_1(r) = \frac{1}{r + a/2b} \quad \text{and} \quad f_2(r) = \frac{1}{\sqrt{4\pi b}}\left(\sqrt{4\pi b}\, e^{br^2}\right), \\ \text{then} \quad & F_1(\tau) = e^{-a/2b\,\tau} , \quad F_1(t-\tau) = e^{-a/2b(t-\tau)} \\ \text{and} \quad & F_2(\tau) = \left(1/\sqrt{4\pi b}\right) e^{-\tau^2/4b} \end{aligned}\right\} . \qquad (148)$$

Combining equations (146), (147), and (148) gives

$$c/c_0 = \frac{e^{-a^2/4b + at/2b}}{\sqrt{4\pi b}} \int_0^t e^{-at/2b + a\tau/2b - \tau^2/4b}\, d\tau \quad . \qquad (149)$$

Simplifying and completing the square in equation (149), leads to

$$c/c_0 = \frac{1}{\sqrt{4\pi b}} \int_0^t e^{-(\tau - a)^2/4b}\, d\tau \quad . \qquad (150)$$

Letting $\eta = \tau - a/\sqrt{4b}$, the integral becomes

$$c/c_0 = 1/2\left(2/\sqrt{\pi} \int_{-a/\sqrt{4b}}^{t - a/\sqrt{4b}} e^{-\eta^2}\, d\eta\right) . \qquad (151)$$

From the definition of the error function, equation (151) can be expressed as

$$c/c_0 = 1/2\left\{\operatorname{erf}\left(a/\sqrt{4b}\right) + \operatorname{erf}\left(t-a/\sqrt{4b}\right)\right\} \quad . \tag{152}$$

Close to the source, it can be shown that $a/\sqrt{4b}$, a, and b $\approx$ 0, and thus, equation (152) reduces to

$$c/c_0 \approx 1/2 \operatorname{erf}\left(t/\sqrt{4b}\right) \quad . \tag{153}$$

As t increases, $c/c_0 \rightarrow 1/2$; at the source, $c/c_0 = 1/2$ for all t. This result violates the boundary condition of equation (134), and equation (152) cannot be applied close to the source. Away from the source, $a/\sqrt{4b}$ increases; for $a/\sqrt{4b} > 2$, erf($a/\sqrt{4b}$) $\approx$ 1. For these conditions, equation (152) becomes

$$c/c_0 = 1/2 \operatorname{erf}_c\left(\frac{a-t}{\sqrt{4b}}\right) \tag{154}$$

which satisfies the boundary condition of equation (134). The restriction on equation (154) of $a/\sqrt{4b} > 2$ can be shown to limit the application of equation (154) to distances greater than $0.04x_0$ (2% of the well spacing) from the source. Thus, equation (154) describes the spatial and temporal tracer distributions along any streamline, resulting from a step function injection at the recharge well, and provided that the observation point is greater than $0.04x_0$ from the source. The quantities a and $\sqrt{4b}$ in equation (154) are equal to the mean travel time (based upon the seepage velocity) for a fluid particle to move from the source to any point along the streamline and the spread of the tracer distribution with respect to the mean travel time, respectively).

Molecular diffusion becomes important for small flow rates, Q, large well spacings, $2x_0$, and along the streamlines $\pi/2 < \psi/A < \pi$ (see Fig. 4-5). Its influence on the tracer distribution can be accounted for by adding the term $\left(\mathcal{D}_m/q^2\right)\frac{\partial^2 c}{\partial t^2}$ to equation (133). The solution to (133), including molecular diffusion, is given by equation (154) in which the quantities

$$\frac{\mathcal{D}_m x_0^4}{7A^3}\left\{\frac{2}{5} + \frac{\sinh\eta}{\cosh\eta+1}\left[\frac{1}{(\cosh\eta+1)^3} + \frac{3}{(\cosh\eta+1)^2} + \frac{2}{(\cosh\eta+1)} + \frac{2}{5}\right]\right\} \tag{155}$$

for $\psi/A = 0,\ 2\pi$ and

$$\begin{aligned}&\frac{\mathcal{D}_m x_0^4}{3A^3\sin^2\xi}\Bigg\{\frac{\sinh\eta}{(\cosh\eta+\cos\xi)^3}+\frac{2}{\sin^2\xi}\Bigg[1+\frac{\sinh\eta}{(\cosh\eta+\cos\xi)}+\cot\xi\Bigg(\sin^{-1}\Bigg[\frac{\cosh\eta\cos\xi+1}{\cosh\eta+\cos\xi}\Bigg]-\\&-\sin^{-1}(\cos\xi)\Bigg)\Bigg]-\frac{5\cos\xi}{2\sin^2\xi}\Bigg[\frac{\sinh\eta}{(\cosh\eta+\cos\xi)^2}-\frac{3\cos\xi}{2\sin^2\xi}\Bigg\{1+\frac{\sinh\eta}{(\cosh\eta+\cos\xi)}+\cot\xi\Bigg(\sin^{-1}\Bigg[\frac{\cosh\eta\cos\xi+1}{\cosh\eta+\cos\xi}\Bigg]-\\&-\sin^{-1}(\cos\xi)\Bigg)\Bigg\}+\frac{1}{2\sin\xi}\Bigg[\sin^{-1}(\cos\xi)-\sin^{-1}\Bigg(\frac{\cosh\eta\cos\xi+1}{\cosh\eta+\cos\xi}\Bigg)\Bigg]\Bigg]\Bigg\}\end{aligned}\tag{156}$$

for $0 < \psi/A < 2\pi$ are added to the expressions for b, given by equations (141) and (143). However, as molecular diffusion is not important in this study (see Section 4.4.2), the expressions for b given by equations (141) and (143) will be used.

In order to apply the results to any combination of well spacing and flow rate, it is convenient to make the argument of the complementary error function in equation (154) dimensionless, using the parameter x_0^2/A. Thus, equation (154) can be written as

$$\frac{c}{c_0} = \frac{1}{2}\,\mathrm{erf}_c\left[\frac{a'-\tau}{\sqrt{4b'}}\right] \tag{157}$$

where $\tau = At/x_0^2$, $a' = aA/x_0^2$, and $b' = bA^2/x_0^4$.

Equations (154) and (157) satisfy the boundary condition of equation (134); however, they do not satisfy the initial condition that c = 0 when t = 0 for $-\infty \leqslant \phi/A \leqslant \infty$ and $0 \leqslant \psi/A < 2\pi$ Changing the spatial concentration gradients to temporal gradients in the dispersion term of equation (129), introduced the requirement for an initial condition on $\partial c/\partial t$ as well as on c. Away from the vicinity of the well (line source), $\partial c/\partial t$ will be very nearly zero at t = 0; however, very close to the well, $\partial c/\partial t$ will not be zero at t = 0(within 10 - 20 particle diameters of the well). Thus, close to the well there will be a finite amount of tracer in the flow field at t = 0. In order to determine the influence of the amount of tracer in the flow field at t = 0 on the tracer distribution at later times throughout the flow field,and to compare the tracer distribution based on the approximate solution (equation (157)) with the tracer distribution subject to exact convective-dispersion equation, (129), a numerical solution of equation (129) was carried out for the $\psi/A = 0$ streamline.

To carry out a numerical solution of equation (129), the method of finite differences was used. In this method, the continuous derivatives are replaced by finite approximations, based upon Taylor series expansions of the tracer concentration about the point (ϕ, t).

Letting

$$\left.\begin{aligned} G &= c/c_0 & q' &= x_0 q/A = \cosh\eta + \cos\xi \\ \tau &= At/x_0^2 & \beta &= \alpha_1'/x_0 \\ \eta &= \phi/A & \xi &= \psi/A \end{aligned}\right\}, \qquad (158)$$

equation (129) can be written as

$$\frac{\partial G}{\partial \tau} + (q')^2 \frac{\partial G}{\partial \eta} = (q')^2 \frac{\partial}{\partial \eta}\left(\beta q' \frac{\partial G}{\partial \eta}\right) \qquad (159)$$

or

$$\frac{\partial G}{\partial \tau} + (q')^2 \frac{\partial G}{\partial \tau} = \beta (q')^3 \frac{\partial^2 G}{\partial \eta^2} + \beta (q')^2 \sinh\eta \frac{\partial G}{\partial \eta} . \qquad (160)$$

From Taylor series expansions of G about any point (η, τ), the spatial and temporal derivatives can be expressed as

$$\left.\begin{aligned} \left(\frac{\partial G}{\partial \tau}\right)_{m,n} &= \frac{G_{m,n+1} - G_{m,n}}{\Delta \tau} \\ \left(\frac{\partial G}{\partial \rho}\right)_{m,n} &= \frac{G_{m+1,n} - G_{m-1,n}}{2\Delta \eta} \\ \left(\frac{\partial^2 G}{\partial \rho^2}\right)_{m,n} &= \frac{G_{m+1,n} + G_{m-1,n} - 2G_{m,n}}{(\Delta \eta)^2} \end{aligned}\right\} . \qquad (161)$$

where the continuous (η, τ) plane (the computations are carried out along a streamline so that ξ = constant) has been replaced by a grid or mesh of points, spaced $\Delta\eta$ and $\Delta\tau$ apart, and each mesh point is given the co-ordinates ($m\Delta\eta$, $n\Delta\tau$). The quantities, m and n, are the integer variables 1, 2, 3, ... Substituting (161) into (160) and solving for $G_{m,n+1}$ gives

$$\begin{aligned} G_{m,n+1} = {} & G_{m,n}\left\{1 - 2\beta(q')^3_{m,n}\left(\frac{\Delta\tau}{(\Delta\eta)^2}\right)\right\} + \\ & + G_{m+1,n}\left\{\beta(q')^3_{m,n}\left(\frac{\Delta\tau}{(\Delta\eta)^2}\right) - (q')^2_{m,n}\left(\frac{\Delta\tau}{2\Delta\eta}\right) + \beta(q')^2_{m,n}(\sinh\eta)_{m,n}\left(\frac{\Delta\tau}{2\Delta\eta}\right)\right\} + \\ & + G_{m-1,n}\left\{\beta(q')^3_{m,n}\left(\frac{\Delta\tau}{(\Delta\eta)^2}\right) + (q')^2_{m,n}\left(\frac{\Delta\tau}{2\Delta\eta}\right) - \beta(q')^2_{m,n}(\sinh\eta)_{m,n}\left(\frac{\Delta\tau}{2\Delta\eta}\right)\right\}. \end{aligned} \tag{162}$$

In order for the finite difference solution (equation (162)) to describe the tracer distribution, $\Delta\eta$ and $\Delta\tau$ must be chosen so that the numerical solution will be both stable (i.e., no oscillations in the results) and converge to the exact solution of equation (129). These two conditions on the numerical solutions will be met provided that the coefficients of each of the G terms in (162) is positive and less than 1, and that the sum of the coefficients is equal to 1 (see Ritchmyer [88]). These requirements give the following conditions:

$$\left.\begin{aligned} \frac{\Delta\tau}{(\Delta\eta)^2} &> \frac{1}{2\beta(q')^3_{m,n}} \\ 0 < \left(\frac{\Delta\tau}{2\Delta\eta}\right)(q')^2_{m,n}&\left\{-1 + \frac{2\beta q'_{m,n}}{\Delta\eta} + \beta(\sinh\eta)_{m,n}\right\} < 1 \\ 0 < \left(\frac{\Delta\tau}{2\Delta\eta}\right)(q')^2_{m,n}&\left\{1 + \frac{2\beta q'_{m,n}}{\Delta\eta} - \beta(\sinh\eta)_{m,n}\right\} < 1 \end{aligned}\right\}. \tag{163}$$

After considering several possible choices of $\Delta\eta$ and $\Delta\tau$, which satisfied the conditions of equation (163), a fixed time increment,

$$\Delta\tau = \frac{9}{4}\beta^2 , \tag{164}$$

and a variable space increment,

$$\Delta\eta = 3(\beta q'_{m,n})^{3/2}, \tag{165}$$

were chosen. The choice of $\Delta\tau$ = constant was made to avoid interpolation along the time scale, and the $\Delta\eta$ was chosen to satisfy equation (163), having fixed $\Delta\tau$. Now, as the line source is located at $\eta = -\infty$, an infinite number of $\Delta\eta$ steps would be required in order to start the solution at the line source. As a result, the numerical solution was started with the boundary condition of (134) applied at a finite η value of -3.79611 instead of $\eta = -\infty$. For a similar reason, the numerical solution was stopped at $\eta = 3.79611$ instead of at the line sink at $\eta = \infty$. These values of η were chosen so that no change in the numerical solution occurred when the boundary condition of (134) was applied for η values less than -3.79611 (i.e., closer to the recharge well). For these η values and $\Delta\eta$ given by equation (165), there were 196 spatial or $\Delta\eta$ steps from the recharging well to the pumping well. The mean travel time from the line source to $\eta = -3.79611$ and from $\eta = 3.79611$ to the line sink is only 0.3% of the mean travel time between the source and the sink, and the change in the slope of the distribution, caused by starting the numerical solution at $\eta = -3.79611$, instead of $\eta = -\infty$ is only 0.02% of the total change in slope from the recharging to the pumping well.

Having selected $\Delta\tau$ and $\Delta\eta$, equation (162) was programmed for numerical solution on the IBM 7090-4 computer using the boundary and initial conditions given by

$$\left.\begin{aligned} G_{0,0} &= G(\eta = -3.79611, t = 0) = \tfrac{1}{2} \\ G_{0,n>0} &= G(\eta = -3.79611, t > 0) = 1 \\ G_{m>0,0} &= G(\eta > -3.79611, t = 0) = 0 \end{aligned}\right\} . \tag{166}$$

These conditions, expressed by equation (166), represent a step function change in tracer concentration at $\eta = -3.79611$, at $t = 0$. Since the step function is discontinuous at $t = 0$, the mean value of the step function on each side of the discontinuity was used at $t = 0$, see Crandall [28].

The results of the numerical solution for the tracer distribution along the $\xi = 0$ streamline are shown in Figure 4-7. In addition, the approximate solution for the tracer distribution, given by equation (157), is also plotted in Figure 4-7, for $\eta = 0$ and $\eta = \infty$. A value of β equal to .0154 was used in each of the solutions. Comparing these two solutions for $\eta = 0$ and ∞ , it can be seen that the two solutions have very nearly the same shape and time history (time differences between the two solutions are about 1.5% for $\eta = 0$ and 0.5% for $\eta = \infty$). Though a comparison was only carried out for the $\psi/A = 0$ streamline, it is expected that the agreement between the approximate and the numerical solution for any other streamline would be as good as for the $\psi/A = 0$ streamline, since the relative influences of dispersion to convection will be approximately the same for all streamlines. Thus, away from the immediate vicinity of the recharging well (i.e., greater than 20 particle diameters), the approximate solution, (157), may be used to predict the tracer distribution along any streamline in the flow field.

The temporal distribution of tracer at the pumping well can be obtained by integrating equation (157) over all the streamlines (i.e., $\xi = 0 \rightarrow 2\pi$) at each time, τ . Thus,

$$\frac{C_p(\tau)}{C_0} = \frac{1}{4\pi}\int_0^{2\pi} erf_c\left[\frac{a'_p-\tau}{\sqrt{4b'_p}}\right] d\xi \quad , \qquad (167)$$

where $C_p(\tau)$ is the pumping well concentration at any τ and a'_p and b'_p are the values of a' and b' at the pumping well. Setting $\eta = 0$ in equations (140), (141), (142), and (143),

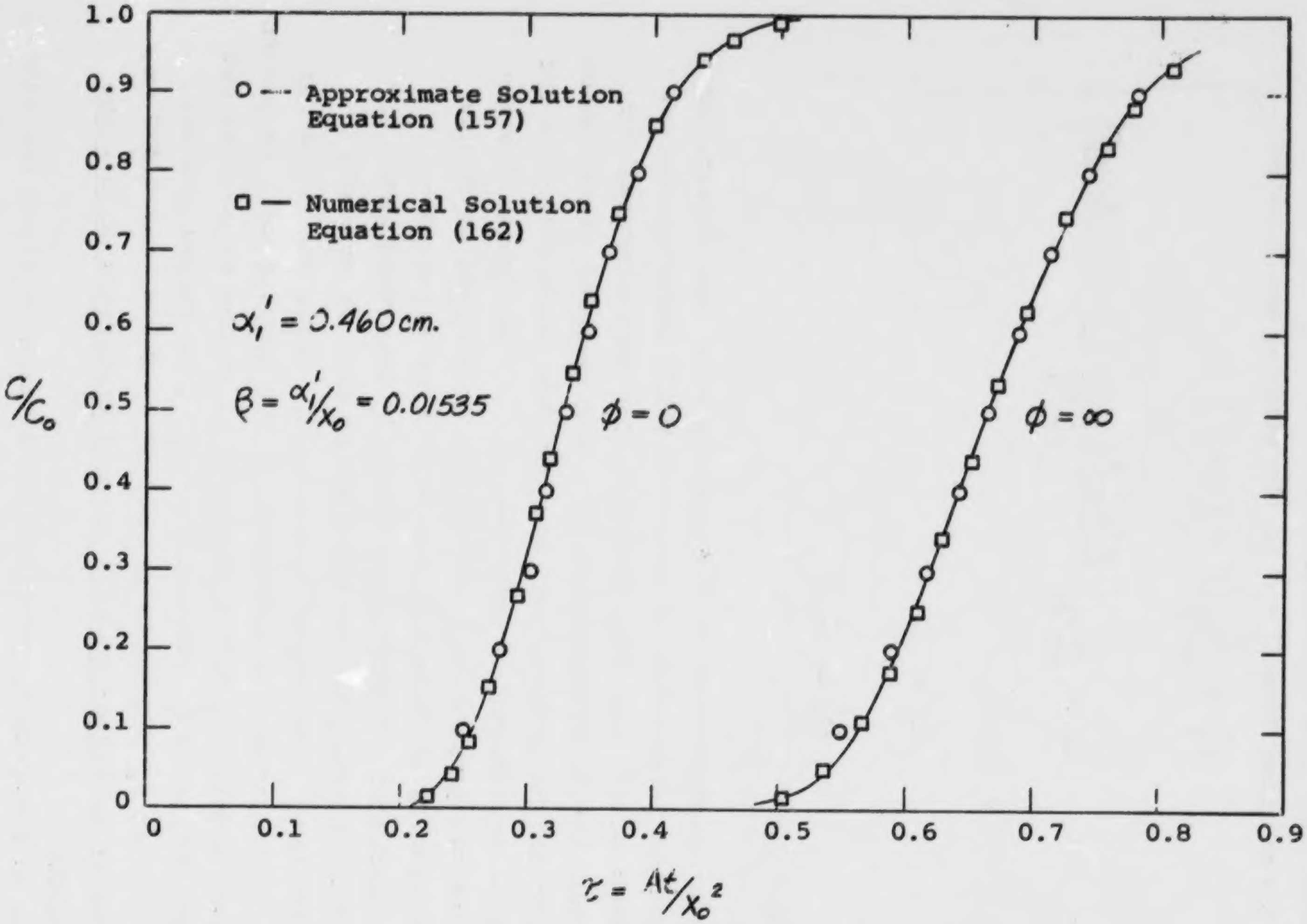

Figure 4-7 Comparison of Numerical and Approximate Solutions for the Concentration Distribution along $\psi = 0$ at $\phi = 0$ and $\phi = \infty$.

and multiplying by 2 (the flow field is symmetrical and hence, the travel time from the recharging well to $\eta = 0$ is the same as the travel time from $\eta = 0$ to the pumping well) gives

$$\left.\begin{aligned} a'_p &= \frac{2}{\sin^2\xi}\left(1-\xi\cot\xi\right) \\ &\text{and} \\ b'_p &= \frac{\beta}{\sin^2\xi}\left[\frac{\xi\left(3\cos^2\xi+\sin^2\xi\right)-3\sin\xi\cos\xi}{\sin^3\xi}\right] \\ &\text{for } 0<\xi<2\pi,\ \text{while} \\ a'_p &= \frac{2}{3} \\ &\text{and} \\ b'_p &= \frac{4}{15}\beta \\ &\text{for } \xi = 0, 2\pi. \end{aligned}\right\} . \quad (168)$$

The tracer distribution at the pumping well was determined by numerical integration of equation (167) using streamline increments of 3° and Simpson's Rule for approximating the area under the distribution curve. The temporal distribution of tracer at the pumping well was not measureably altered for streamline increments of less than 3°. The tracer distribution at the pumping well, $C_p(\tau)/C_0$, is plotted in Figure 4-6 for several different β values. From Figure 4-6, it can be seen that at very small times, τ less than about 0.7, the tracer distribution at the pumping well is strongly dependent upon longitudinal dispersion. While for τ greater than 0.7, the tracer distribution at the pumping well is governed almost completely by convection. It should be pointed out that the choice of β values, $\beta = \alpha'_1/x_0$, in Figure 4-6 was based upon an x_0 of 30.48 cm. and α'_1 = 0.294, and 0.920 cm.

(c) Tracer Distribution with Lateral Dispersion across the Streamlines

In this approach, longitudinal dispersion along the streamlines is neglected; thus, setting $\alpha'_1 = 0$ in equation (109), the convective-dispersion equation simplifies to

$$\frac{\partial c}{\partial t} + q^2\frac{\partial c}{\partial \phi} = q^2\frac{\partial}{\partial \psi}\left(\alpha_2' q \frac{\partial c}{\partial \psi}\right) \tag{169}$$

with $q = \frac{A}{X_0}\left(\cosh\left(\phi/A\right) + \cos\left(\psi/A\right)\right)$ or from equation (108),

$$\frac{\partial c}{\partial t} + q\frac{\partial c}{\partial s} = \alpha_2' q \frac{\partial^2 c}{\partial n'^2} \tag{170}$$

with s and n' defined by equations (111), (112), and (113). Since dispersion along the streamlines has been neglected in equations (169) and (170), these equations predict that the lateral tracer distribution (normal to a streamline) will be established instantaneously when the tracer arrives at any point along the streamline. This fact can be seen more clearly if we introduce the following change of variables

$$\left.\begin{aligned} \gamma &= s \\ \beta &= t - a \end{aligned}\right\} \tag{171}$$

where a is the mean travel time along a streamline from the recharge well to any point s and is defined by equations (140) and (142). In terms of the variables, η and β ,

$$\left.\begin{aligned} \frac{\partial}{\partial t} &= \frac{\partial}{\partial \beta} \\ \frac{\partial}{\partial s} &= \frac{\partial}{\partial \gamma} - \frac{1}{q}\frac{\partial}{\partial \beta} \end{aligned}\right\} . \tag{172}$$

Replacing the derivatives in equation (170), using equation (172), gives

$$q\frac{\partial c}{\partial \gamma} = \alpha_2' q \frac{\partial^2 c}{\partial n'^2} \tag{173}$$

or

$$\frac{\partial c}{\partial \gamma} = \alpha_2' \frac{\partial^2 c}{\partial n'^2} \qquad (174)$$

Thus, since γ = s and since equation (174) is independent of time, equation (174) predicts that the steady-state lateral tracer distribution is established instantaneously after the arrival of the tracer to any point, s, along the streamline. Though in actuality this conclusion is not true (since longitudinal dispersion is not zero), yet a solution to (174) should give an indication of the maximum influence of lateral dispersion on the tracer distribution in the flow field due solely to convection along the streamlines. This conclusion, concerning the instantaneous lateral tracer distribution, can also be obtained by expressing the solution to equation (170) in the form of a product [25]. Thus,

$$c(s,n',t) = c_1(s,t)\,c_2(s,n') \qquad (175)$$

where $c_1(s,t)$ is the solution of

$$\frac{\partial c_1}{\partial t} + q\frac{\partial c_1}{\partial s} = 0 \qquad (176)$$

(i.e., the tracer distribution along the streamlines subject to convection only, equation (123)) and $c_2(s,n')$ is the solution of equation (174) for the steady-state lateral tracer distribution. Equation (175) can be shown to be a solution of equation (170) by direct substitution; in addition, since $c_1(s,t)$ is equal to 0 for $t < a$ (the mean travel time from the source to any point on a streamline), equation (175) predicts that the steady-state lateral tracer distribution, $c_2(s,n')$, will be established instantaneously when $t = a$.

A solution to (174) for the case of an infinitesimal amount of tracer introduced at the source (recharge well) on one streamline leaving the source is given by

$$dc = \frac{dM}{\rho\sqrt{4\pi\alpha_2' s}}\, e^{-\left[n'/\sqrt{4\alpha_2' s}\right]^2} , \qquad (177)$$

where dc is the concentration at any point (s,n') and dM is the increment of tracer introduced at the source along one streamline.

Equation (177) describes the steady-state tracer distribution throughout the flow field resulting from a continuous injection of mass, dM, on one streamline. In addition, equation (177) also describes the instantaneous tracer distribution as seen by an observer moving with the seepage velocity along the streamline on which the tracer was injected (see equation (175)). Hence, for a step function change in concentration (i.e., from c = 0 to $c = c_0$) at t = 0 on all streamlines at the source, the resulting temporal distribution of tracer at any point (s_0 ,n_0') or (ϕ_0, ψ_0) in the field can be obtained by integrating equation (177) over all the streamlines which arrive at the equipotential line ϕ_0 at each instant of time, t. Thus, at the pumping well (sink) the tracer distribution is given by

$$C_p(t) = \frac{\xi(t)}{\pi}\int_{-m(t)}^{m(t)} \frac{c_0}{\sqrt{4\pi\alpha_2' s_p}}\, e^{-\left[n'/\sqrt{4\alpha_2' s_p}\right]^2}\, dm , \qquad (178)$$

where n' = n - m (the lateral co-ordinate of a point relative to its streamline location, m, see equation (113)), s_p is the distance along each streamline location from the recharge well to the pumping well, m(t) is the co-ordinate of the streamline arriving at the well at time, t, and $\xi(t)/\pi$ is that fraction of the tracer, introduced at the recharge well at t = 0, which arrives at the pumping well after a time, t, (assuming no dispersion (see equation (126)).

Since m(t) and n' approach zero at the pumping well for all streamlines, and since the flow field is symmetrical about the line of symmetry between the wells (i.e., $\eta = x = 0$, see Figure 4-5), equation (178) will be integrated along $\eta = x = 0$. In the integration of equation (178), s_p must be expressed as a function of m; however, close to the line joining the two wells ($\psi = y = 0$), s_p is very nearly constant with changes in m at a value of $2x_0$ (the well spacing). Thus, for the region close to $\psi = y = 0$, equation (178) becomes

$$\frac{C_p(t)}{C_0} = \left(\frac{\xi(t)}{\pi}\right)\frac{2}{\sqrt{\pi}}\int_0^{m(t)/\sqrt{8\alpha_2' x_0}} e^{-\mu^2}\,d\mu \qquad (179)$$

where

$$\mu = \frac{n'}{\sqrt{8\alpha_2' x_0}} \ , \ dm = -dn' \ , \text{ and} \int_{-m(t)}^{m(t)} dm = 2\int_0^{m(t)} dm \ .$$

Finally, using the definition of the error function, equation (179) can be expressed as

$$\frac{C_p(t)}{C_0} = \frac{\xi(t)}{\pi}\,\mathrm{erf}\left[\frac{m(t)}{\sqrt{8\alpha_2' x_0}}\right] . \qquad (180)$$

Equation (180) expresses that fraction of the tracer, injected into the flow at the recharge well at t = 0, which arrives at the pumping well after a time, t. However, since s_p was assumed to be constant in the integration of equation (178), equation (180) is valid only for small times (i.e., $t < 0.7\, x_0^2/A$), see equation (127). This restriction on the application of equation (180) to small times is not serious, for, as will be shown in section 4.4.2, α_2' is very small; hence, the greatest influence of lateral dispersion on the tracer distribution is confined to the region close to the line joining the two wells.

4.2 Experimental Equipment and Procedure

4.2.1 Radial and Two Well Flow Equipment

To investigate the validity of the theoretical predictions of the previous section and to determine α_1', the dispersion coefficient along the radial streamlines, a sand model was built and tested. The over-all layout of the model, including the devices for controlling and measuring the flow rate and piezometric head, is shown in Figures 4-8 and 4-9. The model represented a horizontal, confined aquifer with fully penetrating wells along one boundary and a perforated screen around the outer circular boundary. The model shape, a sector of 180°, was chosen in order to take advantage of the fact that the tracer distribution in the two well flow case is symmetrical with respect to the line joining the two wells. The circular boundary and open channel around the outer boundary of the model enabled either a constant head during the radial flow tests, or a variable head distribution (created by causing a flow through the channel) during the two well flow experiments to be maintained on the outer radius. The outer radius of 4'-9" was selected so that in the two well experiments, 75-80% of the tracer leaving the recharge well at $t = 0$ would arrive at the pumping well before the remaining 20-25% of the tracer reached the outer radius. After the tracer reached the outer radius, the tracer boundary conditions would no longer be valid.

The sand was confined between a varnished 3/4 in. thick plywood base and a 1/2 in. thick lucite cover. The plywood base stood about 3-1/2 ft. above the floor and was supported by a wooden and steel frame. The frame was pivoted along one edge so that the model could be tilted on a 10°-20° slope to allow the air to escape when the sand was initially filled with water. A 3/4 in. thick sheet of polyurethane sponge, placed on the plywood base, and a 1/8 in. thick sheet of the same sponge glued to the lucite cover prevented the fluid from short circuiting along the top or bottom boundaries of themodel, and, when compressed by the lucite cover, gave a uniform and dense packing of the sand between the two boundaries. The boundary along which the wells were mounted was varnished 3/4 in. thick plywood with sand particles gluid to it in order to prevent short circuiting of fluid along it. The outer boundary, confining the sand, was a 1/32 in. stainless steel screen with 1/32 in. holes and an open area of about 30% of the total screen area.

The location of the wells in the model is indicated in Figure 4-8, and the details of the well construction and operation are illustrated in Figure 4-10. The wells were made from a 1 in. O.D. brass pipe with a fine mesh brass screen soldered to the pipe over 1/2 of its circumference. The wells extended above and below the boundaries of the model so that connections for supplying water and for inserting a conductivity probe could be made external to the model. A lucite manifold, extending the full depth of the well, rapidly distributed the fluid entering the well over its full length and helped to provide a uniform rate of withdrawal over the depth of the sand layer. The wells were packed with the same sand as in the model in order to reduce the volume of dead space above and below the model and to reduce any influence of differences between the mixing characteristics inside and outside the well on the measured tracer distributions. Conductivity probes, mounted in a slot in the lucite manifold, measured tracer concentrations within the well at a point about mid-depth in the sand model.

The general layout and locations of the piezometer taps and conductivity probes is shown in Figure 4-8. The locations were chosen in order that measurements of both radial and angular variations in the head and tracer distributions could be detected. The piezometer taps were made from 1/4 in. (O.D.) lucite tubes with one open end plugged and a series of radial slots, about 0.020 in. wide x 1/4 in. long, spaced evenly around the tube just inside the plugged end. The tubes were all mounted in the lucite cover of the model such that the slots extended about a 1/2 in. into the sand layer. Each piezometer tap was individually connected by means of a valve to a manifold (see Fig. 4-9). The manifolds, in turn, were connected in series to a micromanometer. In this way, either the absolute head at a point, or the difference in head between any two points, could be determined. Since the tubes in the micromanometer were about 1 in. in diameter, capillary effects were not important. The vernier on the manometer had a least reading of 0.001 in.; however, a slight wobble in the point gage probably reduced the accuracy to the nearest 0.002-0.003 in..

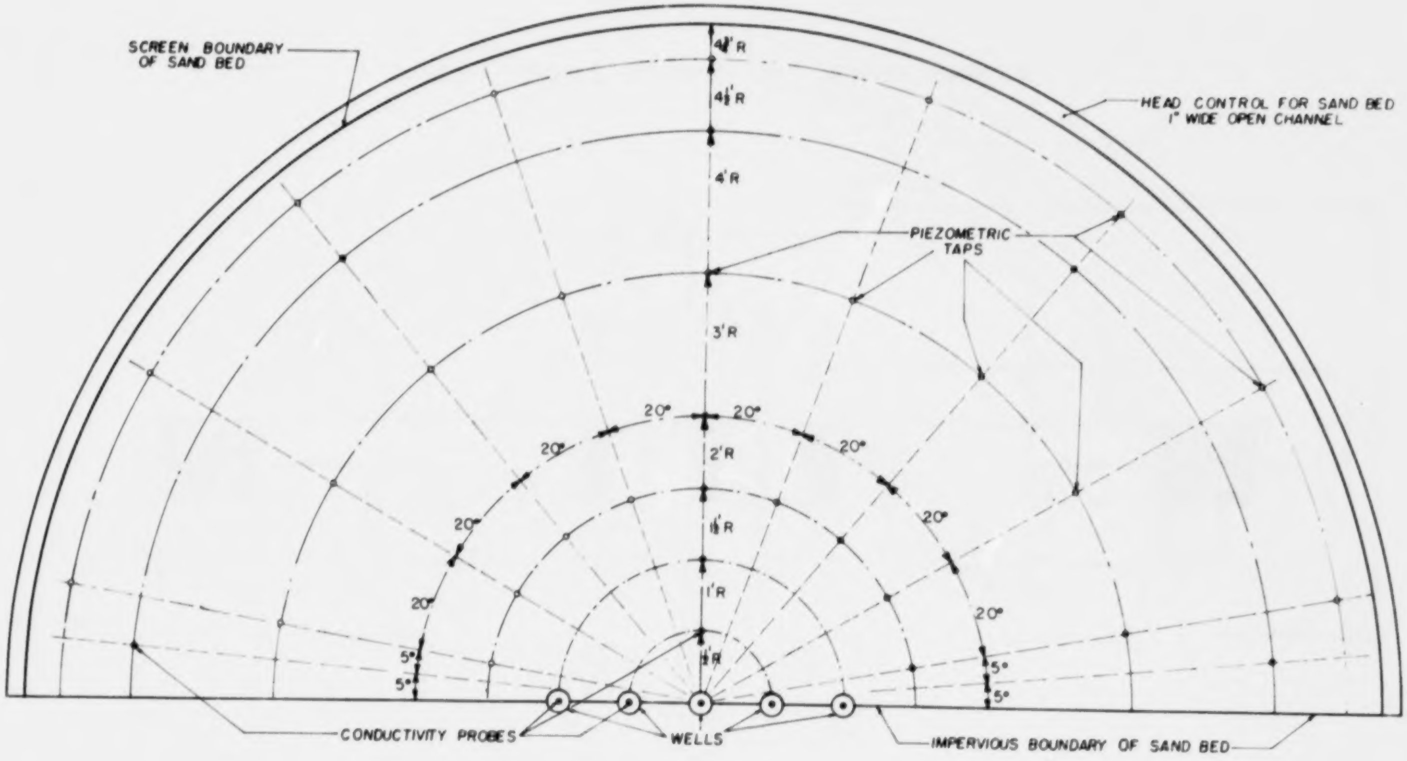
SCREEN BOUNDARY OF SAND BED
HEAD CONTROL FOR SAND BED 1" WIDE OPEN CHANNEL
4¾'R
4½'R
4'R
PIEZOMETRIC TAPS
3'R
20°
20°
20°
20°
20°
20°
20°
20°
20°
20°
2'R
1½'R
1'R
½'R
5°
5°
5°
5°
CONDUCTIVITY PROBES
WELLS
IMPERVIOUS BOUNDARY OF SAND BED

FIGURE 4-8 GENERAL LAYOUT OF WELL RECHARGE APPARATUS

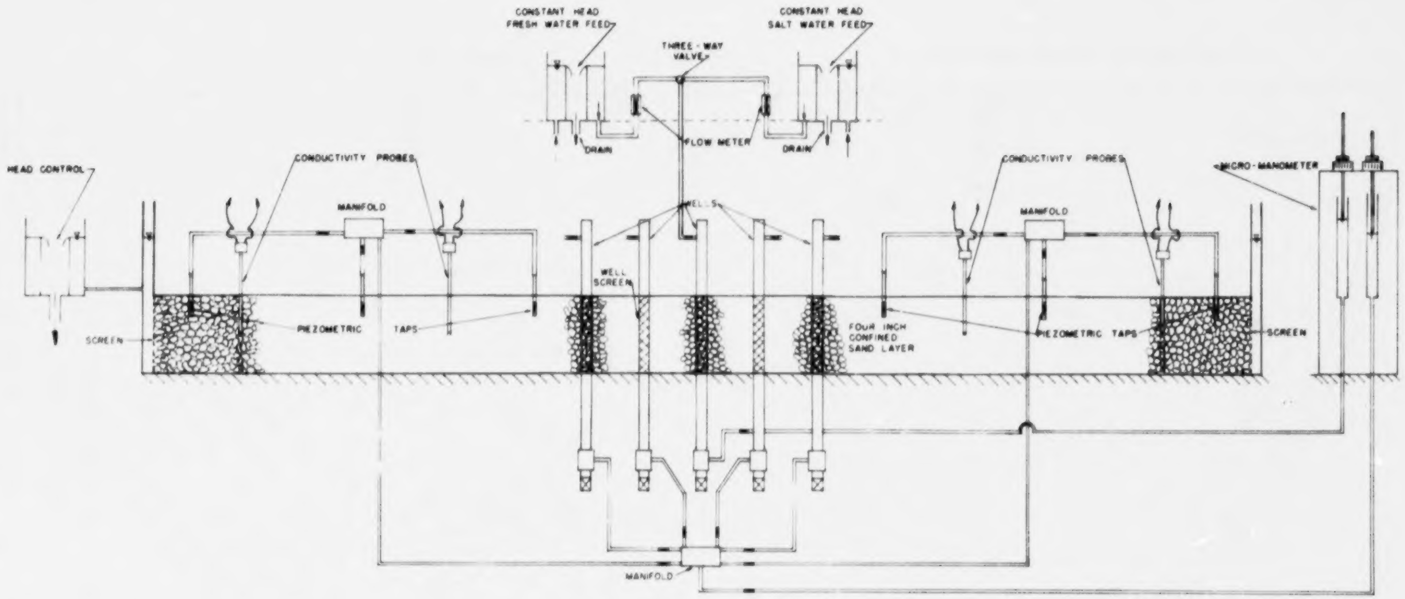

CONSTANT HEAD FRESH WATER FEED
THREE-WAY VALVE
CONSTANT HEAD SALT WATER FEED
FLOW METER
DRAIN
DRAIN
HEAD CONTROL
CONDUCTIVITY PROBES
MANIFOLD
WELLS
CONDUCTIVITY PROBES
MANIFOLD
MICRO-MANOMETER
WELL SCREEN
SCREEN
PIEZOMETRIC TAPS
FOUR INCH CONFINED SAND LAYER
PIEZOMETRIC TAPS
SCREEN
MANIFOLD

FIGURE 4-9 SCHEMATIC SECTION OF WELL RECHARGE APPARATUS

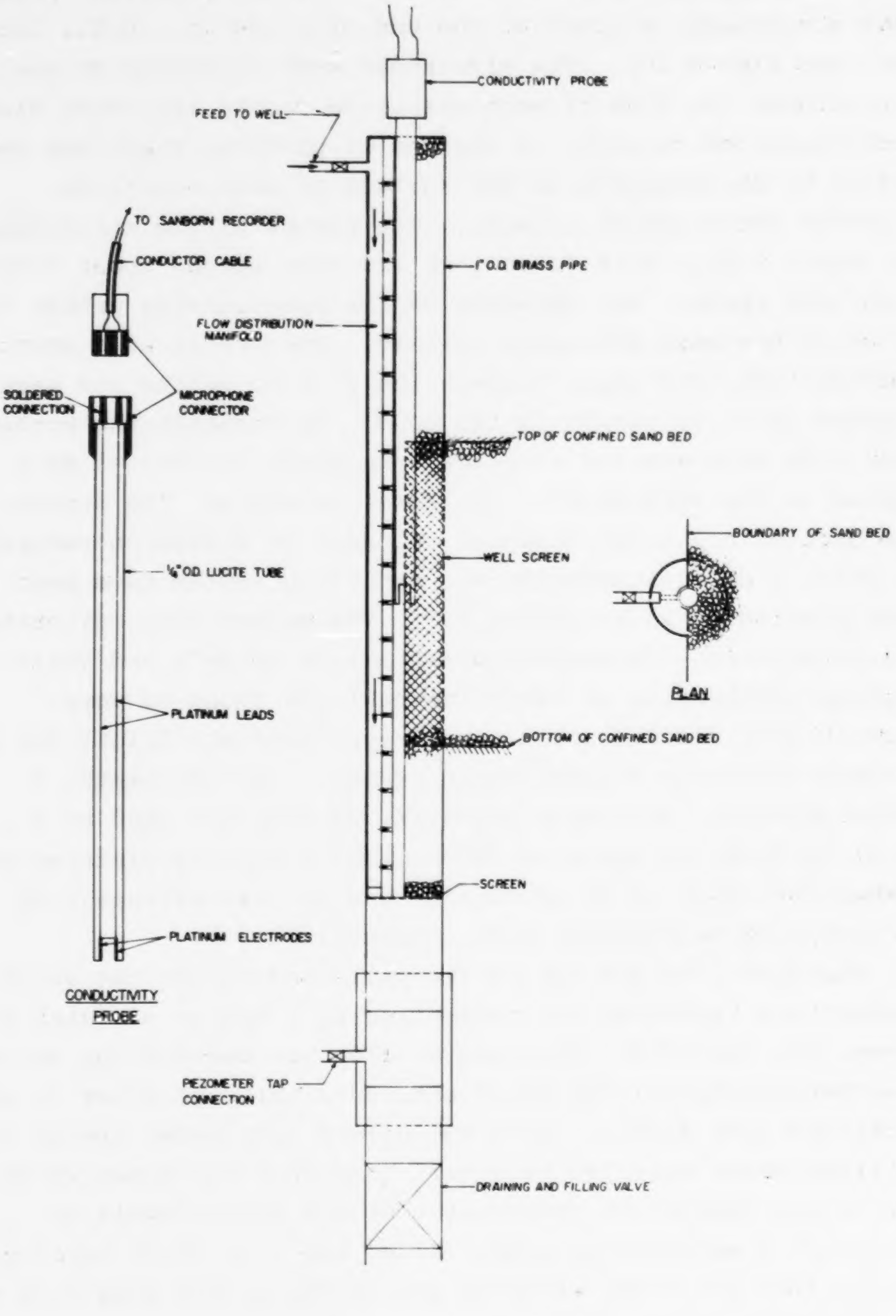
CONDUCTIVITY PROBE
FEED TO WELL
TO SANBORN RECORDER
CONDUCTOR CABLE
1" O.D. BRASS PIPE
FLOW DISTRIBUTION MANIFOLD
SOLDERED CONNECTION
MICROPHONE CONNECTOR
TOP OF CONFINED SAND BED
BOUNDARY OF SAND BED
WELL SCREEN
¼" O.D. LUCITE TUBE
PLAN
PLATINUM LEADS
BOTTOM OF CONFINED SAND BED
SCREEN
PLATINUM ELECTRODES
CONDUCTIVITY PROBE
PIEZOMETER TAP CONNECTION
DRAINING AND FILLING VALVE

FIGURE 4-10 CONSTRUCTION AND OPERATION DETAILS OF THE WELLS AND CONDUCTIVITY PROBES

The conductivity probes consisted of two parallel, platinum plate electrodes, mounted at one end of a 1/4 in., O.D., lucite tube (see Fig. 4-10). The electrodes were insulated on one side so that only the side of each electrode facing the other electrode conducted current. A coating of platinum black was deposited by electrolysis on the surface of each electrode to reduce polarization effects. The plates of the electrodes were about 3/16 x 3/16 of an inch and were spaced about 5/32 of an inch apart. The location of the conductivity probes in the wells has been discussed earlier. The probes were mounted within the sand layer through the plywood bottom and were situated about mid-depth in the sand. By rotating the probes after they were mounted in place, the probe electrodes were aligned in the direction of the local velocity. The probes were excited and their response recorded on a Sanborn recorder, the details of this exciting and recording system have been given previously in section 3.2.1. The probes were calibrated against solutions of known concentrations of NaCl and their response (deflection of recording pen) was found to vary linearly with concentration (up to approximately 0.12%) for a ten-fold change in concentration of NaCl. In the tests, a dilute solution, approximately 0.1%, of NaCl was used as a tracer in order to minimize density and viscosity differences between the fresh water and tracer and to take advantage of the linear probe response with concentration.

The flow into and out of the wells and across the outer boundary was regulated and controlled by a system of weirs and valves, see Fig. 4-9. The rate of flow was measured by means of rotameters before the fluid entered a well and after it was discharged from a well. Both the dilute salt water tracer and the fresh water were fed to a well through a three-way valve. In this way either all fresh water or all tracer would be flowing to a well at any time. Also, the flow could rapidly be changed from all fresh water to all tracer at the same flow rate with only minor effects on the established head distribution within the sand layer. Overflow weirs, located at different points around the outer boundary of the model enabled a constant head to be maintained along the outer boundary in the case of the radial flow experiments. In the case of the two well tests, a variable head distribution around the outer boundary of the model was established by a flow of fresh water from one end of the outer channel to the other. This flow was introduced and withdrawn from the channel through manifolds, and the rate of flow was controlled by constant head reservoirs at each end of the channel.

The sand medium used in the tests was the No. 2, New Jersey Beach sand, used in the longitudinal and lateral dispersion tests. Its mean diameter (d_{50}) was 0.167 cm and its uniformity coefficient (d_{60}/d_{10}) was 1.35. Dry sand was placed in the model in two approximately 2 in. thick layers. Both layers were rodded individually and together to insure a dense, uniform arrangement of the particles. The top of the sand was then leveled at an elevation about 1/8 of an inch above the screen and plywood boundaries. Then the lucite cover was placed on the sand and pulled down into contact with the screen and plywood boundaries. The cover was uniformly pulled down onto the sand by means of beams which ran across the cover and were spaced 1 foot apart. The beams were loaded by tightening tie rods, anchored in the frame of the model and located at each end of the beams. In this way, a uniform thickness and tight packing of the sand layer was obtained. Variations in thickness of the sand layer of about one particle diameter, about 2-3% of the total thickness, were found over the whole model. Due to the dead weight of the sand and the pulling down of the lucite cover, both the top and bottom pieces of sponge would be compressed; however, it was not possible, after putting the cover on, to determine how much compression of either piece of sponge took place. Thus, in order to determine the thickness and porosity of the sand layer, an estimate of the compression of the sponge was made on the following basis:

Since the sponge was very compressible and the piece of sponge attached to the lucite cover was only 1/8 of an inch thick, it was assumed that this piece of sponge would compress to negligible thickness. In addition, since the sand layer was thoroughly rodded to obtain a dense particle packing, it was therefore assumed that, when the lucite cover was pulled down 1/8 of an inch, the sand layer thickness did not change and the bottom piece of sponge was compressed by 1/8 of an inch. Finally, some tests were made of the compression of the bottom piece of sponge under the dead weight of a four inch rodded sand layer. Combining these three assumptions, the average sand layer thickness was found to be 3-1/2 inches. The porosity of the sand packing, estimated from the weight and volume of a 4 inch rodded layer of the same sand, was found to be 0.374.

After the model had been packed with sand and sealed around the edges, the whole model was tilted on a $10^\circ - 20^\circ$ slope and slowly filled with de-aired water which was supplied through the bottom of the wells. When the filling was completed, the model was lowered to its horizontal position, and then the testing program was begun. In all of the tests, de-aired fresh water and de-aired salt water were used in order to prevent any air entrappment within the media.

4.2.2 Radial Flow Testing Procedure

Prior to beginning a dispersion test, a steady flow of fresh water was introduced into the model through the central well, and a constant head was maintained in the outer channel. After a steady-state flow pattern had been established throughout the model, the rate of flow, determined by the rotameter, was recorded. The piezometric head distribution was measured, using the micromanometer, and its measurements were checked to make sure that the head was a constant at different positions on the same radius. The radial variation of piezometric head also was checked by plotting the measurements on semi-log graph paper. Having determined the head distribution, the conductivity probes were connected to the Sanborn recorder and balanced to read zero deflection in the fresh water flow. Probe measurements were made at the central or recharging well, at the two wells situated 12 inches on either side of the center well, and at locations 6, 12, and 24 inches into the media from the center well. As the oscillograph had only 4 recording channels, the probe at 24 inches and one of the probes at 12 inches had to be connected to the Sanborn in place of the probes at the recharge well and 6 inches into the media after the tracer front had moved beyond these locations. With the probes balanced, the 3-way valve was quickly changed to stop the fresh water flow and to start the salt water flow. At the same time, the timer on the Sanborn recorder was started. The salt water flow was measured and was found to be within 1-2% of the fresh water rate of flow for all of the runs. The experimental measurements were continued until the tracer front had moved beyond the probe at a radius of 24 inches. When the tracer measurements were completed, the timer was stopped; however, the salt water flow was maintained. The conductivity probes were rebalanced to read zero deflection in the salt water flow, and another run was begun, following the same procedure as before; in this case, however, fresh water displaced salt water. Experiments were carried out at different flow rates, but, in all cases, the flow rate was adjusted so that the Reynolds number at the edge of the well was less than 6. This limit was placed on the flow rate in order that Darcy's equation would apply throughout the model.

4.2.3 Two Well Flow Testing Procedure

In this phase of the testing program, the experiments were begun by establishing a steady flow of fresh water from the recharging to the pumping well. The rate of flow through both wells was measured and adjusted so that the two flow rates were equal. In addition to the flow between the wells, a steady fresh water flow in the outer channel of the model (see Fig. 4-9) was established in runs 2 and 3 in order that the head distribution throughout the aquifer might more nearly approximate the head distribution due to two wells in an infinite sand layer. The establishment of a steady flow was determined by the constancy of the piezometric head at several points in the aquifer. When equilibrium conditions were established, the piezometric head distribution was measured with the micromanometer and compared to the theoretical head distribution (for a line source and a line sink in an infinite sand layer), calculated using the measured fresh water flow rate into the aquifer from the recharge well. If the measured heads at several points differed by more than 0.002-0.003 inches from the theoretical heads at those same points, the flow in the outer channel was adjusted until the measured and the predicted head distributions were in close agreement.

With a steady flow of fresh water established, the conductivity probes were connected to the recorder and balanced to read zero deflection in the fresh water flow. Probe measurements were made at the pumping and the recharging wells and at radii of 6 and 12 inches into the media along the line midway between the recharging and pumping wells. With the probes balanced, the 3-way valve on the recharging well was quickly changed to start the salt flow and to stop the fresh water flow. At the same time, the timer on the recorder was started. The salt water flow rate was determined from the rotameter reading and found to be slightly smaller (1-2%) than the fresh water flow rate in each of the three runs. Measurements of the tracer distribution at locations within the media were continued until the conductivity probes indicated that the tracer front had moved beyond their locations (i.e., until the tracer concentration was equal to the concentration in the recharge well). At the pumping well, however, the measurements were stopped when the rate of change of the tracer concentration became very small, $c/c_0 \cong 0.7$ (the tracer concentration at the pumping well never reached the concentration at the recharge well because of the continual addition of fresh water, see the two well flow pattern in Figure 4-5). The flow rates were adjusted in these tests so that the Darcy equation would apply throughout the sand model.

4.3 Method of Analysis

4.3.1 Radial Flow Dispersion

In order to determine the dispersion coefficient, α_1' , from the experimental measurements, the approximate solution, equation (94), was used. The assumptions underlying equation (94) were satisfied in the experiments (i.e., the tracer measurement points were located far enough from the recharge well so that $\partial/\partial r \cong -r/A\, \partial/\partial t$ (equation (92)) and $\frac{\partial c}{\partial t} \cong 0$) at t = 0, but close enough to the recharge well so that molecular diffusion had a negligible influence on the tracer distributions); however, a further discussion of this point is given in Section 4.4.1 in connection with a discussion of the results themselves.

If we define new variables

$$\left.\begin{aligned} \xi &= \frac{2At_*}{r^2} \\ \eta &= \frac{8}{3}\frac{\alpha_1'}{r} \end{aligned}\right\} \qquad (181)$$

where $t_* = t - t_{50_r}$; then equation (94) becomes

$$\frac{c}{c_0} = \frac{1}{2}\,\mathrm{erf}_c\left[\frac{1-\xi}{\sqrt{2\eta'}}\right] \qquad (182)$$

(Note: In equation (181), $A = Q/\pi b\theta$, since the flow field was a width of 180°.) The correction, t_{50_r} , was subtracted from all of the time measurements in order to account for the fact that the tracer concentration did not rise instantaneously to c_0 in the recharging well. This correction varied between 8 and 15 sec. and never constituted more than 2% of the travel time to any probe.

Now, for any radial position, η is a constant, and, since the $\mathrm{erf}_c(\;)$ is the integral of the Gaussian probability distribution, a plot of c/c_0 versus $1-\xi$ on arithmetic probability paper will result in a straight line with a standard deviation equal to $\sqrt{\eta'}$. Thus, knowing η , equation (181) can be solved for α_1' , and gives

$$\alpha_1' = \frac{3}{8} r\eta = \frac{3}{8} r\sigma^2 \qquad (183)$$

where σ is the standard deviation, determined from the plot of c/c_0 versus $1-\xi$.

The quantity A in equation (181) can be determined from the tracer distribution at any radius or from the rate of flow, Q, the aquifer thickness, and the porosity ($A = Q/\pi b\theta$). As the aquifer thickness and porosity could not be determined from direct measurement (see section 4.2.1), A was determined from the tracer distribution using the condition that

$$A = \frac{r^2}{2t_{50_*}} \qquad (184)$$

when $c/c_0 = 1/2$ in equation (94). t_{50_*} is the time at which $c/c_0 = 1/2$ at any radius, r, corrected for the time to reach

t_{50} in the recharge well.

The permeability of the packing was determined by using measurements of the head gradient, flow rate, and an estimate of the sand thickness, b, in equation (77). Rearranging (77), we have

$$K = \frac{h_1 - h_2}{Q/\pi b \ln(r_2/r_1)} \qquad (185)$$

where the 2π in (77) has been changed to π since the experimental model has an angular width of 180°. The measurements of piezometric head versus the radial position of measurement were plotted on semi-log paper. From the slope of the line of best fit through the measurements, the quantity $h_1 - h_2/\ln(r_2/r_1)$ was determined and used in equation (185) to calculate K.

A typical radial dispersion test (run #3) and its analysis are presented below to illustrate the method of data reduction. Figure 4-11 shows a plot of c/c_0 versus time at the positions 6, 12, and 24 inches into the media from the recharging well. The values of c/c_0 were read directly from the deflections recorded by the Sanborn since concentration varied linearly with Sanborn deflection. Using the values of t_{50*} at each probe in equation (184), the quantity $A = Q/\pi b \theta$ was determined at each of the three radial positions. Knowing A, r, and t_* for each position, the quantities ξ and $1-\xi$ were calculated and plotted against c/c_0 on arithmetic probability paper, as shown in Figure 4-12. The lines of best fit through the data at 6, 12, and 24 inches, give $\sigma = .166, .115, .081$ at the three positions, respectively; using these σ values in equation (183) gives α_1' values of 0.16, 0.15, and 0.15 cm. at 6, 12, and 24 inches, respectively, from the recharging well. The Reynolds number at each of the three positions was 0.47, 0.23, and 0.12, respectively; the Reynolds number at the well was 5.6.

4.3.2 Dispersion in Flow Between Two Wells

The experimental measurements of the temporal variations of the tracer distribution, at various points within the media, were reduced to a dimensionless form using C_0 (the tracer concentration in the recharge well) and x_0^2/A as a reference concentration and time, respectively. The measurements were then plotted on arithmetic graph paper and compared with the theoretical predictions of equations (126) and (157).

Measurements of the piezometric head distribution in the aquifer were compared with the theoretical head distribution for an infinite layer of sand. The theoretical head distribution was determined from equation (103), using the measured well flow rate and the permeability, determined in the radial flow tests.

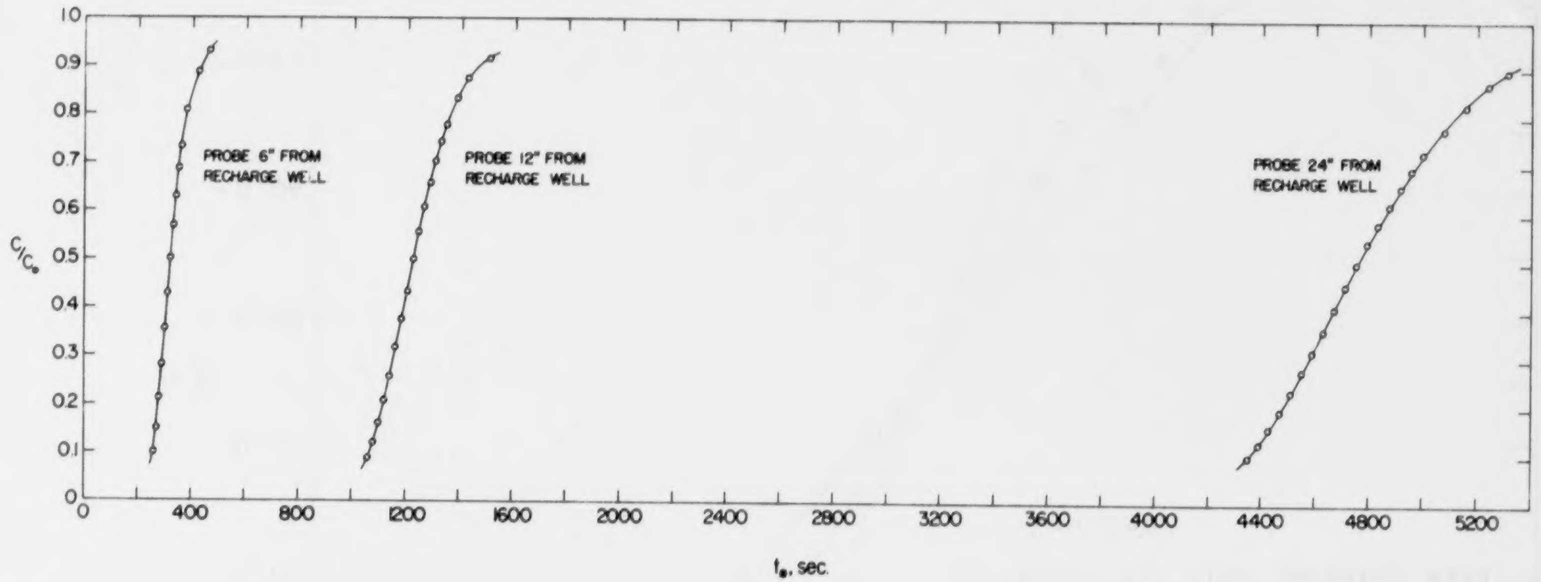

FIGURE 4-11 PLOT OF RELATIVE CONCENTRATION, C/C_o, VERSUS TIME, t_*, FOR THREE RADII IN RADIAL DISPERSION TEST 3

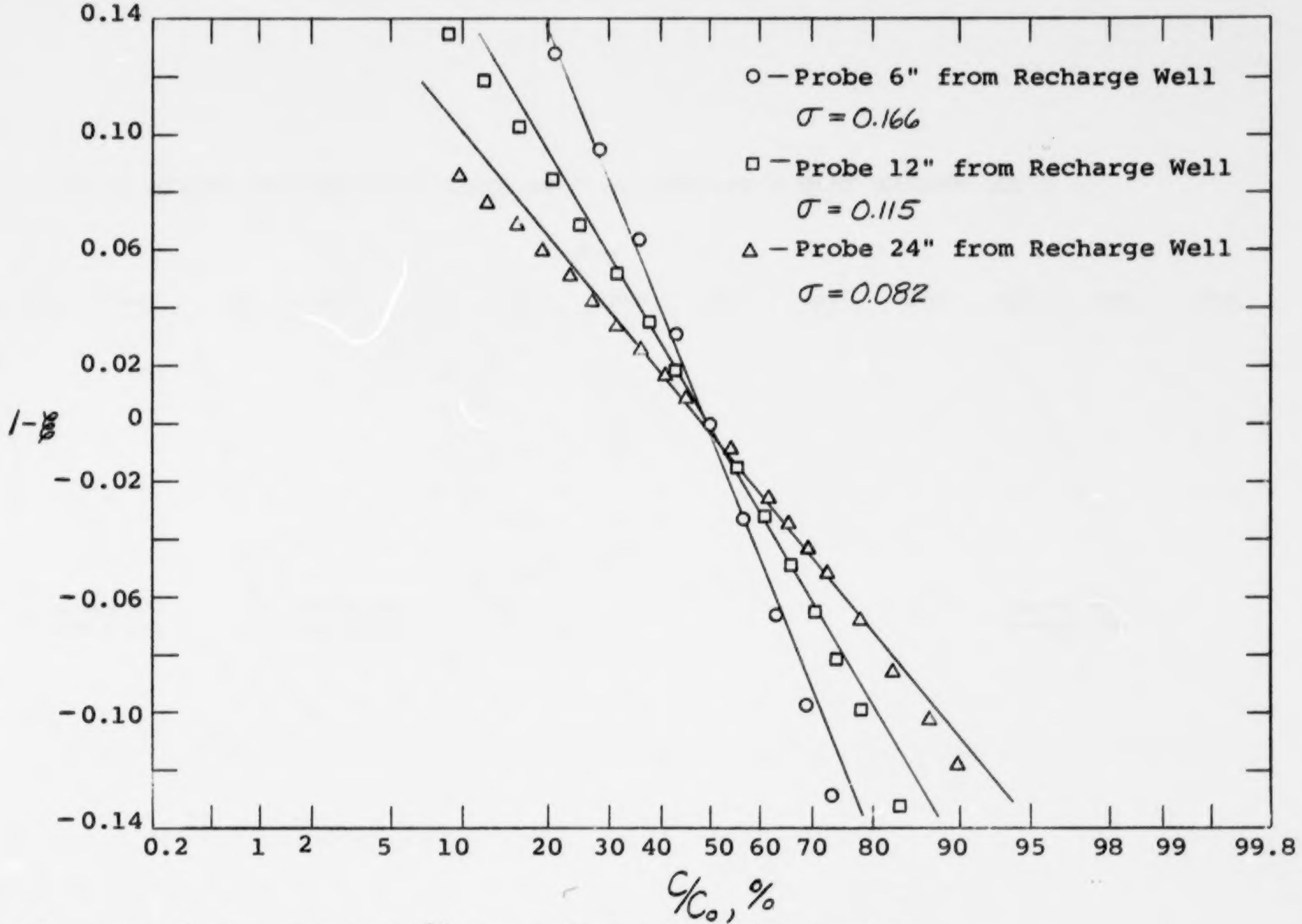

Figure 4-12 Plot of c/c_0 versus $1-\frac{\ell}{\ell}$ for Radial Dispersion Test 3

4.4 Presentation and Discussion of Results

4.4.1 Radial Flow Dispersion

Table III summarizes the radial dispersion constants, α_1', obtained from the experimental investigation along with the flow rates and the properties of the media used in the tests. For the Reynolds number range of this study, the experimental results indicate that α_1' has a constant value of 0.15 cm. independent of the distance from the recharging well (hence the local velocity) and the well flow rate. This average value of α_1' agrees very well with the results from the longitudinal dispersion testing, reported in Section 3.4.1, if n_1 is set equal to 1.0 instead of 1.2 as obtained from the longitudinal dispersion experimental results. Letting

Table 4-1 - Summary of Radial Dispersion Tests

Test	Radial Position from Recharge Well, in.	Q cm^3/sec	$\mathbb{R} = \frac{q_r d_{50}}{\nu}$	α_1' cm	Remarks
1	6	2.82	0.34	0.15	No.2 Sand d_{50}=0.167cm U.C.=1.35= d_{60}/d_{10} θ =0.374 K = 1.87cm/sec k = $1.71\times10^{-5}cm^2$ $\mathcal{D}_m$ =0.95×10^{-5} cm^2/sec
	12		0.17	0.15	
	24		0.09	0.15	
2	6	2.72	0.33	0.16	
3	6	3.82	0.47	0.16	
	12		0.24	0.15	
	24		0.12	0.15	
4	6	3.72	0.45	0.16	
5	6	1.98	0.24	0.15	
	12		0.12	0.14	
	24		0.06	0.15	
6	6	1.90	0.23	0.15	

$n_1 = 1$ also agrees with the theoretical analysis for radial flow dispersion, since it was assumed that the dispersion coefficient along the streamlines varied linearly with the velocity (see Section 4.1.1). Fitting an equation, $D_1/\nu = \psi_1\left(\frac{Wd_{50}}{\nu}\right)$ (see equation (58)) through the data of Rumer, Mehlhorn, and Mohtadullah in Figure 3-15 at a Reynolds number of 1 gives

$$D_1 = 0.86 d_{50} W = \alpha_1 W \qquad (186)$$

The data of Rumer and others has been used since their measurements of the longitudinal dispersion coefficient were made using conductivity probes similar to those of this study. Using the d_{50} of 0.167 cm. for this sand gives

$$\alpha_1 = (0.86)(0.167) = 0.14\,\text{cm} \qquad (187)$$

Thus, since this value of α_1 is very nearly equal to the experimentally determined value of $\alpha_1' = 0.15$ cm, it would appear that the dispersion coefficient along a streamline, D_1, is the same for both uniform and non-uniform flows at the same velocity; hence, experimental results for the longitudinal dispersion coefficient, obtained for uniform flow, can be applied to dispersion problems involving non-uniform flows.

Lau's experimental work [65] on radial flow dispersion indicates that α_1' decreases with distance from the well; however, he points out that sampling errors in the determination of the tracer distribution may have led to this result. His findings indicate that at 9 and 18 inches from the source, α_1' is approximately equal to α_1; however, at 36 inches from the source, α_1' is about 35% less than α_1.

Harpaz and Bear [49] have presented laboratory and field measurements of tracer distributions in radial flow, which were obtained by injecting a salt tracer through a well at a constant rate into a media for a fixed period of time. After this time period, the flow was stopped, and fluid was pumped out of the media at the same rate as it was pumped into the media; during the pumping of the fluid out of the media, the tracer concentration was measured in the well. No analysis of the measurements for the longitudinal dispersion coefficient was given since a numerical solution of the convective-dispersion equation was still being carried out. The solution presented in this study could not be used to analyze their measurements because of the different boundary conditions and the change in sign, due to flow reversal, of the convective term in equation (82).

In the analysis of the experimental results, the approximate solution equation (94) to the radial flow dispersion was used. For run 5, with the minimum flow rate, the mean τ value at the probe 6 inches from the recharge well (i.e., when $c/c_0 = 1/2$) is approximately 5000. For this τ, the numerical solution lags in time the approximate solution by about 1%; thus, any errors introduced through the use of the approximate solution will be very small. At the probes 12 and 24 inches from the recharge well, any errors in arrival time, arising from the use of the approximate solution, will be less than 0.25% and 0.07% respectively.

In addition, molecular diffusion will have a negligible influence on the measured tracer distributions. Consider equation (95); the ratio of the two terms in the denominator of the argument of the complementary error function will give the relative importance of molecular diffusion to radial dispersion. Letting μ be this ratio gives

$$\mu = \frac{\mathcal{D}_m r^4/A}{4/3\,\alpha_1' r^3} = \frac{3}{4}\frac{\mathcal{D}_m r}{\alpha_1' A} \qquad (188)$$

Using the results for run 5 at the probe farthest from the recharge well (α_1' = 0.15 cm, r = 61 cm, A = 0.196 cm^2/sec) gives μ = 0.015. Thus, for the run with the minimum flow rate, the error due to the neglect of molecular diffusion is about 1 1/2% at the probe farthest from the recharge well.

The volume of the dispersed region in the radial displacement process as compared to the volume of fluid recharged can be estimated from the standard deviation of the tracer distribution at any radius. Using ± 2 σ of the mean radius r as a measure of the width of the dispersed zone (the relative tracer concentration, c/c_o , varies from 0.025 to 0.975 in this region), the ratio of the volume of the dispersed region to the volume of the fluid recharged is given by

$$\frac{4\sigma}{r} = \sqrt{\frac{32}{3}\frac{\alpha_1'}{r} + 8\frac{\mathcal{D}_m}{A}} \qquad (189)$$

For the conditions of run 5 at the probe farthest from the recharge well (i.e., r = 61 cm), $\frac{4\sigma}{r}$ = 0.16. Thus, for this radius and flow rate in the model, the volume of the dispersed region is 16% of the total recharged volume.

Though the theoretical predictions developed in this investigation have been applied to the study of radial dispersion in a small sand model, these results may also be applied to field situations. As an example, consider a confined aquifer, 100 feet thick, composed of a fine sand, (d_{50} = 0.001 ft.), which contains small amounts of gravel and silt. The aquifer has a porosity of 0.35 and a permeability of 1000 gal/day/ft^2. (These conditions are typical of the confined aquifer at Manhattan Beach in Los Angeles, California [7] and [115].) For a single 12 inch diameter well, fully penetrating and steadily recharging the aquifer with treated waste water at a rate of 0.7 cfs, the quantity $A = Q/2\pi b\theta$ in equations (78), (94), and (184) will be 2.91×10^{-3} ft^2/sec. The flow in the aquifer will be laminar since the Reynolds number at the well is $\mathbb{R} = \frac{q_r d_{50}}{\nu} = (5.81 \times 10^{-3})(.001)/10^{-5} = 0.6$. α_1', the radial dispersion coefficient, for this sand is 0.0008 ft. (α_1' may be determined from Figure 3-15 using d_{50} or from Figure 3-16 using the permeability).

The relative influence of molecular diffusion to radial dispersion on the distribution of recharged water in the mixed region between the recharged water and the native groundwater is given by $\mu = (3/4)\mathcal{D}_m r/\alpha_1' A$ (equation (188)). For these field conditions, $\mu = 3.53 \times 10^{-3} r$, where r is the radius from the well in feet (a $\mathcal{D}_m$ of 1.08×10^{-8} ft^2/sec was used). At 100 feet from the well, μ is equal to 0.35; whereas, at 1000 feet from the well, μ is equal to 3.5. From these calculations, it is clear that radial dispersion will determine the distribution of recharged water in the mixed zone between the recharged water and the native ground water close to the well ($r <$ 50 - 100 ft for these conditions); whereas, molecular diffusion will govern the distribution of recharged water at large distances from the well ($r >$ 1000 - 2000 ft for these conditions).

The extent of the mixed or dispersed region during recharging can be estimated using equation (189), in which $4\sigma/r$ is the ratio of the volume of the dispersed region to the volume of the fluid recharged. For a point 100 feet from the well, $4\sigma/r$ is equal to 0.011, and at 1000 feet from the well, $4\sigma/r$ is equal to 0.006. Thus, the zone of mixing of the recharged water with the native ground water for this recharging well is confined to a 1 foot region at a radius of 100 feet from the well and a 6 foot region at a radius of 1000 feet from the well.

The values of the sand layer thickness, b, and porosity, θ, obtained by an estimate of the foam rubber compression (see Section 4.2.1) were very close to the values obtained from the dispersion tests. Using the value of $A = Q/\pi b\theta$ obtained from the dispersion curves (see equation (184)) and the flow rate, Q, the average value of the quantity, $\pi b\theta$, from all the radial dispersion tests was found to be 10.16 cm. Using the values of b = 3 1/2 inches and $\theta = 0.374$, estimated in Section 4.2.1, the value of $\pi b\theta$ is 10.45 cm. As the difference between these two calculations of $\pi b\theta$ is only 3%, and since b and θ were determined independently, the estimates of b = 3 1/2 inches and $\theta = 0.374$ should be very close to the actual sand layer thickness and porosity.

Experimental measurements of the dispersion constant, α_1', were carried out with salt water displacing fresh water (tests 1, 3, and 5) and fresh water displacing salt water (tests 2, 4, and 6). For the tests with fresh water displacing salt water, the values of α_1' obtained at 12 inches and 24 inches into the media were 30% and 60% greater, respectively, than the average α_1' value; the α_1' values at 6 inches into the media agreed very well with the average α_1' of 0.15 cm. This increase of α_1' with distance from the recharge well for tests 2, 4, and 6 is apparently due to the density difference between the fresh and salt water. Since the fresh water is slightly less dense than the salt water, and the model is horizontal, a slight overturning may take place during the displacement process. This overturning would increase the slope of the elution curve with distance from the well, and hence, the α_1' value.

With salt water displacing fresh water, tests 1, 3, and 5, the ringed electrode probe (used in the longitudinal and lateral dispersion tests) was inserted in the media and moved from the top to the bottom of the sand layer to determine the vertical distribution of the salt tracer. The measurements indicated that the concentration of the salt tracer at any time and radial position was the same at all depths in the sand layer.

Measurements of the displacement process were also made with probes in the two wells, 12 inches on either side of the recharging well (see Fig. 4-9). However, as the tracer distributions measured by these two probes both lagged the distribution measured by the probe 12 inches into the media and gave greater α_1' values than it, the results of the probes in these two wells were not used. The different result for the probes in the wells 12 inches on either side of the recharging well, as compared to the probes in the media, was due to the fact that these probes within the wells are partially sheltered by the manifolds within the wells (see Fig. 4-10). As a result of this sheltering, the flow velocity between the electrodes of these probes is less than the flow velocity at that same radius in the media. Hence, the response of these probes within the wells lags the response of the probe in the media at the same radius.

The piezometric head before and during each of the tests was essentially constant at all angular positions on each radii. The maximum variations of head were 0.002 to 0.003 inches between any two angular positions on the same radius.

4.4.2 Dispersion in Flow Between Two Wells

The tracer and piezometric head distributions for the three experimental runs are presented in Figures 4-13 through 4-21. For comparison, the piezometric head distribution, arising from the flow between a line source and a line sink in an infinite field, equation (103), is also given. In addition, the tracer distribution at each of the conductivity probes is compared with the theoretical distribution, given by equations (157) and (167), which neglect the influence of lateral dispersion.

Lateral dispersion will tend to retard the rate of increase of the tracer at a measuring point within the media or in the pumping well; however, since the coefficient of lateral dispersion is small, in comparison to the longitudinal dispersion coefficient ($D_2'/D_1' = 1/16$ at $\mathbb{R} = 1$), the influence of lateral dispersion on the tracer distribution can be neglected. Consider the tracer distribution at the pumping well, defined by the equation

$$\frac{C_p(t)}{C_0} = \frac{\xi(t)}{\pi} \operatorname{erf}\left[\frac{m(t)}{\sqrt{8\alpha_2' x_0}}\right] \qquad (180)$$

where erf $\left[m(t)/\sqrt{8\alpha_2' x_0}\right]$ represents the influence of lateral dispersion. Now, as the erf (2) is equal to 0.995, lateral dispersion will have a negligible influence on the tracer at the pumping well for

$$m(t)/\sqrt{8\alpha_2' x_0} \geqslant 2 \qquad (190)$$

In the development of the differential equation describing the tracer distribution, it was assumed that the lateral dispersion coefficient varied linearly with the velocity (equation (66)). Hence, in order to determine α_2' , let us fit an equation

$$\frac{D_2}{\nu} = \psi_2\left(\frac{w d_{50}}{\nu}\right) \qquad (191)$$

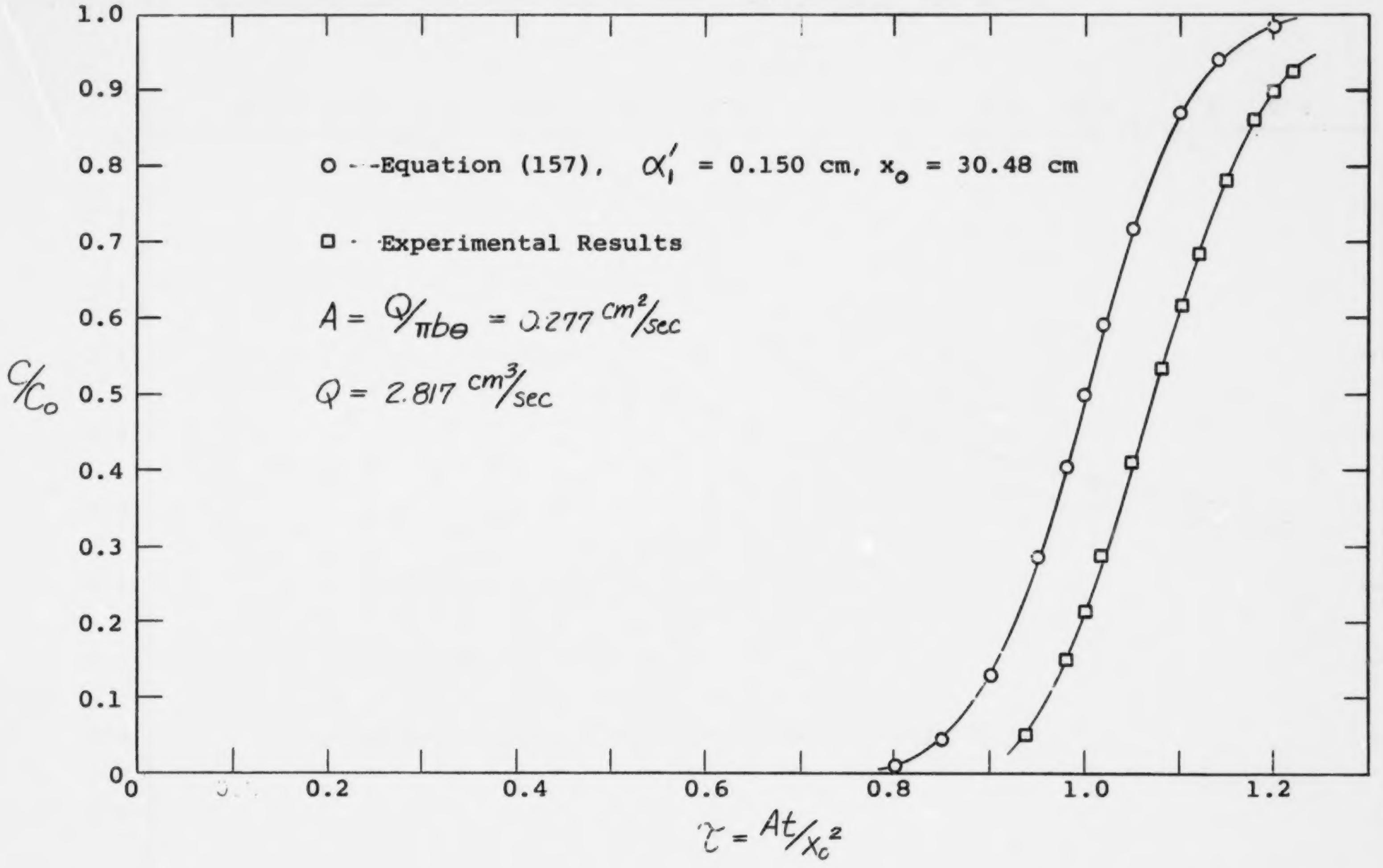

Figure 4-13 Concentration Distribution on Line of Symmetry between the Wells for Run I

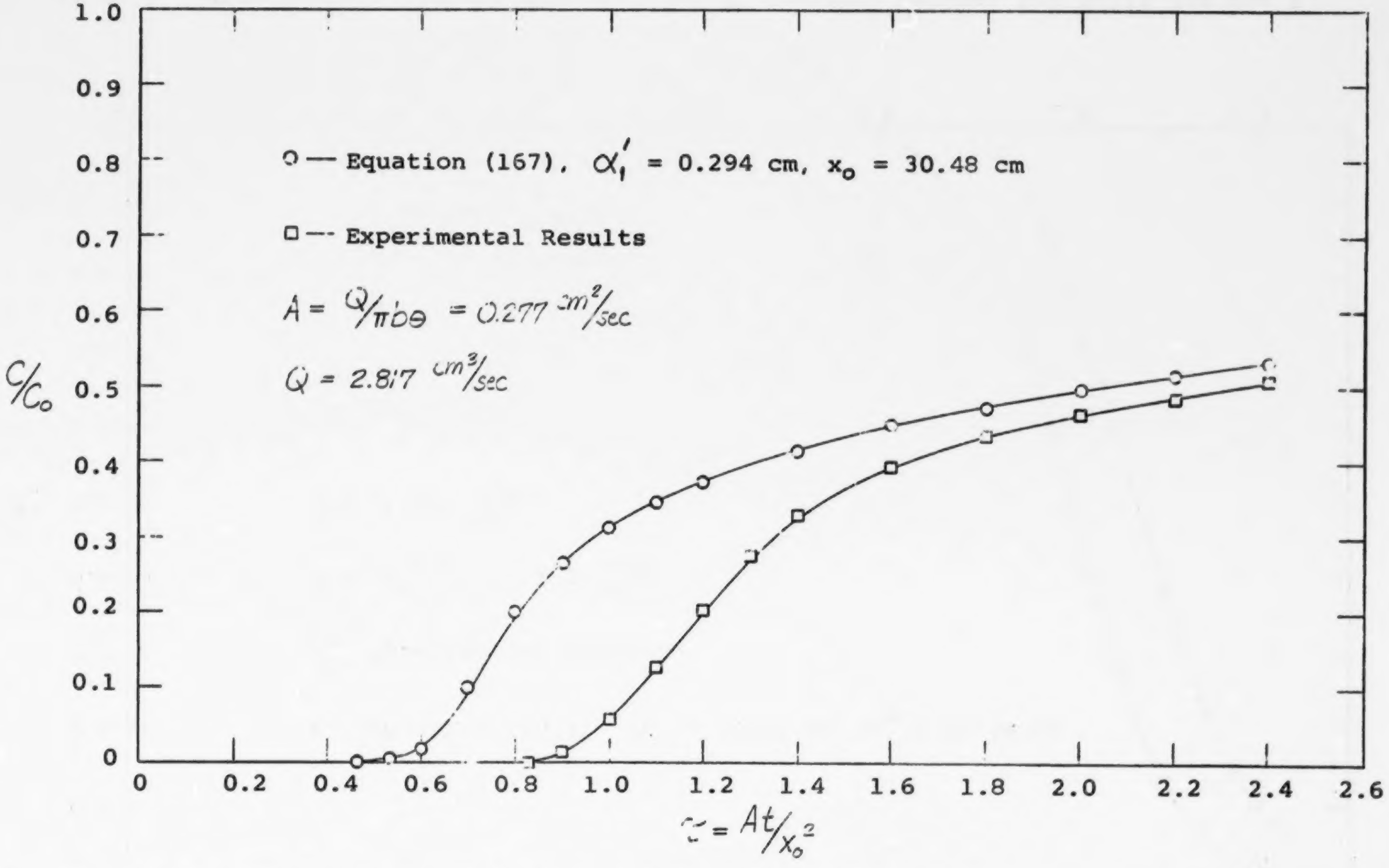

Figure 4-14 Concentration Distribution at the Pumping Well for Run I

The upper number at each piezometer tap is the theoretical differential head for an infinite sand layer, based upon the measured well flow rate, inches. The bottom number at each piezometer tap is the measured differential head, inches.

The differential head is determined with respect to the head on the line of symmetry between the two wells.

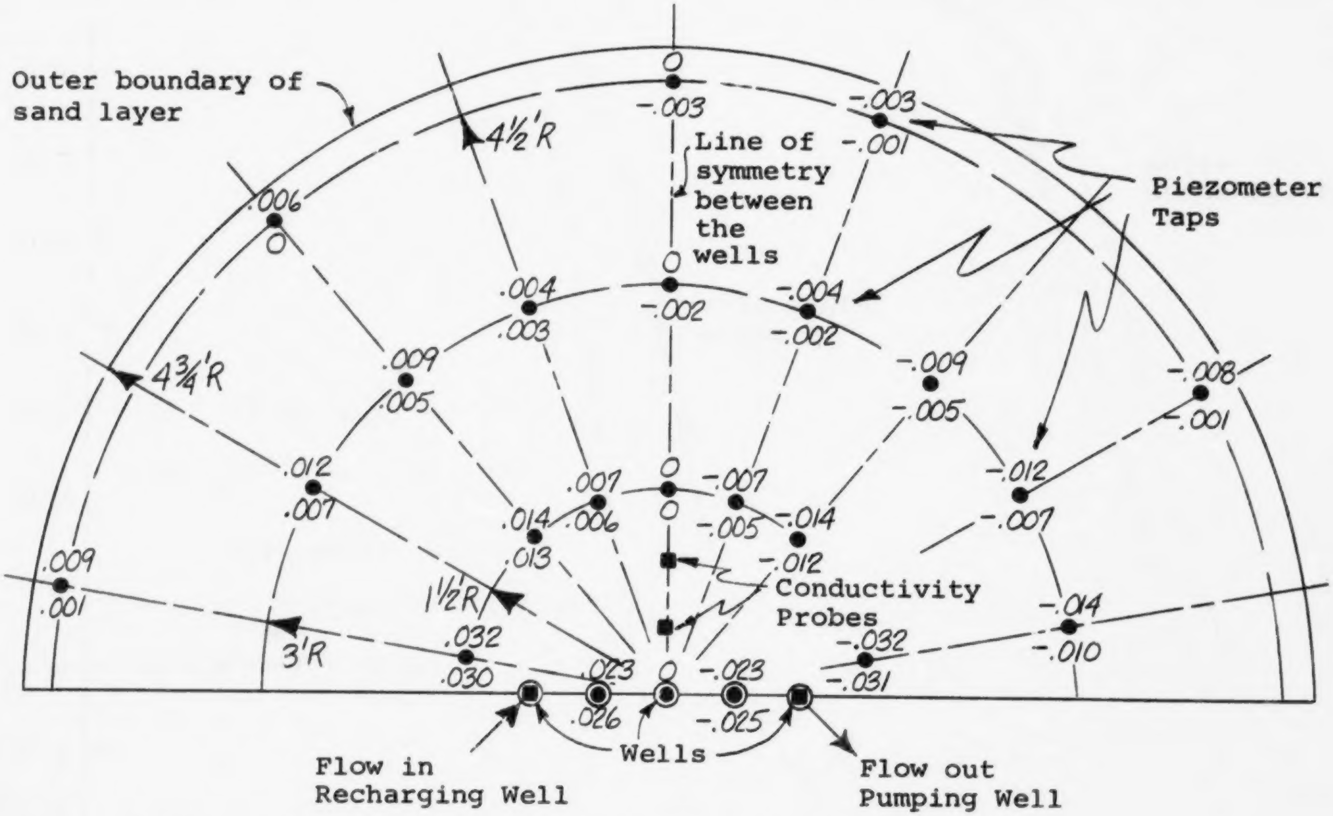
Outer boundary of sand layer
Piezometer Taps
Line of symmetry between the wells
Conductivity Probes
Wells
Flow in Recharging Well
Flow out Pumping Well
4½'R
4¾'R
1½'R
3'R
0
-.003
-.003
-.001
.006
0
0
-.002
.004
.003
-.004
-.002
.009
.005
-.009
-.005
-.008
-.001
.012
.007
.007
.006
0
0
-.007
-.005
-.014
-.012
-.012
-.007
.014
.013
.009
.001
.032
.030
.023
.026
0
-.023
-.025
-.032
-.031
-.014
-.010

Figure 4-15 Differential Piezometric Head Distribution for Run I

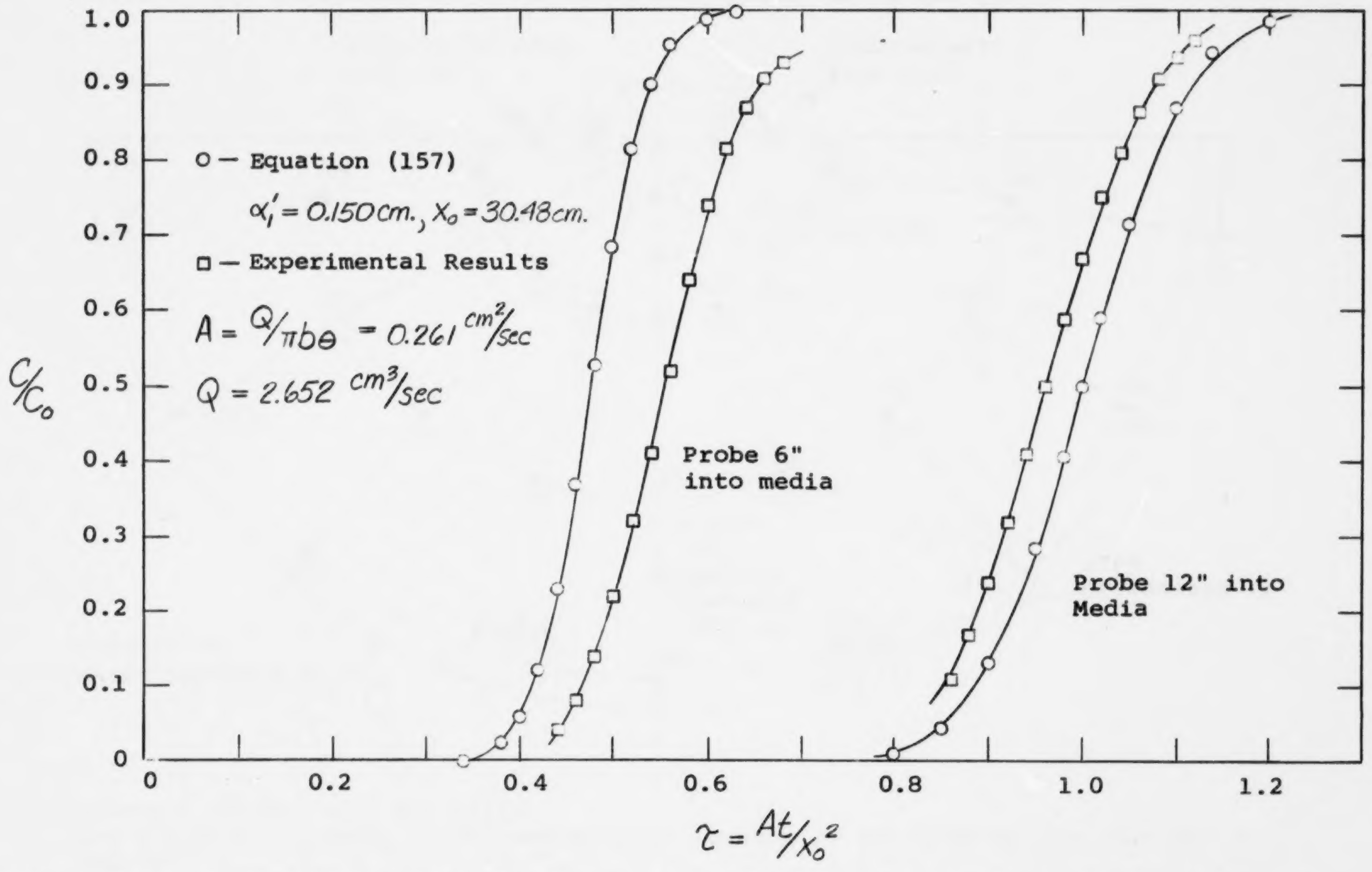

Figure 4-16 Concentration Distribution on Line of Symmetry between the Wells for Run II

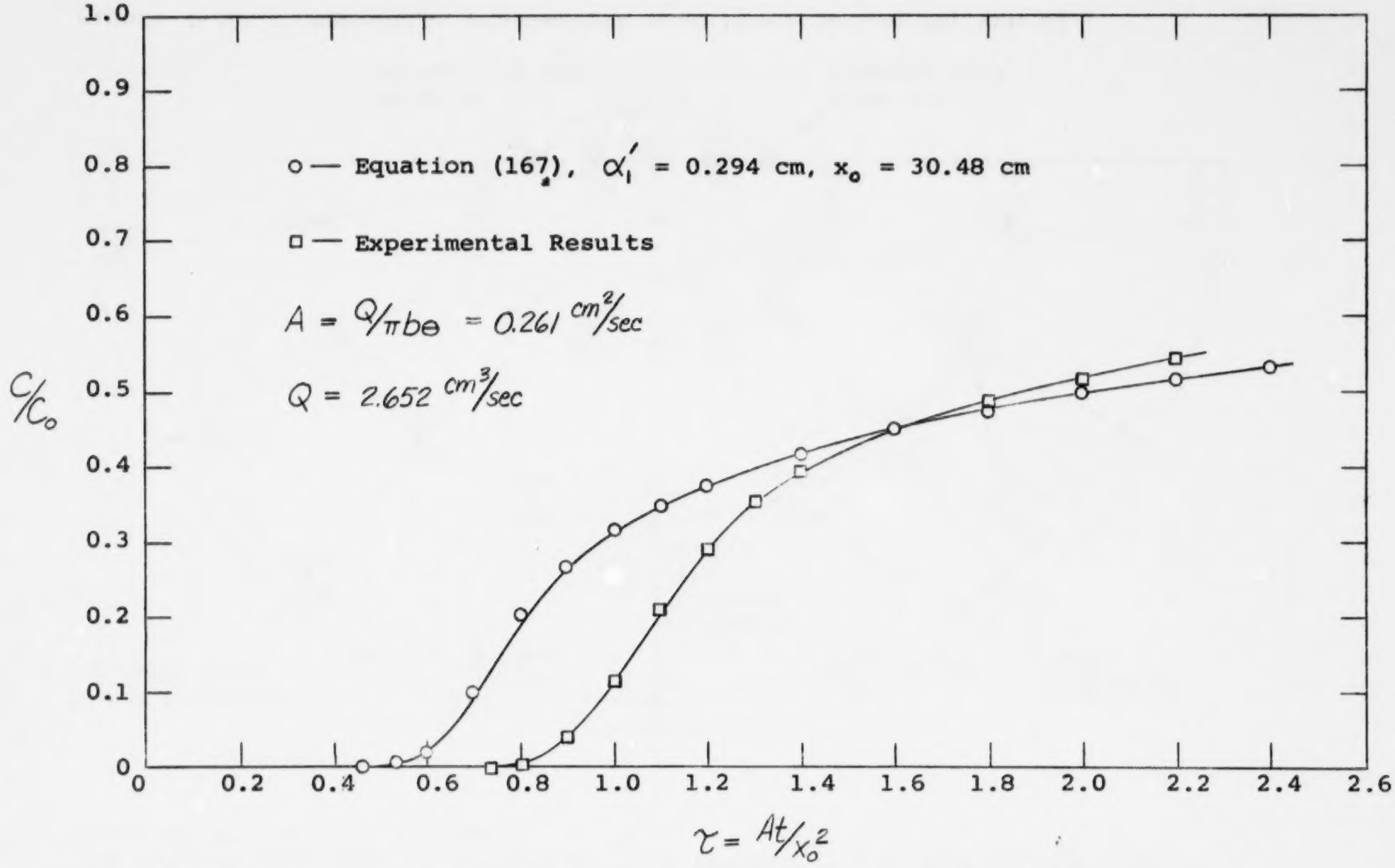

Figure 4-17 Concentration Distribution at the Pumping Well for Run II

The upper number at each piezometer tap is the theoretical differential head for an infinite sand layer, based upon the measured well flow rate, inches.
The bottom number at each piezometer tap is the measured differential head, inches.
The differential head is determined with respect to the head on the line of symmetry between the two wells.

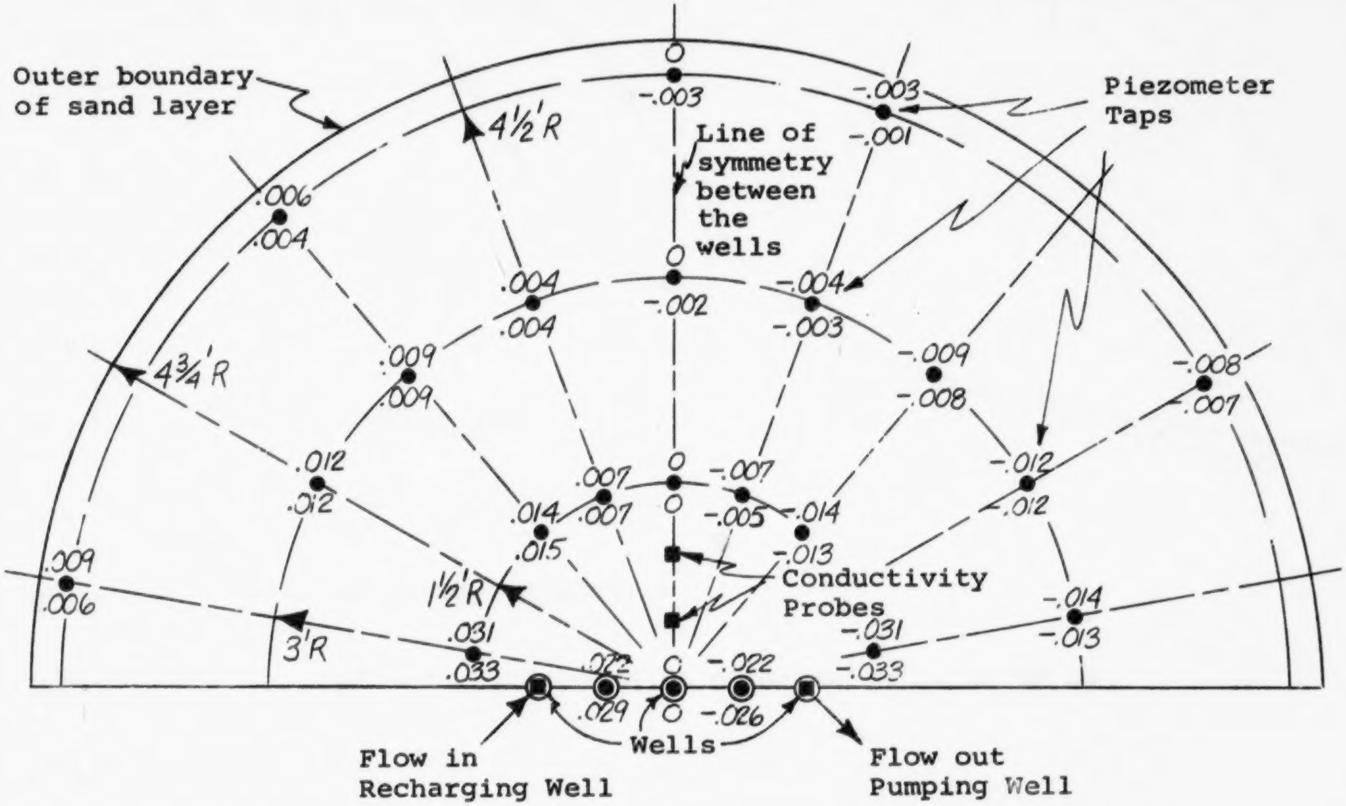
Outer boundary of sand layer
4½'R
4¾'R
1½'R
3'R
Line of symmetry between the wells
Piezometer Taps
Conductivity Probes
Flow in Recharging Well
Wells
Flow out Pumping Well
0
-.003
-.003
-.001
.006
.004
0
-.002
.004
.004
-.004
-.003
.009
.009
-.009
-.008
-.008
-.007
.012
.012
0
0
.007
.007
-.007
-.005
.014
.015
-.014
-.013
-.012
-.012
.009
.006
.031
.033
.022
.029
0
0
-.022
-.026
-.031
-.033
-.014
-.013

Figure 4-18 Differential Piezometric Head Distribution for Run II

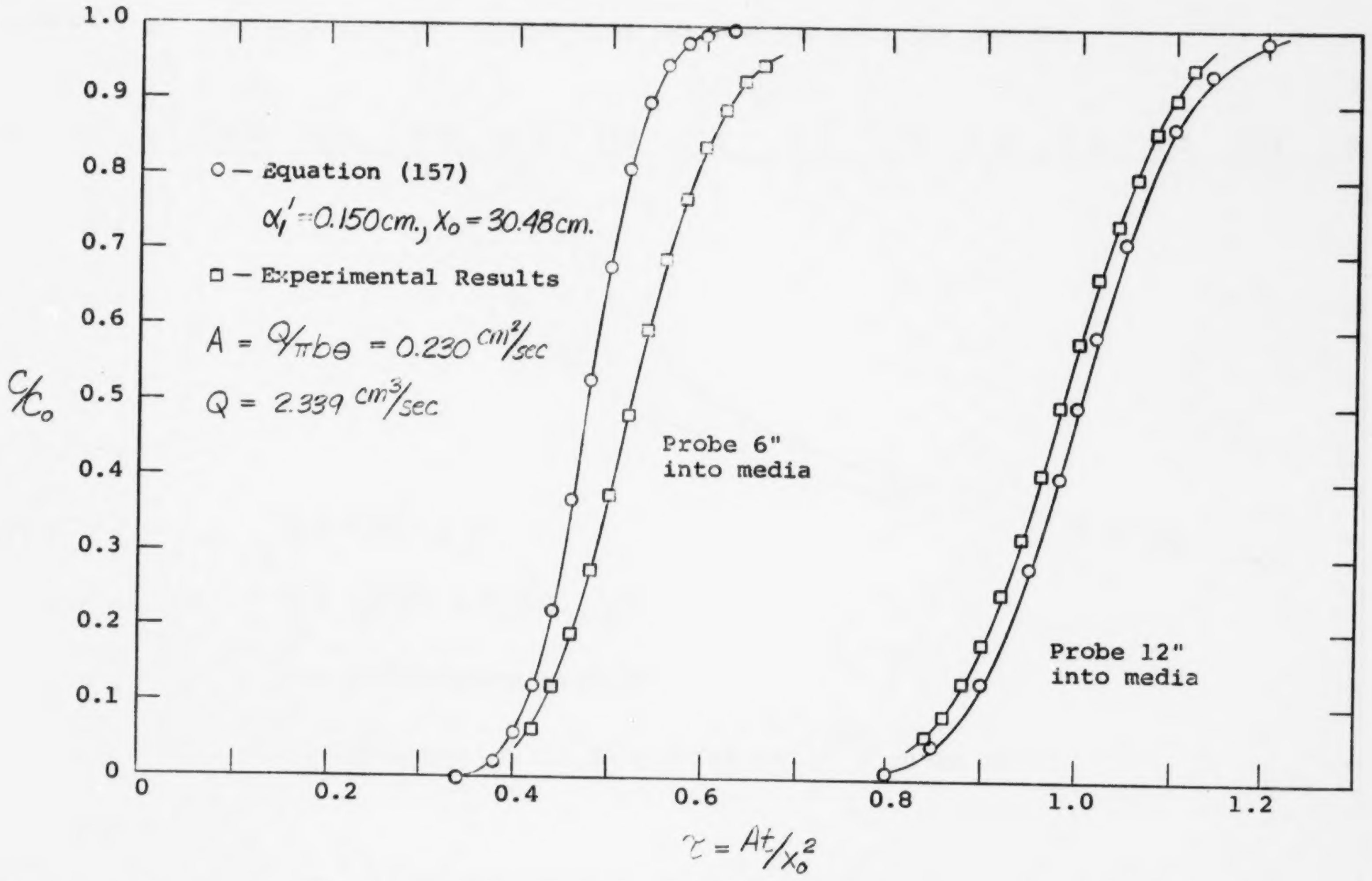

Figure 4-19 Concentration Distribution on Line of Symmetry between the Wells for Run III

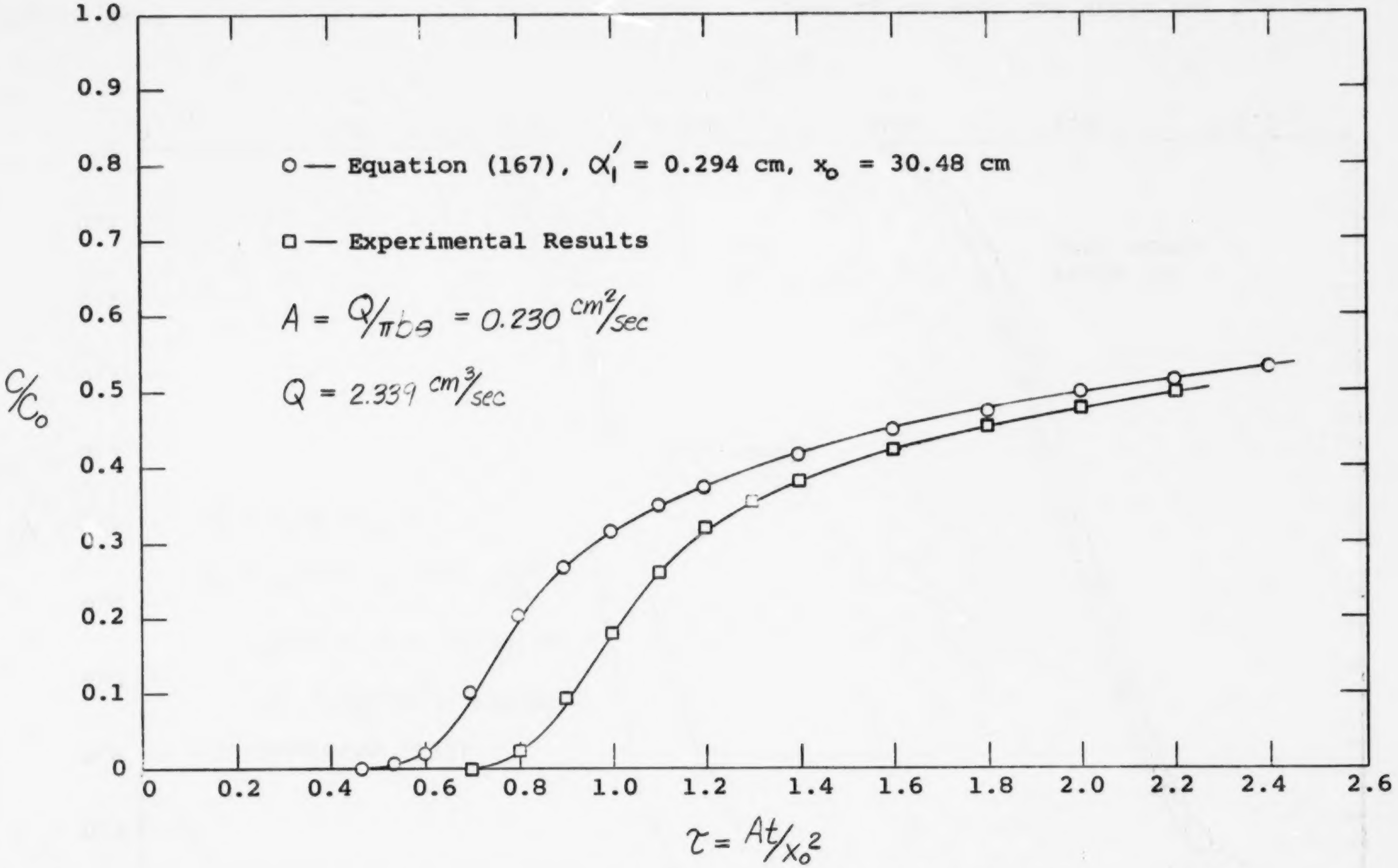

Figure 4-20 Concentration Distribution at the Pumping Well for Run III

The upper number at each piezometer tap is the theoretical differential head for an infinite sand layer, based upon the measured well flow rate, inches.
The bottom number at each piezometer tap is the measured differential head, inches.
The differential head is determined with respect to the head on the line of symmetry between the two wells.

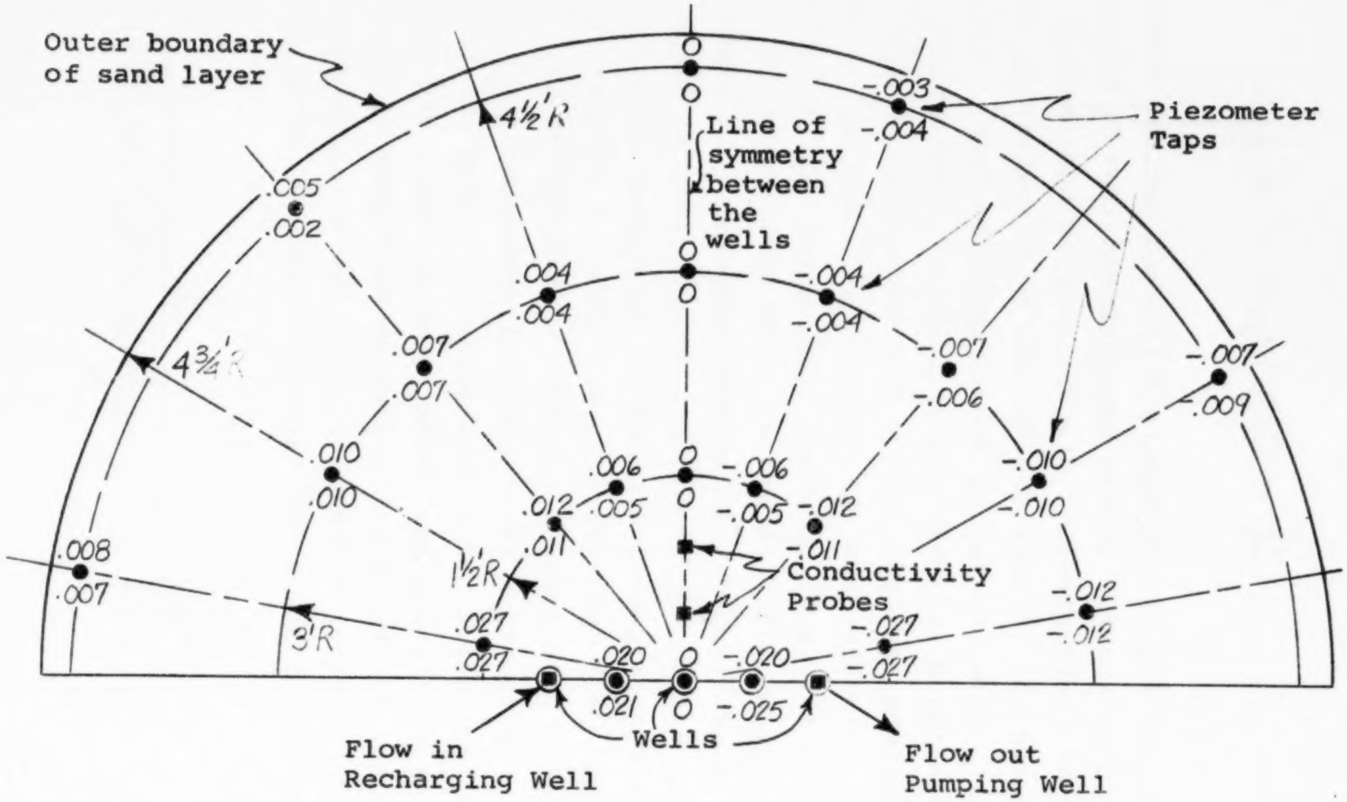
Outer boundary of sand layer
Piezometer Taps
Line of symmetry between the wells
4½'R
4¾'R
1½'R
3'R
Conductivity Probes
Wells
Flow in Recharging Well
Flow out Pumping Well
.008
.007
.005
.002
.010
.010
.007
.007
.004
.004
.027
.027
.012
.011
.006
.005
.020
.021
0
0
0
0
0
0
0
0
-.006
-.005
-.020
-.025
-.012
-.011
-.027
-.027
-.004
-.004
-.003
-.004
-.007
-.006
-.010
-.010
-.012
-.012
-.007
-.009

Figure 4-21 Differential Piezometric Head Distribution for Run III

through the experimental results of Blackwell in Figure 3-15 at a Reynolds number of 1. Carrying out this procedure, we are led to the relationship

$$D_2 = 0.060 d_{50} W = \alpha_2' q \,. \tag{192}$$

Since the results of Figure 3-15 were derived from uniform flow experiments, it has been assumed that $\alpha_2' = \alpha_2$ (i.e., the lateral coefficient of dispersivity in non-uniform flow is equal to the lateral coefficient of dispersivity for uniform flow). From the radial flow dispersion tests, Section 4.4.1, it was found that the coefficients of longitudinal dispersivity in uniform and non-uniform flow were equal ($\alpha_1' = \alpha_1$). Thus, it would seem reasonable that $\alpha_2' = \alpha_2$. Using $d_{50} = 0.167$ cm in equation (192) gives $\alpha_2' = 0.010$ cm. Letting $\alpha_2' = 0.010$ cm and $x_o = 30$ cm in equation (190) leads to the conclusion that lateral dispersion is important for $m(t) \leqslant 3$ cm or $\xi(t) < \pi/45$. Hence, lateral dispersion has a significant influence on the tracer distribution at the pumping well only for $c/c_o < 0.025$. A similar conclusion can also be reached for points within the media.

For the flow rates and well spacings of this study, molecular diffusion had a negligible influence on the measured tracer distributions. From equation (65), the relative importance of the mass transfer by molecular diffusion to that by longitudinal dispersion along the streamlines is given by the ratio of these two terms. Letting μ be this ratio, we have that

$$\mu = \frac{\mathcal{D}_m}{\alpha_1' q} = \frac{\mathcal{D}_m}{\alpha_1' \frac{A}{x_o}\left(\cosh(\phi/A) + \cos(\psi/A)\right)} \,. \tag{193}$$

For any streamline, ψ, this ratio is a maximum on the line of symmetry between the wells (i.e., $\phi = 0$). For run 3 at the probe 12 inches into the media along the line $\phi = 0$ ($\alpha_1' = 0.150$ cm, $A = 0.230$ cm^2/sec, $x_0 = 30$ cm, and $\psi/A = \pi/2$) the ratio μ is 0.009.

The shapes of the experimental tracer distributions presented in Figures 4-13 through 4-21 are very similar to the theoretical distributions at the same locations, including only the influence of longitudinal dispersion (this is also a further indication that lateral dispersion has a negligible influence on the tracer distribution). However, there is a time difference between the occurrence of the same c/c_0 value, as predicted theoretically and measured experimentally in the model. In Run I, the measured piezometric head distribution, Figure 4-15, differed significantly from the theoretical head distribution for a line source and a line sink in an infinite flow field. These differences resulted from the constant head condition which was maintained in the outer channel (i.e., for this run there was no flow in the outer channel). The piezometric heads on the recharging well side of the line of symmetry were lower than the theoretical heads at the same locations, and the piezometric heads on the pumping side of the line of symmetry were higher than the theoretical heads. Thus, since the piezometric head gradients leaving the recharging well and entering the pumping well are greater than the theoretical head gradients, a greater percentage (compared with the theoretical source-sink flow) of the flow from the recharge well will move outwards to the outer boundary, and a greater percentage (compared with the theoretical source-sink flow) of the flow to the pumping well will come from the outer boundary. This flow pattern, then, will cause the measured c/c_0 values at points along the line of symmetry and in the pumping well to occur later than the same c/c_0 values predicted, assuming the flow pattern is that of a line source and sink in an infinite flow field.

This time difference in the occurrence of the same c/c_0 values for Run I, $\Delta\tau$, at a point on the line of symmetry between the wells and at the pumping well, can be seen in Fugures 4-13 and 4-14. Measurements of the tracer distribution at a point 6 inches into the media along the line of symmetry are not reported for run I, for the conductivity probe was not working properly. The tracer distribution at the pumping well is compared with a theoretical distribution based upon $\alpha_1' = 0.294$ cm instead of 0.150 cm (the coefficient of longitudinal dispersivity found in the radial flow tests). However, from Figure 4-6, it can be seen that for $c/c_0 > 0.7$, the theoretical tracer distributions for $\alpha_1' = 0$ and 0.294 cm are almost identical; thus, for $c/c_0 > 0.7$, the tracer distribution based upon $\alpha_1' = 0.294$ cm will be the same as the tracer distribution based upon $\alpha_1' = 0.150$ cm. For $c/c_0 < 0.7$, the tracer distribution with $\alpha_1' = 0.15$ cm will lie between the distributions for $\alpha_1' = 0$ and 0.294 cm.

For Run I, the time difference, $\Delta\tau$, in the appearance of the same c/c_0 value, predicted theoretically and measured experimentally at the pumping well (Figure 4-14) is about 4-5 times greater ($\Delta\tau = 0.28 - 0.35$) than the time difference ($\Delta\tau = 0.07$) between the same c/c_0 values at the probe on the line of symmetry (Figure 4-13). As the mean travel time along a streamline between the wells is twice the mean travel time along the same streamline from the recharge well to the line of symmetry between the wells, the time difference, $\Delta\tau$, between the appearance of the same c/c_0 values at the pumping well should be about twice ($\Delta\tau = 0.14$) the time difference at the probe on the line of symmetry ($\Delta\tau = 0.07$). This additional time difference ($\Delta\tau = .14-.21$) at the pumping well is due to the flow pattern around the probe in the well. The probe was mounted in a groove in the manifold, Figure 4-10, with its electrodes positioned about mid-depth in the sand model. As the probe and its electrodes were sheltered by the groove in the manifold, the flow, which entered the well from the media and left at the top of the well, did not pass directly between the probe electrodes. With this flow pattern, then the response of the probe to the tracer would lag the arrival of the tracer in the well.

In Runs II and III, the measured piezometric head distributions, Figures 4-18 and 4-21, were within 0.002 inches of the theoretical head distributions at every measuring point except along the line joining the two wells. At the two measuring points along the line joining the two wells, differences of 0.004, 0.005, and 0.007 inches between the theoretical and experimental piezometric heads were found. The shapes (i.e., rate of increase) of the measured tracer distributions, Figures 4-16, 4-17, 4-19, and 4-20, have the same form as the theoretical predictions; however, as in the case of Run I, there are time differences between the appearance of the same c/c_o values for the theoretical and measured distributions. The experimental results for the probe 6 inches into the media along the line of symmetry (Figures 4-16 and 4-19) show that the c/c_o values occur later than the same c/c_o values for the theoretical distributions. In addition, the slope of the measured tracer distribution is greater than the predicted distribution. Since the distributions at the probe 12 inches into the media have the same shape (rate of increase of the tracer distribution) and time of occurrence ($\Delta \tau = 0.02 - 0.04$) as the theoretical distributions, the differences between the shape and time of occurrence of the measured and the predicted distributions at the probe 6 inches into the media, are due either to distortions in the flow field locally, caused by differences in the local piezometric head distribution (similar to that along the line joining the two wells, see Figures 4-18 and 4-21), or to a misalignment of the probe electrodes and the local direction of flow. This latter condition, shown in Figure 4-22, may have occurred when the probe, initially aligned parallel to the streamlines for measurements in radial flow, was turned 90° in order that the electrodes would be parallel with the streamlines in the two well flow experiments.

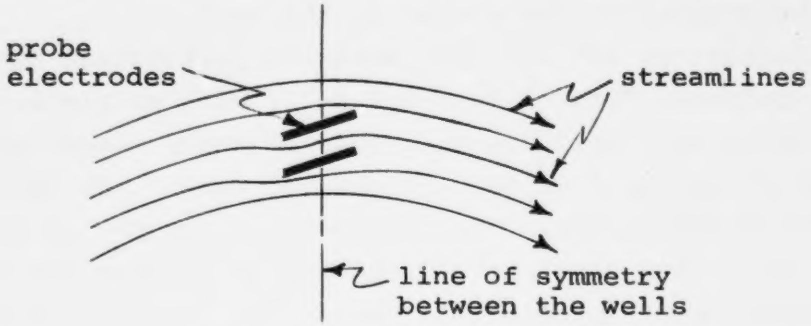

Figure 4-22 Distortion of Flow Pattern due to Probe Misalignment with Flow

If the electrodes were not aligned with the streamlines, the flow of tracer between the electrodes would be reduced, and the response of the probe to the tracer would lag the arrival of the tracer at the probe. The increased slope of the measured tracer distributions would also have been the result of the altered flow pattern through the probe electrodes.

The measured c/c_0 values at the pumping well, Figures 4-17 and 4-20, also occurred later than the same c/c_0 values predicted by the theoretical distributions. The flow pattern in these two runs, except very close to the line joining the two wells, was the same as the flow pattern between a line source and sink in an infinite flow field. Thus, the time difference between the theoretical and experimental tracer distributions in the pumping well, then, is a result of the flow pattern about the probe in the well. For Run I, the time difference due to the flow pattern in the well was found to be $\Delta\tau = 0.14 - 0.21$. This time difference, $\Delta\tau = 0.14 - 0.21$, is the same as that observed in Run III, see Figure 4-20. However, for Run II, the time difference, $\Delta\tau$, was greater than 0.14 - 0.21, and the measured tracer distribution increased more rapidly than the predicted distribution. As the flow rate remained constant, the increase in $\Delta\tau$ and the slope of the tracer distribution may have been due to a change in the response characteristics of the probe.

From this discussion of the three experimental tests, it is clear that the differences between the measured and the predicted tracer distributions are the result of a time lag between the response of the conductivity probe to the tracer and the arrival of the tracer at the probe. In Run I, an additional time lag between the measured and the predicted tracer distributions resulted from the differences between the measured and the theoretical piezometric head distributions. Thus, the theoretical expressions for the tracer distribution, equation (157) within the aquifer and equation (167) at the pumping well, may be used to describe the distribution of a recharged fluid in the flow between two wells, one recharging and one pumping, provided that molecular diffusion and lateral dispersion do not effect the tracer distribution. If molecular diffusion exerts a significant influence on the tracer distribution, as compared to longitudinal dispersion (i.e., for large well spacings and small flow rates), equations (155) and (156) should be used along with equation (157) in order to describe the tracer distribution within the media.

Equations (157) and (167) may be applied to the prediction of the distribution of recharged water in field problems as well as to laboratory model studies, provided the conditions under which equations (157) and (167) were derived are satisfied in the field (i.e., steady flow between a single recharging and a single pumping well in a confined aquifer with no natural groundwater flow in the aquifer). To illustrate the application of these results to a field situation, consider the confined aquifer, discussed previously in Section 4.4.1, in which there are now two 12 inch diameter wells, one recharging the aquifer at a rate of 0.7 cfs and the other pumping from the aquifer at the same rate. The distance between the wells is 500 ft. (thus x_o = 250 ft.), and the aquifer has the same properties as discussed earlier: thickness, b = 110 ft.; porosity, θ = 0.35; mean grain size, d_{50} = 0.001 ft.; permeability, K = 1000 gal/day/ft^2; and coefficient of longitudinal dispersivity, α_1' = 0.0008 ft. For these conditions, the quantity A, given by $Q/2\pi b\theta$, in equations (107) and (157) and in $\tau = At/x_o^2$ is equal to 2.91 x 10^{-3}ft^2/sec, and α_2', the coefficient of lateral dispersivity, is equal to 0.000048 ft. (determined using Figure 3-15 with d_{50} or using Figure 3-16 with k, the intrinsic permeability).

Thus, the dimensionless time parameter, $\tau = At/x_o^2$, in equations (157) and (167) is given by τ = 40 x 10^{-4}t, where t is the time from the beginning of recharging in days. In Figure 4-6, it can be seen that longitudinal dispersion has a significant influence on the temporal distribution of recharged water at the pumping well for $\tau < 0.7$. Thus, at times, t, less than 175 days, the distribution of recharged water at the pumping well is determined by longitudinal dispersion; whereas, for times, t, greater than 175 days, the distribution of recharged water at the pumping well is governed by convection.

The extent of the mixed region between the recharged water and the native ground water is determined by the combined mechanisms of longitudinal and lateral dispersion and molecular diffusion. Using the values of α_2' and x_o in equation (190) leads to the conclusion that lateral dispersion has an appreciable influence on the distribution of recharged water for $c/c_o < 0.01$ at any point in the aquifer. The relative importance of molecular diffusion to longitudinal dispersion on the distribution of recharged water can be calculated using equation (193). For this flow rate, μ (the ratio of the mass transfer by molecular diffusion to the mass transfer by longitudinal dispersion) is equal to 0.6 at $\phi = 0$ (the line of symmetry between the wells) and $\psi = 0$ (the line joining the two wells). For $\psi = \pi/2$ (see Figure 4-5) and $\phi = 0$, $\mu = 1.2$. Closer to the wells, longitudinal dispersion becomes more important than molecular diffusion in determining the distribution of recharged water; at 25 feet from the wells, μ is equal to 0.1.

Harpaz and Bear [49] reported on some field testing involving the flow of a tracer between a recharging and a pumping well. The tracer was introduced as a step function change in concentration at the recharge well, and its temporal distribution was measured at several observation wells in the aquifer and at the pumping well. The measured tracer distributions indicated that either the aquifer was not isotropic and homogeneous or the flow pattern in the aquifer was not the same as the flow pattern of a recharging and a pumping well (or a combination of these reasons), for the tracer distributions at two of the three observation wells did not approach the injected tracer concentration after a long period of time. Thus, it was not possible to compare the theoretical expression for the tracer distribution, equation (157), with these field measurements. In addition, the tracer concentration in the pumping well increased to $c/c_0 = 0.30$ and then appeared to remain constant instead of continuing to increase as predicted by equations (126) or (167). Also, the rate of increase of the tracer concentration in the pumping well to $c/c_0 = 0.30$ was slower than predicted by equations (126) or (167).

V. SUMMARY AND CONCLUSIONS

This investigation has dealt with miscible fluid displacement problems which occur in the recharge and disposal of treated and untreated water by wells in groundwater basins. For the idealized conditions of a homogeneous, isotropic, confined aquifer, analytical predictions of the distribution of a tracer during recharging have been made and compared with experimental measurements of the tracer distribution. In addition, the analytical solutions have been used to study the relative influences of convection, longitudinal and lateral dispersion, and molecular diffusion on the tracer distribution.

In the first part of this study, analytical solutions were obtained which describe the influences of longitudinal and lateral dispersion on the tracer distribution in uniform flow through a sand column. Longitudinal and lateral dispersion coefficients were determined from experimental measurements of the tracer distribution and were correlated with the Reynolds number in the following relationships:

$$\frac{D_1}{\nu} = 1.70\left(\frac{wd_{50}}{\nu}\right)^{1.2},\ 0.2 < \frac{wd_{50}}{\nu} < 10\ ;\quad \frac{D_1}{\nu} = 223\left(\frac{w\sqrt{k}}{\nu}\right)^{1.2},\ 0.004 < \frac{w\sqrt{k}}{\nu} < 0.1$$

$$\frac{D_2}{\nu} = 0.11\left(\frac{wd_{50}}{\nu}\right)^{0.7},\ 0.2 < \frac{wd_{50}}{\nu} < 5\ ;\quad \frac{D_2}{\nu} = 1.86\left(\frac{w\sqrt{k}}{\nu}\right)^{0.7},\ 0.004 < \frac{w\sqrt{k}}{\nu} < 0.1$$

$$\frac{D_1}{D_2} = 15.5\left(\frac{wd_{50}}{\nu}\right)^{0.5},\ 0.2 < \frac{wd_{50}}{\nu} < 5\ ;\quad \frac{D_1}{D_2} = 120\left(\frac{w\sqrt{k}}{\nu}\right)^{0.5},\ 0.004 < \frac{w\sqrt{k}}{\nu} < 0.1$$

D_1 and D_2 are the coefficients of longitudinal and lateral dispersion; ν is the kinematic viscosity; w is the seepage velocity, d_{50} is the mean particle size; and k is the intrinsic permeability. For uniform materials, either $\sqrt{k}$ or d_{50} may be used as a characteristic pore size in the Reynolds number correlation; however, with non-uniform media, and in field investigations, the Reynolds number correlation based upon $\sqrt{k}$ should be used, since the intrinsic permeability includes the effect of a distribution of pore sizes and is more easily measured in the field. Finally, an examination of the variations in the measured dispersion coefficients of different investigators at the same Reynolds number (see Figures 3-15 and 3-16) revealed that these differences were due primarily to the measurement of the tracer distribution outside of the media. It is recommended that measurements of the tracer distribution be made within the media with a probe designed to respond to changes in the tracer concentration in a small volume of media at the probe.

From the study of the tracer distribution in radial flow from a well, an approximate solution for the radial tracer distribution,

$$\frac{C}{C_0} = \frac{1}{2}\,erf_c\left[\frac{r^2/2 - At}{\sqrt{\frac{4}{3}\alpha_1' r^3 + \frac{\mathcal{D}_m}{A} r^4}}\right] \qquad (95)$$

was obtained. Neglecting molecular diffusion, a comparison of equation (95) with a numerical solution of the differential equation describing the tracer distribution equation (82) (see Figures 4-3 and 4-4) indicated that equation (95) was a close approximation of the tracer distribution for distances greater than 20 particle diameters from the well. The influence of molecular diffusion on the tracer distribution was not important in the experimental study; however, in field operations at distances of only 300 feet from the well, molecular diffusion may be of equal importance with radial dispersion in determining the tracer distribution. Finally, the results of the experimental study showed that the coefficient of longitudinal dispersion in radial flow was equal to the coefficient of longitudinal dispersion in uniform flow at the same velocity; thus, measurements of dispersion coefficients in uniform flow may be used in the study of dispersion and displacement problems in non-uniform flow.

For the steady flow between two wells, one pumping tracer into the media at the same rate as the other one is pumping the mixture of fresh water and tracer out of the media, the tracer distribution, including the influence of longitudinal dispersion, is given by

$$\frac{c}{c_o} = \frac{1}{2}\,\mathrm{erfc}\left[\frac{a' - \tau}{\sqrt{4b'}}\right] \qquad (157)$$

in which a', b' are given by equations (140), (141), (142), and (143), and $\tau = At/x_o^2$. Lateral dispersion was shown to have a negligible influence on this tracer distribution, except very close to the line joining the two wells. The influence of molecular diffusion on the tracer distribution, as expressed by equation (157), can be accounted for by combining equations (155) and (156) with equations (141) and (143). In this experimental study, molecular diffusion was not important; however, in field situations, molecular diffusion may exert an influence on the tracer distribution equal to that of longitudinal dispersion in the region near the line of symmetry between the wells. (The extent of this region increases with decreasing flow rates and increasing well spacings.) The longitudinal dispersion coefficient determines the shape of the tracer distribution at points within the media. At the pumping well, however, it has an important influence on the tracer distribution only for small concentrations $c/c_o < 0.1$, and for short times, $\tau < 0.7$ (corresponds to times up to 175 days for the example field problem worked out in section 4.4.2). For $c/c_o > 0.1$ and $\tau > 0.7$ (see Fig. 4-6), the tracer distribution at the pumping well is dominated by convection along the streamlines and is given by

$$\frac{C_p(\tau)}{C_0} = \frac{\xi(\tau)}{\pi} \qquad (126)$$

in which ξ is equal to ψ/A and τ is the time at which the streamline ξ arrives at the pumping well.

The application of the above results to field operations is limited to homogeneous, isotropic, and confined aquifers; however, for unconfined aquifers with small water table slopes, these results should give a good approximation to the tracer distributions. An important extension of this study would be to investigate the tracer distributions for these same flow patterns in nonhomogeneous and anisotropic media, in aquifers of variable thickness and shape, in aquifers with partially penetrating wells, and in aquifers in which a uniform flow is superimposed on the well flow pattern.

VI. REFERENCES

1. Aris, R., "Notes on the Diffusion-Type Model for Longitudinal Mixing in Flow," Chemical Engineering Science, Vol. 9, 1959, pp. 266-267.

2. Aris, R., and N. R. Amundson, "Some Remarks on Longitudinal Mixing or Diffusion in Fixed Beds," American Institute of Chemical Engineers, Journal, Vol. 3, No. 2, June 1957, pp. 280-282.

3. Bachmat, Y. and J. Bear, "The General Equations of Hydrodynamic Dispersion in Homogeneous, Isotropic, Porous Mediums," Journal of Geophysical Research, Vol. 69, No. 12, June 15, 1964, pp. 2561-2567.

4. Banks, R. B., S. Jerasate, and R. F. H. Owston, "Studies on Dispersion in Porous Media Flow," Final Report of a Research Program, Technological Institute, Northwestern University, Evanston, Illinois, IV Parts, January 1962.

5. Banks, R. B., and S. Jerasate, "Dispersion in Unsteady Porous Media Flow," Proceedings, ASCE (Hydraulics Division), paper No. 3109, HT3, May 1962, pp. 1-21. --with discussion by:

   Harleman, D. R. F., R. R. Rumer, Jr., and J. A. Hoopes, Proceedings, ASCE (Hydraulics Division); HY6, November. --and closure by:

   Banks, R. B., and S. Jerasate, Proceedings, ASCE, (Hydraulics Division), Vol 89, HY3, May 1963, p. 297.

6. Baron, T., "Generalized Graphical Method for the Design of Fixed Bed Catalytic Reactors," Chemical Engineering Progress, Vol. 48, No. 3, March 1952, pp. 118-124.

7. Bauman, P., "Theoretical and Practical Aspects of Well Recharge," Transactions, ASCE, Part I, 1963, pp. 739-764.

8. Bear, J., "On the Tensor Form of Dispersion in Porous Media," Journal of Geophysical Research, Vol. 66, No. 4, April 1961, pp. 1185-1197.

9. Bear, J., "Some Experiments in Dispersion," Journal of Geophysical Research, Vol. 66, No. 8, August 1961, pp. 2455-2467.

10. Bear, J., and D. K. Todd, "The Transition Zone between Fresh and Salt Waters in Coastal Aquifers," Contribution No. 29, Water Resources Center, University of California, Berkeley, September 1960, 156 pp..

11. Benham, A. L., W. E. Dowden, and W. J. Kunpman, "Miscible Fluid Displacement - Prediction of Miscibility," *A.I.Ch.E. - S.P.E. Joint Symposium on Fundamental Concepts of Miscible Fluid Displacement: Part I*, Preprint 27, San Francisco, December 1959.

12. Beran, M. J., "Dispersion of Soluble Matter in Slowly Moving Fluids," Ph.D. Thesis, Division of Applied Science, Harvard University, Cambridge, Massachusetts, 1955.

13. Bernard, R., and R. Wilhelm, "Turbulent Diffusion in Fixed Beds of Packed Solids," *Chemical Engineering Progress*, Vol. 46, No. 5, 1950, pp. 233-244.

14. Biggar, J. W., and D. R. Nielsen, "Some Comments on Molecular Diffusion and Hydrodynamic Dispersion in Porous Media," *Journal of Geophysical Research*, Vol. 65, No. 9, September 1960, pp. 2887-2895.

15. Biggar, J. W., and D. R. Nielsen, "Some Comments on Molecular Diffusion and Hydrodynamic Dispersion in Porous Media," *Journal of Geophysical Research*, Vol. 67, No. 9, August 1962, pp. 3636-3637.

16. Bird, R. B., Stewart, W. E., and E. N. Lightfoot, *Transport Phenomena*, John Wiley and Sons, Inc., New York, 1960.

17. Bischoff, K. B., "Notes on the Diffusion-Type Model for Longitudinal Mixing in Flow," *Chemical Engineering Science*, Vol. 12, 1962, pp. 69-70.

18. Bischoff, K. B., and O. Levenspiel, "Fluid Dispersion - Generalization and Comparison of Mathematical Models, I - Generalization of Models," *Chemical Engineering Science*, Vol. 17, 1962, pp. 245-255.

19. Bischoff, K. B., and O. Levenspiel, "Fluid Dispersion - Generalization and Comparison of Mathematical Models, II - Comparison of Models," *Chemical Engineering Science*, Vol. 17, 1962, pp. 257-264.

20. Blackwell, R. J., "Laboratory Studies of Microscopic Dispersion Phenomena in Porous Media," *A.I.Ch.E. - S.P.E. Joint Symposium on Fundamental Concepts of Miscible Fluid Displacement: Part I*, Preprint 27, San Francisco, December 1959.

21. Brenner, H., "The Diffusion Model of Longitudinal Mixing in Beds of Finite Length, Numerical Values," *Chemical Engineering Science*, Vol. 17, 1962, pp. 229-243.

22. Brigham, W. E., P. W. Reed, and J. N. Dew, "Experiments on Mixing during Miscible Displacement in Porous Media," *A.I.Ch.E. - S.P.E. Joint Symposium on Fundamental Concepts of Miscible Fluid Displacement*, Preprint 44, San Francisco, December 1959.

23. Cairns, E. J., and J. M. Prausnitz, "Longitudinal Mixing in Packed Beds," *Chemical Engineering Science*, Vol. 12, No. 1, 1960, pp. 20-34.

24. Carberry, J. J., and R. H. Bretton, "Axial Dispersion of Mass in Flow through Fixed Beds," *American Institute of Chemical Engineering Journal*, Vol. 4, No. 3, September 1958, pp. 367-375.

25. Carslaw, H. S. and J. C. Jaeger, *Conduction of Heat in Solids*, Oxford University Press, London, 2nd edition, 1959, 510 pp..

26. Cole, F. W., J. V. Cowan, and M. L. Jackson, "Miscible Displacement Studies Using Radial Cores," *A.I.Ch.E. - S.P.E. Symposium on Fundamental Concepts of Miscible Fluid Displacement: Part I*, Preprint 46, San Francisco, December 1959.

27. Converse, A. O., "The Effect of Velocity Profile on Axial Dispersion in Packed Beds," *American Institute of Chemical Engineering Journal*, Vol. 6, No. 2, June 1960, pp. 344-345.

28. Crandall, S. H., *Engineering Analysis*, McGraw-Hill Book Co., Inc., New York, 1956, 417 pp..

29. Crank, J., *The Mathematics of Diffusion*, Oxford University Press, London, 1956, 347 pp..

30. Danckwerts, P. V., "Continuous Flow Systems; Distribution of Residence Times," *Chemical Engineering Science*, Vol. 2, 1953, pp. 1-13.

31. Day, P. R., "Dispersion of a Moving Salt-Water Boundary Advancing Through Saturated Sand," Transactions, AGU, Vol. 37, No. 5, October 1953, pp. 595-601.

32. de Josselin De Jong, "Longitudinal and Transverse Diffusion in Granular Deposits," Transactions, AGU, Vol. 39, No. 1, February 1958, pp. 67-74.

33. de Josselin De Jong, G., and M. J. Bossen, "Discussion of Paper by Jacob Bear, 'On the Tensor Form of Dispersion in Porous Media,'" Journal of Geophysical Research, Vol. 66, No. 10, October 1961, pp. 3623-3624.

34. de Wiest, R. J. M., Geohydrology, John Wiley and Sons, Inc., New York, 1965, 366 pp.

35. de Witte, A. J., "A Kinetic Theory of Liquid Displacement," Physics of Fluids, Vol. 3, No. 2, June 1959, pp. 139-144.

36. Dorweiler, V.P., and R. W. Fahien, "Mass Transfer at Low Flow Rates in a Packed Column," American Institute of Chemical Engineering Journal, Vol. 5, No. 2, June 1959, pp. 139-144.

37. Ebach, E. A., and R. R. White, "Mixing of Fluids Flowing through Beds of Packed Solids," American Institute of Chemical Engineering Journal, Vol. 4, No. 2, June 1958, pp. 161-169.

38. Eriksson, E., "A Note on the Dispersion of a Salt-Water Boundary Moving Through Sand," Transactions, AGU, Vol. 39, No. 5, October 1958, pp. 937-938.

39. Everett, J. P., F. W. Gooch, and J. C. Calhoun, Jr., "Liquid-Liquid Displacement in Porous Media as Affected by the Liquid-Liquid Viscosity Ratio and Liquid-Liquid Miscibility," Transactions, AIME, Vol. 189, 1950, pp. 215-224.

40. Goldstein, S., "On Diffusion by Discontinuous Movements, and on the Telegraph Equation," Quarterly Journal of Mechanics and Applied Mathematics, Vol. 4, 1951, pp. 129-156.

41. "Ground Water Contamination," Proceedings of the 1961 Symposium, Technical Report W61-5, Robert A. Taft Sanitary Engineering Center, U. S. Department of Health, Education, and Welfare, 218 pp.

42. Grane, F. E., and G. H. F. Gardner, "Measurements of Transverse Dispersion in Granular Media," *Journal of Chemical and Engineering Data*, Vol. 6, No. 2, April 1961, pp. 283-287.

43. Handy, L. L., "An Evaluation of Diffusion Effects in Miscible Liquid Displacement," *Transactions*, *AIME*, Vol. 216, T.N.2030, 1959, pp. 382-384.

44. Hantush, M. S., "Hydraulics of Wells," in *Advances in Hydroscience*, Academic Press, N. Y., Vol. 1, 1964.

45. Harleman, D. R. F., and R. R. Rumer, Jr., "The Dynamics of Salt-Water Intrusion in Porous Media," Report No. 55, Hydrodynamics Laboratory, M. I. T., August 1962, 125 pp..

46. Harleman, D. R. F., P. F. Mehlhorn, and R. R. Rumer, Jr., "Longitudinal Dispersion in Uniform Porous Media," Report No. 57, Hydrodynamics Laboratory, M. I. T., August 1962, 30 pp..

47. Harleman, D. R. F., P. F. Mehlhorn, and R. R. Rumer, Jr., "Dispersion Permeability Correlation in Porous Media," *Proceedings*, *ASCE* (Hydraulics Division), HY2, March 1963, pp. 67-85.

48. Harleman, D. R. F., and R. R. Rumer, Jr., "Longitudinal and Lateral Dispersion in an Isotropic Porous Medium," *Journal of Fluid Mechanics*, Vol. 16, Part I, May 1963, pp. 1-12.

49. Harpaz, Y., and J. Bear, "Investigations on Mixing of Waters in Underground Storage Operations," Publication No. 64, International Union of Geodesy and Geophysics, Association of Scientific Hydrology, General Assembly of Berkeley, 1964, pp. 132-153.

50. Harr, M. E., *Groundwater and Seepage*, McGraw Hill Book Co., Inc., New York, 1962, 315 pp..

51. Hennico, A., G. Jacques, and T. Vermeulen, "Longitudinal Dispersion in Packed Extraction Columns," Lawrence Radiation Laboratory, University of California (UCRL - 10696, 1963), 190 pp..

52. Hildebrand, F. B., *Advanced Calculus for Applications*, Prentice-Hall, New Jersey, 1964, 646 pp..

53. Irmay, S., "On the Theoretical Derivation of Darcy and Forchheimer Formulas," *Transactions*, *AGU*, Vol. 39, No. 4, August 1958, pp. 702-707.

54. Jacob, C. E., "Flow of Ground Water," in *Engineering Hydraulics*, John Wiley and Sons, New York, 1950, pp. 321-386.

55. Jacques, G. L., and T. Vermeulen, "Longitudinal Dispersion in Solvent Extraction Columns: Peclet Numbers for Ordered and Random Packings," University of California Berkeley (UCRL - 8029), November 1957.

56. Kaufman, W. J., "Ground Disposal of Radioactive Wastes," Sanitary Engineering Research Laboratory, *Conference Proceedings*, Sanitary Engineering Research Laboratory, University of California Berkeley, August 25-27, 1959.

57. Kimura, M., K. Ueda, and T. Ofuka, "Effective Diffusivity of Packed Bed," *American Institute of Chemical Engineering Journal*, Vol. 6, No. 2, June 1959, pp. 267-268.

58. Kitagawa, K., "Sur le Dispersement et L'Ecart Moyen de l'Ecoulement des Eaux Sout Erranines: L'Experiences avec un Modele de Laboratoire," Memoirs of College of Science, Kyoto Imperial University, Series A, Vol. 17, 1934, pp. 37-42.

59. Klinkenberg, A., H. J. Krajenbrink, H. A. Laruverier, "Diffusion in a Fluid Moving at Uniform Velocity in a Tube," *Industrial and Engineering* Chemistry, Vol. 45, No. 6, 1953, pp. 1202-1208.

60. Klinkenberg, A., and H. Sjinitzer, "Holding Time Distributions of the Gaussian Type," *Chemical Engineering Science*, Vol 5, 1956, pp. 258-270.

61. Kramers, H., and G. Alberda, "Frequency Response Analysis of Continuous Flow Systems," *Chemical Engineering Science*, Vol. 2, No. 4, 1953, pp. 173-181.

62. Lapidus, L., "Flow Distribution and Diffusion in Fixed-Bed Two-Phase Reactors," *Industrial and Engineering Chemistry*, Vol. 49, 1957, pp. 1000-1006.

63. Lau, L. K., W. J. Kaufman, and D. K. Todd, "Studies of Dispersion in a Radial Flow System," Progress Report No. 3, Sanitary Engineering Research Laboratory, Department of Engineering and School of Public Health, July 1957, pp. 44.

64. Lau, L., W. J. Kaufman, G. T. Orlob, and D. K. Todd, "Studies of Flow Dispersion in Porous Media," Progress Report No. 4, Canal Seepage Research, Sanitary Engineering Research Laboratory, University of California Berkeley, July 1958, 67 pp..

65. Lau, L. K., W. J. Kaufman, and D. K. Todd, "Dispersion of a Water Tracer in Radial, Laminar Flow through Homogeneous Porous Media," Progress Report No. 5, Canal Seepage Research, Hydraulic Laboratory and Sanitary Engineering Research Laboratory, University of California Berkeley, July 1959, 78 pp..

66. Le Grand, H. E., "Management Aspects of Groundwater Contamination," Journal Water Pollution Control Federation, September 1964, pp. 1133-1145.

67. Levenspiel, O., Chemical Reaction Engineering, John Wiley and Sons, Inc., N. Y., 1962, 501 pp..

68. Levenspiel, O., and W. K. Smith, "Notes on the Diffusion-type Model for the Longitudinal Mixing of Fluids in Flow," Chemical Engineering Science, Vol. 6, 1957, pp. 227-233.

69. Li, Wen-Hsiung, "Band Diffusion with Variable Parameters along Flow," Proceedings,ASCE (Engineering Mechanics Division), EM5, paper No. 4106, October 1964, pp. 343-361.
--with discussion by:

Hoopes, J. A., and D. R. F. Harleman, Proceedings, ASCE (Engineering Mechanics Division), (to be published in 1965).

70. Liles, A. W., and C. J. Geankoplis, "Axial Diffusion of Liquids in Packed Beds and End Effects," American Institute of Chemical Engineering Journal, Vol. 3, No. 1, March 1957, pp. 591-595.

71. McHenry, Jr., K. W., and R. H. Wilhelm, "Axial Diffusion of Binary Gas Mixtures Flowing in a Random Bed of Spheres," American Institute of Chemical Engineering Journal, Vol. 3, No. 1, March 1957, pp. 83-92.

72. Mohtadullah, K., "Longitudinal Dispersion in Non-Uniform Media," M. S. Thesis, Department of Civil Engineering, M. I. T., Cambridge, Massachusetts, May 1964, 84 pp..

73. Muskat, M., The Flow of Homogeneous Fluids Through Porous Media, McGraw-Hill Book Co., Inc., N. Y., 1937, 763 pp..

74. Nelson, R. W., and A. E. Reisenauer, "Application of Tracers in Scientific Ground Water Hydrology," in Radioisotopes in Hydrology, Proceedings of the Symposium on the Application of Radioisotopes in Hydrology, March 1963, pp. 207-230.

75. Nielsen, D. R., and J. W. Biggar, "Miscible Displacement in Soils, I, Experimental Information," Proceedings, Soil Science Society of America, Vol. 25, January-February 1961, pp. 1-4.

76. Nikolaevskii, V. N., "Convective Diffusion in Porous Media," in Applied Mathematics and Mechanics (Prikl. Mat. Mech.), Pergamon Press, N. Y., Vol. 23, No. 6, 1959, pp. 1492-1503.

77. Ogata, A., "Dispersion in Porous Media," Ph.D. Thesis, Department of Civil Engineering, Northwestern University, Evanston, Illinois, August 1958, 121 pp..

78. Ogata, A., and R. B. Banks, "A Solution of the Differential Equation of Longitudinal Dispersion in Porous Media," Professional Paper 411-A, U. S. Geological Survey, Department of the Interior, U. S. Government Printing Office, 1961, 7 pp..

79. Ogata, A., "Transverse Diffusion in Saturated Isotropic Granular Media," Professional Paper 411-B, U. S. Geological Survey, Department of the Interior, U. S. Government Printing Office, 1961, 8 pp..

80. Ogata, A., "The Spread of a Dye Stream in an Isotropic Granular Medium," Professional Paper 411-G, U. S. Geological Survey, Department of the Interior, U. S. Government Printing Office, 1964, 11 pp..

81. Orlob, G. T., and G. N. Radhakrishna, "The Effects of Entrapped Gases on the Hydraulic Characteristics of Porous Media," Transactions, AGU, August 1958, pp. 648-659.

82. Perrine, R. L., "Conditional Instability in Miscible Liquid-Liquid Displacement," A.I.Ch.E. - S.P.E. Joint Symposium of Fundamental Concepts of Miscible Fluid Displacement, Part I, Preprint 42, San Francisco, December 1959.

83. Polubarinova-Kochina, P. Ya, Theory of Ground Water Movement, Princeton University Press, Princeton, New Jersey, 1962, 613 pp..

84. Prausnitz, J. M., and R. H. Wilhelm, "Turbulent Concentration Fluctuations in a Packed Bed," Industrial and Engineering Chemistry, Vol. 49, No. 6, June 1957, pp. 978-984.

85. Raimondi, P., G. H. G. Gardner, and C. B. Petrick, "Effect of Pore Structure and Molecular Diffusion on the Mixing of Miscible Liquids Flowing in Porous Media," A.I.Ch.E. - S.P.E. Fundamental Concepts of Miscible Fluid Displacement: Part I, Preprint 43, San Francisco, December 1959.

86. Richardson, J. G., "Flow through Porous Media," Handbook of Fluid Dynamics, Section 16 (compiled by V. L. Streeter), McGraw-Hill Book Co., N. Y., 1961.

87. Richter, R. C., and R. Y. D. Chun, "Artificial Recharge of Ground Water Reservoirs in California," Proceedings, ASCE (Irrigation and Drainage Division), IR4, Paper No. 2281, December 1959, pp. 1-27.

88. Richtmyer, R. D., Difference Methods for Initial-Value Problems, Interscience Publishers, Inc., N. Y., 1962, 238 pp..

89. Rifai, M. N. E., W. J. Kaufman, and D. K. Todd, "Dispersion Phenomena in Laminar Flow through Porous Media," Report No. 3, Sanitary Engineering Research Laboratory, University of California Berkeley, I.E.R. Series 90, July 1956, 157 pp..

90. Robinson, J. M., "Longitudinal Dispersion in Beds of Finely Divided Solids," University of California Berkeley, UCRL-9193), June 1960.

91. Rumer, R. R. Jr., "Longitudinal Dispersion in Steady and Unsteady Flow," Proceedings, ASCE (Hydraulics Division) HY4, Paper No. 3202, July 1962, pp. 147-172.

92. Saffman, P. G., "A Theory of Dispersion in Porous Medium," Journal of Fluid Mechanics, Vol. 6, Part 3, October 1959, pp. 321-349.

93. Saffman, P. G., Dispersion due to Molecular Diffusion and Macroscopic Mixing in Flow through a Network of Capillaries," Journal of Fluid Mechanics, Vol. 7, February 1960, p. 194.

94. Scheidegger, A. E., "Statistical Hydrodynamics in Porous Media," Journal of Applied Physics, Vol. 25, 1954, pp. 994-1001.

95. Scheidegger, A. E., "On the Theory of Flow of Miscible Phases in Porous Media," International Union of Geodesy and Geophysics, International Association of Scientific Hydrology, General Assembly of Toronto, Vol. 2, 1957, PP. 236-242.

96. Scheidegger, A. E., "The Random Walk Model with Auto-correlation of Flow Through Porous Media," Canadian Journal of Physics, Vol. 36, 1958, pp. 649-658.

97. Scheidegger, A. E., "Typical Solutions of the Differential Equations of Statistical Theories of Flow in Porous Media," Transactions, AGU, Vol. 39, No. 5, October 1958, pp. 929-932.

98. Scheidegger, A. E., and V. C. Larson, "Asymmetry of the Concentration Front during Miscible Displacement in Porous Media," Canadian Journal of Physics, Vol. 36, 1958, pp. 1476-1482.

99. Scheidegger, A. E., "Statistical Approach to Miscible Displacement in Porous Media," Bulletin, Canadian Institute of Mining and Metallugry, Vol. 52, No. 561, January 1959, p. 26.

100. Scheidegger, A. E., "Growth of Instabilities on Displacement Fronts in Porous Media," Physics of Fluids, Vol. 3, No. 1, January-February 1960, pp. 94-104.

101. Scheidegger, A. E., "On the Stability of Displacement Fronts in Porous Media: A Discussion of the Muskat-Aronofsky Model," Canadian Journal of Physics, Vol. 38, No. 2, February 1960, pp. 153-162.

102. Scheidegger, A. E., The Physics of Flow through Porous Media, Macmillan Co., N. Y., 1960, 313 pp..

103. Scheidegger, A. E., "General Theory of Dispersion in Porous Media," Journal of Geophysical Research, Vol. 66, No. 10, October 1961, pp. 3273-3278.

104. Schiff, L., "Proceedings Biennial Conference on Ground Water Recharge, University of California Berkeley, June 24-25, 1959," issued by Western Soil and Water Management Research Branch, Fort Collins, Colorado, 1959.

105. Schiff, L., "Proceedings Biennial Conference on Ground Water Recharge, University of California Berkeley, June 28-29, 1961," issued by Ground Water Recharge Laboratory, Southwest Branch, Soil and Water Conservation Research Division, Fresno, California, 1961.

106. Schneebeli, G., "Experiments on the Range of Validity of Darcy's Law and the Appearance of Turbulence in a Filtering Flow," La Houille Blanche, No. 2, March-April 1955, pp. 141-149.

107. Shima, S., "On the So-Called Diffusion Phenomena of Seepage Flow," International Association for Hydraulic Research Conference, Part III, Dubrovnik, Yugoslavia, 1961, 9-1 to 9-6.

108. Simpson, E. S., "Transverse Dispersion in Liquid Flow through Porous Media," Professional Paper 411-C, Geological Survey, United States Government Printing Office, Washington, 1962, 30 pp..

109. Sinkoff, M. D., R. Parges, and J. H. McDernott, "Mean Residence Time of a Liquid in a Trickling Filter," Proceedings, ASCE (Sanitary Engineering Division), Vol. 85, SA-6, November 1959.

110. Strang, D. A., and C. J. Geankoplis, "Longitudinal Diffusivity of Liquids in Packed Beds," Industrial and Engineering Chemistry, Vol. 50, 1958, pp. 1305-1308.

111. "Studies in Water Reclamation," Technical Bulletin 13, I. E. T. Series 37, Sanitary Engineering Research Laboratory, University of California, July 1955, 65 pp..

112. Taylor, G. I., "Dispersion of Soluble Matter in Solvent Flowing Slowly through a Tube," Proceedings, Royal Society of London, Series A, Vol. 219, 1953, pp. 186-205.

113. Taylor, G. I., "The Dispersion of Matter in Turbulent Flow Through a Pipe," Proceedings, Royal Society of London, Series A, Vol. 223, 1954, pp. 446-468.

114. Todd, D. K., "Annotated Bibliography on Artificial Recharge of Ground Water Through 1954," Paper 1477, U. S. Geological Water Supply Paper, 1959, 115 pp..

115. Todd, D. K., Ground Water Hydrology, John Wiley and Sons, Inc., N. Y., 1959, 336 pp..

116. Yuhara, K., "A Model Experiment for Saline Diffusion in Flow of Water through Porous Media," Geophysics (Japan), Kyoto University, Institute of Geophysics, Vol. 9, April 29, 1954, pp. 127-134.

117. Vallentine, H. R., Applied Hydrodynamics, Butterworths Scientific Publications, London, 1959, 272 pp..

118. Von Rosenberg, D. U., "Mechanics of Steady-State, Single Phase, Fluid Displacement in Porous Media," American Institute of Chemical Engineering Journal, Vol. 2, No. 1, 1956, pp. 55-58.

119. "Water Reclamation," Conference Proceedings, University of California Berkeley, January 26-27, 1956, Sanitary Engineering Research Laboratory, University of California Berkeley, 1956.

120. Wilhelm, R., "Rate Processes in Chemical Reactors," Chemical Engineering Progress, Vol. 49, No. 3, March 1953, pp. 150-154.

DEFINITION OF SYMBOLS

a	coefficient of transient velocity distribution in the column; mean travel time from the source to a point along a streamline	 T
a'	dimensionless mean travel time along a streamline $= \frac{aA}{x_0^2}$	
b	coefficient of transient velocity distribution in the column; thickness of confined aquifer; measure of spread of the tracer distribution along a streamline	 L T^2
b'	dimensionless spread of the tracer distribution along a streamline $= \frac{bA^2}{x_0^4}$	
c	concentration of tracer, mass of tracer/ mass of solution	
c_{max}	maximum tracer concentration at any z below the point source	
c	tracer concentration at point of tracer injection	
$\bar{c}$	Laplace transform of c	T
d_{50}	mean particle size of porous medium	L
$f(\ )$	Laplace transform function	
g	gravitational acceleration	$\frac{L}{T^2}$
h	piezometric head $= \frac{p}{\gamma} + z$	L
$\Delta h'$	dimensionless head gradient during transient column flow	
k	intrinsic permeability of the porous medium	L^2
m	integer, 0, 1, 2, 3, ... ; slope of lateral dispersion plot on probability paper $= \sqrt{4D_2 \frac{z}{w}}$; distance along an equipotential line from $\psi = 0$ to a particular streamline	 L L

n	integer, 0, 1, 2, 3, ...; co-ordinate along an equipotential line	 L
n'	co-ordinate of a point along an equipotential line with respect to a particular streamline = n - m	L
n_1, n_2	exponents on the velocity in the longitudinal and lateral dispersion coefficients	
p	Laplace transform variable; pressure in the fluid; subscript denoting conditions at pumping well	$\frac{1}{T}$ $\frac{F}{L^2}$
q	velocity along a streamline	$\frac{L}{T}$
q'	dimensionless streamline velocity = $\frac{x_o q}{A}$	
r	subscript indicating recharge well	
r, θ, z	cylindrical co-ordinates	L
r_w	radius of a well	L
s	co-ordinate along a streamline	L
t	time	T
t_c, t_c'	time to reach steady-state velocity	T
t'	equivalent time scale for steady flow = $t - \Delta t$	T
Δt	time correction for transient column flow	T
t_{50}	time at which the mean tracer concentration reaches any point	T
t_*	$t - t_{50_r}$	T
u, v, w	velocity components in x, y, z, directions	$\frac{L}{T}$
$\bar{v}$	Darcy or average velocity in any direction	$\frac{L}{T}$
w_o	steady-state velocity along column axis	$\frac{L}{T}$

w'	dimensionless velocity ratio = $\frac{w}{w_o}$	
x, y, z	Cartesian co-ordinates	L
x_o	one-half the well spacing	L
z'	$z - (w_o \Delta t)$	L
A	$\frac{\theta}{K}$;	$\frac{T}{L}$
	$\frac{Q}{\pi b \theta}$	$\frac{L^2}{T}$
B	$\frac{\beta \theta^2}{g d_{50}}$	$\frac{T^2}{L^2}$
C	$\frac{1}{g}$	$\frac{T^2}{L}$
D_1, D_2	coefficients of longitudinal and lateral dispersion in uniform flow	$\frac{L^2}{T}$
D'_1, D'_2	coefficients of longitudinal and lateral dispersion in non-uniform flow	$\frac{L^2}{T}$
$\mathcal{D}_m$	molecular diffusion coefficient	$\frac{L^2}{T}$
F( )	inverse Laplace transform of f( )	
G	dimensionless concentration ratio, $\frac{c}{c_o}$	
H ( )	Hankel transform of zero order	L^2
$J_o( )$, $J_1( )$	Bessel functions of order 0 and 1	
K	Darcy permeability; constant	$\frac{L}{T}$
M	mass of tracer introduced at a point source	$\frac{FT^2}{L}$
Q	volumetric flow rate	$\frac{L^3}{T}$
$\mathbb{R}$	Reynolds number = $\frac{w d_{50}}{\nu}$	

$\mathbb{R}_k$	permeability Reynolds number = $\frac{w\sqrt{k}}{\nu}$	
S	rate of gain of tracer in the control volume	$\frac{FT}{L}$
U.C.	uniformity coefficient of particle size distribution = $\frac{d_{60}}{d_{10}}$	
α_1, α_2	longitudinal and lateral dispersivity coefficients in uniform flow	L
α_1', α_2'	longitudinal and lateral dispersivity coefficients in non-uniform flow	L
β	shape factor of particles in media; packing factor of media; α_1'/χ_0	
γ	media roughness factor; unit weight of solution	$\frac{F}{L^3}$
η	$\sqrt{r^2 + \frac{D_2}{D_1} z^2}$; $\frac{D_1}{wz}$; $\frac{\phi}{A}$; $\frac{8}{3}\,\frac{\alpha_1'}{r}$	L
θ	porosity	
λ	angle between any streamline and the x axis	
ν	kinematic viscosity	$\frac{L^2}{T}$
ξ	$\frac{wt}{z}$; $\frac{\psi}{A}$; $\frac{2At_*}{r^2}$	

ρ	solution density, mass of solution/volume of solution;.	$\frac{FT^2}{L^4}$
	dimensionless radial co-ordinate, $\frac{r}{\alpha_1'}$	
σ	Hankel transform variable;	$\frac{1}{L}$
	standard deviation of concentration distribution	L
τ	time;	T
	dimensionless time co-ordinate = $\frac{At}{x_o^2}$, $\frac{At}{\alpha_1'^2}$	
ϕ	equipotential function	$\frac{L^2}{T}$
ψ	streamfunction	$\frac{L^2}{T}$
ϕ_1, ψ_1	coefficients of dispersion coefficient correlation with Reynolds number	
erf(Δ)	error function of $\Delta = \frac{2}{\sqrt{\pi}}\int_0^{\Delta} e^{-\mu^2} d\mu$	
$erf_c(\Delta)$	complementary error function of $\Delta = 1 - erf(\Delta) = \frac{2}{\sqrt{\pi}}\int_{\Delta}^{\infty} e^{-\mu^2} d\mu$	